

## **INFORMATION TO USERS**

**This manuscript has been reproduced from the microfilm master. UMI films the text directly from the original or copy submitted. Thus, some thesis and dissertation copies are in typewriter face, while others may be from any type of computer printer.**

**The quality of this reproduction is dependent upon the quality of the copy submitted. Broken or indistinct print, colored or poor quality illustrations and photographs, print bleedthrough, substandard margins, and improper alignment can adversely affect reproduction.**

**In the unlikely event that the author did not send UMI a complete manuscript and there are missing pages, these will be noted. Also, if unauthorized copyright material had to be removed, a note will indicate the deletion.**

**Oversize materials (e.g., maps, drawings, charts) are reproduced by sectioning the original, beginning at the upper left-hand corner and continuing from left to right in equal sections with small overlaps.**

**Photographs included in the original manuscript have been reproduced xerographically in this copy. Higher quality 6" x 9" black and white photographic prints are available for any photographs or illustrations appearing in this copy for an additional charge. Contact UMI directly to order.**

**ProQuest Information and Learning  
300 North Zeeb Road, Ann Arbor, MI 48106-1346 USA  
800-521-0600**

**UMI<sup>®</sup>**





# **DETECTION OF HIGH IMPEDANCE FAULTS USING ARTIFICIAL NEURAL NETWORKS**

BY

**Mohammad Hasan Al-Mubarak**

A Thesis Presented to the  
DEANSHIP OF GRADUATE STUDIES

**KING FAHD UNIVERSITY OF PETROLEUM & MINERALS**

DHAHRAN, SAUDI ARABIA

In Partial Fulfillment of the  
Requirements for the Degree of

**MASTER OF SCIENCE**

In

**Electrical Engineering**

**September 2001**

**UMI Number: 1409905**

**UMI<sup>®</sup>**

---

**UMI Microform 1409905**

**Copyright 2002 by ProQuest Information and Learning Company.  
All rights reserved. This microform edition is protected against  
unauthorized copying under Title 17, United States Code.**

---

**ProQuest Information and Learning Company  
300 North Zeeb Road  
P.O. Box 1346  
Ann Arbor, MI 48106-1346**

**KING FAHD UNIVERSITY OF PETROLEUM AND MINERALS**  
**DHAHRAN, SAUDI ARABIA**  
**DEANSHIP OF GRADUATE STUDIES**

*This thesis, written by*

**MOHAMMAD HASAN MOHAMMAD AL-MUBARAK**

*under the direction of his Thesis Advisor, and approved by his Thesis Committee, has  
been presented to and accepted by the Dean of Graduate Studies, in partial fulfillment of  
the requirements for the degree of*

**MASTER OF SCIENCE IN ELECTRICAL ENGINEERING**

**Thesis Committee:**



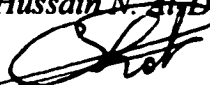
Dr. Ibrahim M. El-Amin (Chairman)



Dr. Youssef L. Abdel-Magid (Member)



Dr. Hussain N. Al-Duwaish (Member)



Dr. Chokri Belhadj Ahmed (Member)



Dr. Mohamed Mohandes (Member)



Dr. Samir A. Al-Baiyat  
Department Chairman



Dr. Osama A. Jannadi  
Dean of Graduate Studies

Date: 7-10-2001



## أهدي هذه الرسالة

إلى والديّ- حفظهما الله - للتنشئة الصالحة و دعائهما المستمر لي بالتوفيق ،

إلى زوجتي الغالية لإخلاصها وصبرها غير المحدود

و تشجيعها الدعوب لإنجاز هذا العمل ،

إلى أخواتي وإخواني : عبد الله ، جعفر ، عباس ، جاسم و أحمد

لمساندتهم و تشجيعهم ،

إلى ابنتي الحبيبة وابني الغاليين : حسن وأحمد ؛

فرحة اليوم و أمل المستقبل

\*\*\*

## THIS THESIS IS DEDICATED TO

**MY PARENTS** for their care and continuous prayers for my success,

**MY BELOVED WIFE** for her faith, unlimited patience and persistent encouragement to complete this work,

**MY SISTERS AND BROTHERS: ABDULLAH, JAFAR, ABBAS,**

**JASIM AND AHMED** for their support and encouragement,

**MY LOVELY DAUGHTER AND SONS: HASAN AND AHMED;**

for the happiness they bring me today, and  
the hope they give me for the future

## **Acknowledgement**

Praise be to Allah who generalized his present and his generosity among his creatures. Blessing and peace be upon our prophet "Mohammad" and his family members.

Acknowledgement is due to King Fahd University of Petroleum and Minerals for providing support for this work.

I wish to express my deep appreciation to Dr. Ibrahim M. El-Amin, who served as my major advisor, for his guidance and invaluable suggestions throughout the course of this work. I also wish to thank the other members of my Thesis Committee Dr. Youssef Abdel-Magid, Dr. Hussain Al-Duwaish, Dr. Chokri Belhadj and Dr. Mohamed Mohandes for their cooperation, encouragement and help. Thanks are also due to the Electrical Engineering Department Chairman, Dr. Samir Al-Baiyat and other faculty members for their interest and support.

I also acknowledge the support of my class and job mates, Ali H. Al-Mohammad and Ahmed H. Al-Mubarak, whose friendship has made a long way short, and a difficult job easy.

Thanks are also due to the Saudi Electricity Company-Eastern Region Branch and all its staff members who provided some of the information needed for this work.

Special thanks are due to my parents who have instilled in me the self confidence and proficiency at work, to my wife whose spirited encouragement has been the prime motivator to finish this work, and to my other family members who have always encouraged and supported my success.

Finally, I wish to thank all my other friends and job colleagues, especially Mohammad J. Al-Jassem, who provided me with the moral support through their sincere interest to complete this work.

# Contents

<b>Acknowledgement</b>	<b>iv</b>
<b>List of Tables</b>	<b>ix</b>
<b>List of Figures</b>	<b>x</b>
<b>Abstract (English)</b>	<b>xviii</b>
<b>Abstract (Arabic)</b>	<b>xix</b>
<b>1 INTRODUCTION</b>	<b>1</b>
1.1 Description of High Impedance Faults (HIFs) .....	1
1.2 Frequency of High Impedance Fault (HIF) Events .....	2
1.3 Review of HIF Detection .....	4
1.3.1 Implementation Issues of HIF Detectors .....	5
1.3.2 HIF Detection Techniques .....	6
1.5 Thesis Motivation .....	9
1.6 Content of the thesis .....	10



<b>2</b>	<b>LITERATURE REVIEW</b>	<b>11</b>
2.1	Review of Previous Research .....	11
2.2	Problem Statement and Intended Work .....	15
<b>3</b>	<b>ARTIFICIAL NEURAL NETWORKS (ANNs)</b>	<b>20</b>
3.1	Introduction to Artificial Neural Networks (ANNs) .....	21
3.2	Architecture of the Feedforward ANN .....	22
3.3	Training with the Backpropagation (BP) Algorithm .....	25
3.4	Description of the Proposed ANN .....	27
<b>4</b>	<b>SIMULATION OF HIGH IMPEDANCE FAULTS (HIFs)</b>	<b>28</b>
4.1	Description of Feeder Model .....	28
4.2	Simulation of the Base Case with EMTP .....	30
4.3	Simulation of HIFs with EMTP .....	35
4.3.1	Types of Events .....	35
4.3.2	Fault Scenarios .....	45
4.3.3	Additional EMTP Cases for ANN Validation .....	75
4.3.4	General Observations on the Waveforms .....	77
4.4	Data Preprocessing .....	77
<b>5</b>	<b>ARTIFICIAL NEURAL NETWORK DESIGN AND TESTING</b>	<b>79</b>
5.1	Overview .....	80
5.2	Description of ANN Design # 1 .....	86

5.3	Description of ANN Design # 2 .....	87
5.4	Description of ANN Design # 3 .....	94
5.5	Test Results .....	100
5.5.1	Design # 1 .....	100
5.5.2	Design # 2 .....	103
5.5.3	Design # 3 .....	106
5.6	Comparison of the Test Results .....	108
5.7	Validation Results of the ANN Designs .....	113
<b>6</b>	<b>CONCLUSIONS AND RECOMMENDATIONS</b>	
	<b>FOR FUTURE WORK</b>	<b>116</b>
6.1	Conclusions .....	116
6.2	Recommendations for Future Work .....	122
	<b>APPENDICES</b>	<b>125</b>
<b>A</b>	<b>EMTP INPUT DATA STRUCTURE</b>	<b>126</b>
A.1	Input Data Structure .....	126
A.2	Three Phase EMTP Data File for the Base Case .....	129
<b>B</b>	<b>VOLTAGE AND CURRENT WAVEFORMS</b>	
	<b>FOR SIMULATED CASES</b>	<b>133</b>
B.1	Normal Load Switching .....	134
B.2	Normal Load and Capacitor Switching .....	134

B.3	HIF with No Load or Capacitor Switching .....	134
B.4	HIF with Load Switching .....	134
B.5	HIF with Load and Capacitor Switching .....	157
B.6	Mid-span HIFs .....	157
B.7	HIF with Varying Fault Current .....	157
B.8	HIF with Varying Line Impedance .....	157
B.9	HIF for Extended Feeder .....	157
B.10	HIF for Lightly Loaded Feeder .....	176
<b>C</b>	<b>MATLAB M-FILES</b>	<b>181</b>
C.1	M-File for Reading the Case Matrices for Design D1F .....	181
C.2	M-File for Building the ANN Input and Test Matrices for Design D1F .....	183
C.3	M-File for ANN Training for Design D1F .....	185
C.4	M-File for ANN Testing for Design D1F .....	185
	<b>Bibliography</b>	<b>186</b>
	<b>Vita</b>	<b>192</b>

## List of Tables

1.1	Typical Fault Currents on Various Surfaces .....	3
1.2	Example of HIF Detector Logic .....	7
4.1	Typical Sequence Impedances at 115 kV Bus .....	32
4.2	Typical Transformer Parameters .....	34
5.1	Summary of the ANN Targets .....	83
5.2	Common Salient Features of the ANN Designs .....	85
5.3	Specific Features of the Various ANN Designs .....	99
5.4	ANN Designs Test Results with Respect to Targets .....	109
5.5	ANN Designs Test Results with Respect to Fault Scenarios .....	110
5.6	Test Results for Validation Cases with Respect to Targets .....	114

## List of Figures

2.1	Typical Phases for HIF Detection Using ANN .....	19
3.1	Neuron Model .....	23
3.2	Commonly Used Transfer Functions For ANN .....	24
3.3	A Typical Three-Layer Feedforward ANN .....	26
4.1	Typical Feeder for HIF Simulation .....	29
4.2	Phase-A Voltage Waveform for Load-1 Switching .....	36
4.3	Phase-A Current Waveform for Load-1 Switching .....	37
4.4	Phase-A Voltage Waveform for Load-4 and C1 Switching .....	39
4.5	Phase-A Current Waveform for Load-4 and C1 Switching .....	40
4.6	Phase-B Current Waveform for Load-4 and C1 Switching .....	41
4.7	Phase-C Current Waveform for Load-4 and C1 Switching .....	42
4.8	Phase-A Voltage Waveform for HIF on Phase-A at Node-1 .....	43
4.9	Phase-A Current Waveform for HIF on Phase-A at Node-1 .....	44

<b>4.10</b>	<b>Phase-A Voltage Waveform for HIF on Phase-A at Node-1 with Load-1 Switching .....</b>	<b>46</b>
<b>4.11</b>	<b>Phase-A Current Waveform for HIF on Phase-A at Node-1 with Load-1 Switching .....</b>	<b>47</b>
<b>4.12</b>	<b>Phase-B Current Waveform for HIF on Phase-A at Node-1 with Load-1 Switching .....</b>	<b>48</b>
<b>4.13</b>	<b>Phase-C Current Waveform for HIF on Phase-A at Node-1 with Load-1 Switching .....</b>	<b>49</b>
<b>4.14</b>	<b>Phase-B Voltage Waveform for HIF on Phase-B at Node-4 with Load-4 and Capacitor C1 Switching .....</b>	<b>50</b>
<b>4.15</b>	<b>Phase-A Current Waveform for HIF on Phase-B at Node-4 with Load-4 and Capacitor C1 Switching .....</b>	<b>51</b>
<b>4.16</b>	<b>Phase-B Current Waveform for HIF on Phase-B at Node-4 with Load-4 and Capacitor C1 Switching .....</b>	<b>52</b>
<b>4.17</b>	<b>Phase-C Current Waveform for HIF on Phase-B at Node-4 with Load-4 and Capacitor C1 Switching .....</b>	<b>53</b>
<b>4.18</b>	<b>Phase-A Voltage Waveform for HIF on Phase-A Between Nodes-1 and 2</b>	<b>55</b>
<b>4.19</b>	<b>Phase-A Current Waveform for HIF on Phase-A Between Nodes-1 and 2</b>	<b>56</b>
<b>4.20</b>	<b>Phase-B Current Waveform for HIF on Phase-B Between Nodes-1 and 2</b>	<b>57</b>
<b>4.21</b>	<b>Phase-C Current Waveform for HIF on Phase-C Between Nodes-1 and 2</b>	<b>58</b>

<b>4.22</b>	<b>Phase-A Voltage Waveform for HIF at Node-1</b>	
	<b>with Zero Fault Impedance .....</b>	<b>60</b>
<b>4.23</b>	<b>Phase-A Current Waveform for HIF at Node-1</b>	
	<b>with Zero Fault Impedance .....</b>	<b>61</b>
<b>4.24</b>	<b>Phase-A Voltage Waveform for HIF at Node-1 with 70 % Fault Current .</b>	<b>62</b>
<b>4.25</b>	<b>Phase-A Current Waveform for HIF at Node-1 with 70 % Fault Current . .</b>	<b>63</b>
<b>4.26</b>	<b>Phase-A Voltage Waveform for HIF at Node-1 (Phase-A)</b>	
	<b>with Line Impedance Reduced by 10 % .....</b>	<b>64</b>
<b>4.27</b>	<b>Phase-A Current Waveform for HIF at Node-1 (Phase-A)</b>	
	<b>with Line Impedance Reduced by 10 % .....</b>	<b>65</b>
<b>4.28</b>	<b>Phase-B Current Waveform for HIF at Node-1 (Phase-B)</b>	
	<b>with Line Impedance Reduced by 10 % .....</b>	<b>66</b>
<b>4.29</b>	<b>Phase-C Current Waveform for HIF at Node-1 (Phase-C)</b>	
	<b>with Line Impedance Reduced by 10 % .....</b>	<b>67</b>
<b>4.30</b>	<b>Phase-B Voltage Waveform for HIF on Phase-A at Node-1</b>	
	<b>with Extended Feeder .....</b>	<b>69</b>
<b>4.31</b>	<b>Phase-B Current Waveform for HIF on Phase-A at Node-1</b>	
	<b>with Extended Feeder .....</b>	<b>70</b>
<b>4.32</b>	<b>Phase-A Voltage Waveform for HIF on Phase-A at Node-1</b>	
	<b>with T3 and C2 Disconnected .....</b>	<b>71</b>

4.33	Phase-A Current Waveform for HIF on Phase-A at Node-1 with T3 and C2 Disconnected .....	72
4.34	Phase-B Current Waveform for HIF on Phase-B at Node-1 with T3 and C2 Disconnected .....	73
4.35	Phase-C Current Waveform for HIF on Phase-C at Node-1 with T3 and C2 Disconnected .....	74
4.36	Single Line Diagram for Simulation of the Additional Validation Cases .....	76
5.1	Error Convergence for ANN Design D1F .....	88
5.2	Error Convergence for ANN Design D1R .....	89
5.3	Error Convergence for ANN Design D2F .....	91
5.4	Error Convergence for ANN Design D2R .....	92
5.5	Error Convergence for ANN Design D2B .....	93
5.6	Error Convergence for ANN Design D3F .....	96
5.7	Error Convergence for ANN Design D3R .....	97
5.8	Error Convergence for ANN Design D3B .....	98
A.1.1	EMTP Input Data Structure .....	128
B.1.1	Phase-A Voltage Waveform for Load-2 Switching .....	135
B.1.2	Phase-A Current Waveform for Load-2 Switching .....	136



B.1.3	Phase-A Voltage Waveform for Load-4 Switching .....	137
B.1.4	Phase-A Current Waveform for Load-4 Switching .....	138
B.1.5	Phase-B Current Waveform for Load-4 Switching .....	139
B.1.6	Phase-C Current Waveform for Load-4 Switching .....	140
B.2.1	Phase-A Voltage Waveform for Load-1 and C1 & C2 Switching .....	141
B.2.2	Phase-A Current Waveform for Load-1 and C1 & C2 Switching .....	142
B.2.3	Phase-B Current Waveform for Load-1 and C1 & C2 Switching .....	143
B.2.4	Phase-C Current Waveform for Load-1 and C1 & C2 Switching .....	144
B.2.5	Phase-A Voltage Waveform for Load-2 and C2 Switching .....	145
B.2.6	Phase-A Current Waveform for Load-2 and C2 Switching .....	146
B.3.1	Phase-B Voltage Waveform for HIF on Phase-B at Node-1 .....	147
B.3.2	Phase-B Current Waveform for HIF on Phase-B at Node-1 .....	148
B.3.3	Phase-A Voltage Waveform for HIF on Phase-A at Node-2 .....	149
B.3.4	Phase-A Current Waveform for HIF on Phase-A at Node-2 .....	150
B.3.5	Phase-B Voltage Waveform for HIF on Phase-B at Node-4 .....	151
B.3.6	Phase-B Current Waveform for HIF on Phase-B at Node-4 .....	152
B.4.1	Phase-B Voltage Waveform for HIF on Phase-B at Node-2 with Load-2 Switching .....	153

<b>B.4.2</b>	<b>Phase-A Current Waveform for HIF on Phase-B at Node-2</b>	
	with Load-2 Switching .....	<b>154</b>
<b>B.4.3</b>	<b>Phase-B Current Waveform for HIF on Phase-B at Node-2</b>	
	with Load-2 Switching .....	<b>155</b>
<b>B.4.4</b>	<b>Phase-C Current Waveform for HIF on Phase-B at Node-2</b>	
	with Load-2 Switching .....	<b>156</b>
<b>B.5.1</b>	<b>Phase-A Voltage Waveform for HIF on Phase-A at Node-1</b>	
	with Load-1 and Capacitor C1 Switching .....	<b>158</b>
<b>B.5.2</b>	<b>Phase-A Current Waveform for HIF on Phase-A at Node-1</b>	
	with Load-1 and Capacitor C1 Switching .....	<b>159</b>
<b>B.5.3</b>	<b>Phase-B Current Waveform for HIF on Phase-A at Node-1</b>	
	with Load-1 and Capacitor C1 Switching .....	<b>160</b>
<b>B.5.4</b>	<b>Phase-C Current Waveform for HIF on Phase-A at Node-1</b>	
	with Load-1 and Capacitor C1 Switching .....	<b>161</b>
<b>B.6.1</b>	<b>Phase-A Voltage Waveform for HIF on Phase-A Between Nodes-3 and 4</b>	<b>162</b>
<b>B.6.2</b>	<b>Phase-A Current Waveform for HIF on Phase-A Between Nodes-3 and 4</b>	<b>163</b>
<b>B.6.3</b>	<b>Phase-B Current Waveform for HIF on Phase-B Between Nodes-3 and 4</b>	<b>164</b>
<b>B.6.4</b>	<b>Phase-C Current Waveform for HIF on Phase-C Between Nodes-3 and 4</b>	<b>165</b>
<b>B.7.1</b>	<b>Phase-A Voltage Waveform for HIF at Node-1 (Phase-A)</b>	
	with 50 % Fault Impedance .....	<b>166</b>

<b>B.7.2</b>	<b>Phase-A Current Waveform for HIF at Node-1 (Phase-A)</b>	
	with 50 % Fault Impedance .....	167
<b>B.7.3</b>	<b>Phase-B Current Waveform for HIF at Node-1 (Phase-B)</b>	
	with 50 % Fault Impedance .....	168
<b>B.7.4</b>	<b>Phase-C Current Waveform for HIF at Node-1 (Phase-C)</b>	
	with 50 % Fault Impedance .....	169
<b>B.8.1</b>	<b>Phase-A Voltage Waveform for HIF at Node-1 (Phase-A)</b>	
	with Line Impedance Increased by 20 % .....	170
<b>B.8.2</b>	<b>Phase-A Current Waveform for HIF at Node-1 (Phase-A)</b>	
	with Line Impedance Increased by 20 % .....	171
<b>B.8.3</b>	<b>Phase-B Current Waveform for HIF at Node-1 (Phase-B)</b>	
	with Line Impedance Increased by 20 % .....	172
<b>B.8.4</b>	<b>Phase-C Current Waveform for HIF at Node-1 (Phase-C)</b>	
	with Line Impedance Increased by 20 % .....	173
<b>B.9.1</b>	<b>Phase-B Voltage Waveform for HIF on Phase-B at Node-4</b>	
	with Extended Feeder .....	174
<b>B.9.2</b>	<b>Phase-B Current Waveform for HIF on Phase-B at Node-4</b>	
	with Extended Feeder .....	175
<b>B.10.1</b>	<b>Phase-A Voltage Waveform for HIF on Phase-A at Node-1</b>	
	with T2 and C1 Disconnected .....	177

<b>B.10.2</b>	<b>Phase-A Current Waveform for HIF on Phase-A at Node-1</b>	
	with T2 and C1 Disconnected .....	<b>178</b>
<b>B.10.3</b>	<b>Phase-B Current Waveform for HIF on Phase-B at Node-1</b>	
	with T2 and C1 Disconnected .....	<b>179</b>
<b>B.10.4</b>	<b>Phase-C Current Waveform for HIF on Phase-C at Node-1</b>	
	with T2 and C1 Disconnected .....	<b>180</b>

# **Abstract**

**Name : Mohammad Hasan Mohammad Al-Mubarak**  
**Title : Detection of High Impedance Faults Using Neural Networks**  
**Major Field : Electrical Engineering**  
**Date of Degree : September 2001**

Till the present, electric utilities are facing the problem of high impedance fault (HIF) detection on electric overhead distribution feeders. These faults often occur when a bare conductor breaks and falls to ground through a high impedance current path. Most HIFs draw little current, which makes them difficult to detect by conventional overcurrent relays. When such faults are not detected, they create a public hazard and threaten the lives of people. The desire to improve public safety has been the primary motivator for the development of HIF detectors.

Detection techniques based on Artificial Neural Network (ANN) have shown a good capability of detecting HIFs. In this thesis, a multi-layer feed-forward ANN, is designed and trained with the Scaled Conjugate Gradient (TRAINSCG) algorithm to analyze the current and voltage waveforms at the substation 13.8 kV bus and indicate whether the feeder is faulty or not. In addition, the ANN can locate the faulty section of the feeder, identity the faulty phase, and most importantly differentiate between faults and fault-like events, such as normal load switching, with a high degree of accuracy.

The Electromagnetic Transients Program (EMTP) is used to simulate the distribution feeder and generate the training cases for the ANN, which is developed and trained using the “ Neural Network Toolbox for MATLAB® ”. The feeder parameters are selected to represent a typical overhead feeder in the distribution network of the Saudi Electricity Company-Eastern Region Branch (SEC-ERB).

**MASTER OF SCIENCE DEGREE**  
**King Fahd University of Petroleum and Minerals**  
**Dhahran, Saudi Arabia**  
**September 2001**

## خلاصة الرسالة

اسم الطالب : محمد حسن محمد المبارك  
عنوان الرسالة : كشف الأعطال ذات المقاومة العالية باستخدام الشبكات العصبية  
التخصص : هندسة كهربائية  
تاريخ الشهادة : رجب ١٤٢٢ هـ

حتى وقتنا الحاضر، ما تزال شركات الكهرباء تعاني من صعوبة اكتشاف الأعطال الكهربائية ذات المقاومة العالية، التي تتعرض لها الخطوط الهوائية لشبكات التوزيع . مثل هذه الأعطال غالبا ما تحدث نتيجة سقوط الموصلات العارية في الخطوط الهوائية و ملامستها للأرض عبر مسار ذو مقاومة عالية . وغالبا ما ينتج عن هذا النوع من الأعطال تيار ضئيل يصعب اكتشافه بواسطة أجهزة الحماية الاعتيادية المستخدمة لكشف التيارات العالية . و عندما تبقى هذه الأعطال دون كشف ، فإنها تشكل خطرا على حياة الناس الذين يعيشون بالقرب منها ، و هذا هو الدافع الرئيس لتطوير أجهزة قادرة على اكتشاف مثل هذه الأعطال . و قد أظهرت أجهزة الكشف المبنية على تقنية الشبكات العصبية نجاحا كبيرا في حل هذه المشكلة .

هذه الرسالة تعرض تصميمًا جديدًا يستخدم شبكة عصبية متعددة الطبقات ، للكشف عن الأعطال الكهربائية ذات المقاومة العالية ، عن طريق تحليل موجات التيار و الجهد المسجلة عند قضيب الجهد ١٣,٨ ك.ف في المحطة الفرعية . و يستطيع هذا التصميم أن يحدد و جود العطل من عدمه ، إضافة إلى تحديد مكان العطل ، والطور المعطل ؛ و الأهم من ذلك كله قدرة هذا التصميم على التمييز بين العطل و الأحداث المشابهة له ، مثل إضافة الأحمال الاعتيادية ، بدرجة عالية من الدقة . و قد تم اختيار جميع مكونات الخط الهوائي المستخدمة في المحاكاة على أساس تلك المستخدمة في خط هوائي نموذجي في شبكة التوزيع الكهربائية للشركة السعودية للكهرباء — فرع المنطقة الشرقية .

درجة الماجستير في العلوم

جامعة الملك فهد للبترول والمعادن

الظهران ، المملكة العربية السعودية

التاريخ : رجب ١٤٢٢ هـ

# **Chapter 1**

## **INTRODUCTION**

Faults on primary distribution feeders can be divided into two major classes, namely low impedance faults (LIFs) and high impedance faults (HIFs). While it is easy to detect and clear LIFs by conventional protection devices, such as reclosers, fuses, overcurrent relays and circuit breakers, it is difficult to detect HIFs by such protection devices. This is due to the fact that currents passing through HIFs normally fall within the unprotected region of conventional overcurrent protection schemes.

### **1.1 Description of High Impedance Faults (HIFs)**

High impedance faults (HIFs) on electric power distribution feeders are of a great concern to electric power utilities. These faults often occur when a bare conductor breaks and falls to ground (referred to as downed conductor) through a high impedance current path, such as a dry tree limb, sand, asphalt or insulator. An open conductor may also be considered

a high impedance fault (HIF). Some HIFs draw sufficient current to be cleared by overcurrent protection, however, many HIFs draw only little current, which makes them difficult to detect by conventional overcurrent relays. Table 1.1 lists typical fault currents due to HIF on various surfaces [1]. As can be seen from the table, HIF current is in the range 0-100 A. This is well below the pick-up current for conventional overcurrent protection.

In addition to having a low level of fault currents, HIFs often exhibit arcing and flashing at the point of contact. They are also characterized by the presence of high frequency components and harmonics [2].

When HIFs are not detected, they create a public hazard and threaten the lives of people. Actually, the desire to improve public safety has been the primary motivator for the development of HIF detectors.

## **1.2 Frequency of High Impedance Fault (HIF) Events**

Presently, there are no exact statistics on how often HIFs occur. This is because utilities normally record system events that result in a breaker or a fuse operation. Another factor that contributes to scarcity of data on HIFs is the legal issues associated with injuries or damages that might result from an undetected HIF.



**Table 1.1: Typical Fault Currents on Various Surfaces**

Surface	Current (A)
Dry asphalt	0
Dry sand	0
Concrete (non-reinforced)	0
Wet sand	15
Dry sod	20
Dry grass	25
Wet sod	40
Wet grass	50
Concrete (reinforced)	75

A report published by General Electric indicates that about 5-20 % of faults on distribution feeders are HIFs [2]. A study of downed conductor faults conducted by Pennsylvania Power and Light Company (PP&L) showed that 32 % of these faults were not cleared by overcurrent protection [3]. Another study indicated that approximately 30-50 % of the downed conductor events are HIFs [1].

Verbal communications with personnel from the Saudi Electricity Company-Eastern Region Branch (SEC-ERB) and Saudi ARAMCO revealed that around 4 % of the faults on their primary distribution networks are HIF type.

### **1.3 Review of HIF Detection**

To date, there is no detection technique that can detect all HIFs and achieve a high degree of security or dependability for distinguishing them from HIF like events, such as load or capacitor switching. This is practically impossible because of the probabilistic nature of HIF detection [4]. Unlike conventional protection which works with predefined decisions based on measured parameters, one cannot tell that a fault is present with complete confidence when HIF detectors are used. Further, the operator will not be able to tell whether the detected fault is really hazardous to the public or not [1].

Some HIFs may be detected by conventional overcurrent protection, however, most HIFs need special techniques to detect and distinguish them from other normal system events. Researchers at Texas A&M University staged more than 200 HIFs on ten feeders at five

different utilities, for a period of eleven years[4]. Only 35 out of these 200 HIFs (17.5%) were cleared by conventional protection.

### **1.3.1 Implementation Issues of HIF Detectors**

As mentioned earlier, the primary motivator for HIF detection is neither system protection nor direct economic benefits. Rather, it is to ensure safety to public and properties, and to avoid legal implications. In the absence of practical and reliable HIF detectors, some HIFs may remain undetected until they are discovered by electricians while doing some preventive maintenance or reported by the public when they notice a downed conductor or experience a disconnection of power supply.

As utilities start to apply HIF detectors to their overhead distribution feeders, a number of issues have to be considered: control action (trip vs. alarm), economics and legal liability.

The most difficult decision to be made after HIF detectors are installed is what action shall be taken after a HIF is detected. This is because HIFs rarely result in damage to electric system secondary equipment and they typically do not exhibit any hazard to the distribution system stability or integrity as the amount of current that flows in HIFs is small when compared to normal load current. Each utility may have different strategy on whether to trip or only initiate an alarm when a HIF is detected based on thorough evaluation of all possible consequences. If a feeder is not tripped or patrolled for a downed conductor events, consequences may include personnel injury, legal liability and

property damages. On the other hand, when a feeder is unnecessarily tripped, it may result in traffic accidents, thefts, medical emergencies and customer inconvenience. One possible strategy for HIF detection is presented in Table 1.2 [1, 2]. For example, according to the table an alarm shall be initiated when there is a load loss with no overcurrent or arcing. But the feeder shall be tripped if there is arcing and overcurrent even when there is no load loss.

On the other hand, utilities also have to evaluate the advantages of installing HIF detectors against the cost of the installation. The only economic advantage of HIF detection is the reduced legal liability. This may not be enough justification for some utilities to install HIF detectors. What makes this decision really complicated is the unknown consequences on public safety from downed conductors. The cost impact for installing HIF detectors can be reduced if the detectors are integrated with distribution automation or load management systems [3].

### **1.3.2 HIF Detection Techniques**

HIFs have been studied since the early 1970's to find some characteristics in the current and voltage waveforms, which would make HIF detection possible and practical [2]. Most of the research has focused on developing more sensitive detectors to detect and clear HIFs [1]. The main difficulty associated with this approach is to maintain the delicate balance between the sensitivity of the detector (overcurrent protection) and the selectivity of the protection scheme. In other words, if the overcurrent relays are set to pick-up for

**Table 1.2: Example of HIF Detector Logic**

<b>Arcing</b>	<b>Load Loss</b>	<b>Overcurrent</b>	<b>Decision</b>
N	N	N	Normal
N	N	Y	Overcurrent *
N	Y	N	Alarm
N	Y	Y	Alarm - Overcurrent *
Y	N	N	Alarm – arcing
Y	N	Y	Trip – down wire
Y	Y	N	Trip – down wire
Y	Y	Y	Trip – down wire

\* trip by conventional protection

small changes in current, such as HIF currents, there will be many unwanted trippings due to normal system operations, like load switching.

Many other HIF detection techniques have been developed by researchers using even/odd harmonic energy contents, sequence components, and features of different combinations of current and voltage waveforms. These will be detailed in Chapter 2. Though some of these detection techniques have shown a good capability of detecting HIFs, the challenge is to make these techniques secure from all disturbances similar to HIFs [5].

HIF detectors can generally be divided into three main categories , namely

1. Falling wire detectors
2. Loss of voltage detectors
3. Waveform detectors

The falling wire detectors are the most expensive to install because at least one detector is required for each span of the overhead feeder. On the other hand, waveform detectors are the cheapest to install [5]. Several waveform detectors, which are based on analysis of the voltage and current waveforms, have been developed over the last two decades. One such detector is presently being manufactured by General Electric [4]. This detector is based on analysis of the harmonic and non-harmonic components of the current in the range 30-780 Hz. It employs expert systems (ES) techniques to detect and classify HIF events.

Researchers have also developed HIF detectors that utilize artificial intelligence techniques other than ES. The most used technique is the artificial neural network (ANN). This is mainly because, unlike ES, ANNs are not based on knowledge base which makes the execution time relatively long. Also, some of the information needed to build a comprehensive database is not readily available for HIFs on distribution networks [6]. Other advantages of ANNs include their excellent noise immunity, robustness and generalization capabilities [7].

## **1.5 Thesis Motivation**

A large percentage of the primary distribution circuits in the Kingdom of Saudi Arabia consists of overhead lines especially in rural areas. For instance, approximately 50 % of all primary distribution circuits (13.8 kV and 34.5 kV) in the system of SEC-ERB are overhead lines [8]. A survey conducted by the Electric Power Research Institute (EPRI) on primary distribution feeders (35 kV and below) found that around 95 % of all faults occurred on overhead lines [9].

The rapid growth of power system complexity makes traditional algorithms for HIF detection quite inadequate. This growth has necessitated the development of protection devices that are capable to generalize and recognize new patterns to keep pace with the system growth. ANNs have proven their effectiveness in solving problems in various fields that are difficult to solve for conventional computer algorithms or human beings. Detection of HIFs is one of the promising applications of ANNs [6, 7].

The thesis is also motivated by the fact that no commercial HIF detector based on ANN is available till this time. On the other hand, HIF Detectors based on ES are available these days but there are no reports about their field performance [4].

Moreover, the advances achieved recently in microprocessor speed encourage the use of more input data to train the ANN. This will give the ANN full picture of the simulated HIF than given by selected characteristics of the HIF, as commonly done in previous research efforts. Furthermore, with the availability of the “ Neural Network Toolbox for MATLAB<sup>®</sup> ”, more training cases can be presented to the ANN and various ANN structures can be tried to select the most appropriate one for the HIF detection problem under consideration.

## **1.6 Content of the thesis**

This thesis is organized as follows: literature survey and problem statement are presented in Chapter 2. Overview of ANN and the backpropagation training algorithm is given in Chapter 3. Simulation of HIF with the Electromagnetic Transients Program (EMTP) is discussed in Chapter 4. Details of ANN designing and testing results are covered in Chapter 5. Finally, conclusions and suggestions for future work are given in Chapter 6.



## **Chapter 2**

# **LITERATURE REVIEW**

This chapter gives a review of the research efforts reported in the literature so far on HIF detection on electric power distribution systems. It also states the problem under consideration and gives a brief review of the work conducted for this thesis.

### **2.1 Review of Previous Research**

Several methods for detection of HIFs on power distribution feeders have been developed using various techniques, such as even/odd harmonic energy contents and sequence component methods [10]. However, the most common HIF detection scheme is based on lowering the settings of overcurrent relays. This method may result in frequent unnecessary power interruptions because most HIFs produce current levels that are similar to normal load switching current [11]. Some HIF detection methods are based on lowering

the settings of ground relays to detect abnormal ground currents. These methods are obviously unreliable for feeders having high degree of imbalance.

The theory behind three techniques for HIF detection on multi-grounded distribution systems are presented by J. Carr [12]. These techniques are based on combining two current measurements, detection of power frequency harmonics and sensing sequence voltage.

Howard Calhoun, Martin T. Bishop and Charles H. Eicher developed a HIF detection method based on the use of Ratio Ground Relay (RGR) [13]. Four different RGR schemes are modeled using analog and digital data to determine the design parameters which have been used to build a prototype RGR by Westinghouse. This method is based on the concept that on a given feeder, the amount of load imbalance does not vary over a small interval of time. Since the current level remains unchanged on most HIFs, this scheme is also unreliable.

A microprocessor based technique for HIF detection based on finding a Chi-squared test statistic using 60 Hz harmonics and sequence components was developed by S. J. Balser, K. A. Clements and D. J. Lawrence [14]. This technique utilizes changes in feeder imbalance to indicate that a HIF is present. When this technique is implemented, it failed to detect a HIF in 60 % of the cases [11].

Another method for HIF detection using the increase in frequency components near 60 Hz is proposed by B. M. Aucoin and B. D. Russell [15]. However, it is difficult to detect significant changes in these frequency components as they normally dominate the frequency spectrum. Since arcing waveforms contain a great deal of high frequency components, another method was proposed by Aucoin and Russell based on the detection of increases in the 2-10 kHz frequency components [16]. However, a major limitation to HIF detection by this method is when capacitors are used for grounding of high frequency signals.

David C. Yu and Shoukat H. Khan described a method to detect HIFs and LIFs [17]. This method is based on measurements of the magnitude of the fault current, the magnitude of the third and fifth harmonic currents, the angle of the third harmonic current, the phase difference between the third harmonic current and the fundamental voltage and the average negative sequence current.

P. R. Silva and A. Santos Jr. presented a technique for detecting HIFs through the analysis of the feeder response to an impulsive signal injected on the feeder from the substation [18]. Different responses are measured at the substation for normal and abnormal conditions. The limitation to this method is that the response to the impulsive signal has to be measured for the real feeder operating in its ultimate configuration. That necessitate repeating the analysis for every possible operating condition of the feeder. A rule based decision support system for detecting single line to ground faults in a delta-delta connected distribution system is proposed by J. A. Momoh, L. G. Dias, T. Thor and D.

Laird [19]. This system is based on knowledge acquired through comprehensive simulations of various fault situations.

In 1990, a strategy for HIF detection was developed using ANNs [11]. Twenty parameters are chosen to represent the feeder operation over one cycle. This strategy showed the great potential of ANNs as a more effective method for HIF detection. A. F. Sultan, G. W. Swift and D. J. Fedirchuk proposed a method that uses a three-layer feed-forward ANN to differentiate between HIFs and fault-like loads [20]. The input to the ANN consists of 33 data points that represent the sampled line current. This method demonstrates some of the advantages of ANNs, namely its ability to generalize and recognize new patterns, and insensitivity to disturbances. The system proposed in [6] for fault diagnosis is also based on ANN. It applies four cascaded, multilayer ANNs to detect the fault occurrence, classify it as a LIF or HIF and identify the faulty section of the distribution feeder. The system uses samples of current and voltage waveforms that are normally available from the substation data acquisition system.

Another promising method based on ANN is proposed by Yasmine Assef, Patrick Bastard and Michel Meunier to detect single phase to ground faults on power distribution systems, with compensated neutral grounding, by comparing the residual and the phase currents [21]. K. L. Butler and J. A. Mamoh described another approach for fault diagnosis on power distribution systems [22]. This approach uses a two-stage supervised clustering ANN for the diagnosis. The inputs to the ANN are the three phase currents for each feeder. The accuracy of this approach is around 90 %.

A. Mohamed and M. D. A. Mazumder developed a diagnosis system for faults on the distribution network. This system employs several feedforward ANN modules, trained with the backpropagation algorithm [23]. The training data are generated based on the analysis of relays and circuit breaker operations to indicate the fault location. Another method is proposed by Shyh-Jier Huang and Cheng-Tao Hsieh to discriminate between HIFs and normal switching events using the Morlet wavelet transform [24]. HIFs are examined under different ground types, including cement, wet soil and grass.

A. M. Sharat, L. A. Snider and K. Debnath presented a new FFT-based relaying scheme for HIF detection on radial distribution feeders [25]. The scheme utilizes a multilayer feedforward ANN and uses the second, third and fifth harmonics of the residual voltage, current and power at the substation distribution bus. Yet another ANN-based approach is designed and tested by A. P. Apostolov, J. Bronfeld, C. H. M. Saylor and P. B. Snow using current data [26]. This approach is able to distinguish between faulted and unfaulted loads.

## **2.2 Problem Statement and Intended Work**

For the purpose of this thesis, a HIF can be defined as a fault on primary distribution system that cannot be detected or cleared by conventional overcurrent protection. Such a fault often occurs when a high impedance object such as a tree limb contacts a bare conductor, or when such a conductor breaks and contacts earth. Most HIFs draw currents

too small to be detected by overcurrent relays, which are usually set to operate in the range 125-200 % of the normal load current [3].

A survey conducted by EPRI showed that around 95 % of all faults on primary distribution feeders occur on overhead lines [9]. The average duration of the faults was less than 8.35 cycles (0.15 seconds). Around 5-20 % of these faults are HIFs [2] and the majority of them are single line to ground faults [10].

When a downed conductor HIF occurs, energized high voltage conductors may fall within the reach of the public which may cause electric shocks and threaten the lives of the public in addition to power supply interruption. Moreover, because arcing often occurs with HIFs, these faults can result in fire and property damage. For these reasons, the primary motivator for HIF detection is to improve public safety rather than electric system protection [11].

The objective of this thesis is to design an ANN that can detect HIFs with high accuracy. In addition, the ANN shall be able to locate the fault, distinguish HIFs from other normal switching events and identify the faulty phase. To achieve this objective, it is necessary to perform the following:

1. Simulate a typical 13.8 kV overhead distribution feeder using EMTP. Single line to ground fault (which is the most frequently occurring fault on overhead lines) will be simulated at different locations along the feeder and at different times. Both heavy and

light load periods will be considered and different system operating conditions will be investigated. The following cases will be simulated:

- a. Normal load switching
- b. Normal load and capacitor switching
- c. High impedance fault with no load or capacitor switching
- d. High impedance fault with load switching
- e. High impedance fault with load and capacitor switching

This will generate the current and voltage waveform samples needed for training the ANN.

2. For all the cases the inputs and targets will be scaled (or normalized) using the MATLAB function `PREMNMX` [27]. This function scales the input and outputs so that they fall in the range  $[-1,1]$ . For some cases additional preprocessing of the input data (voltage and current waveforms) will be performed using the Fast Fourier Transform (FFT).
3. An ANN will be developed and trained using some of the waveform samples. Numerous ANN architectures, as required, will be examined till the appropriate architecture (number of hidden layers and number of neurons in each layer) is obtained.

4. The ANN will then be tested using the remaining waveform samples that have not been used for the ANN training.
5. Generalization of the ANN will be checked using waveform samples for new cases that are totally different from those used to train and test the ANN.

Figure 2.1 shows a schematic diagram of the typical phases needed for detecting HIFs using ANN.



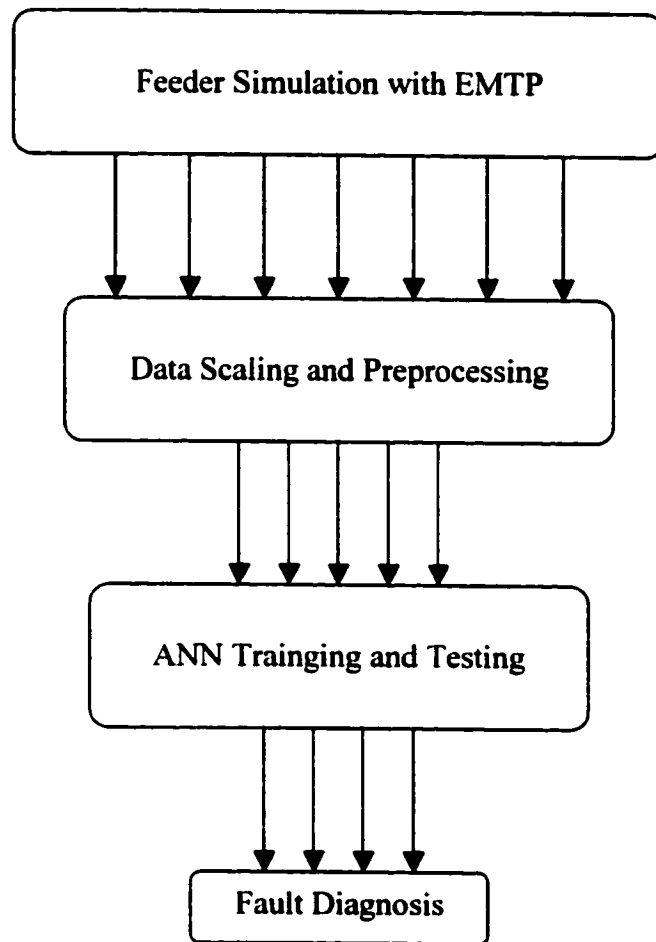


**Figure 2.1: Typical Phases for HIF Detection Using ANN**

## **Chapter 3**

# **ARTIFICIAL NEURAL NETWORKS**

As mentioned earlier, the difficulty of HIF detection problem has prompted the use of artificial intelligence (IA) techniques in general and ANN in particular. The most important advantages of ANN for HIF applications are [28]:

1. Its generalization capabilities which allows using ANN with noisy and non-linear inputs. ANN can also predict meaningful solutions to problems that are not presented to it during training.
2. Its shorter response time than other IA techniques, such as expert systems (ES).
3. ANN can be built much easier than ES which requires availability and entry of a huge amount of data. Such data is not available for HIFs.

The following sections give a brief introductory to ANN in general with emphasis on the ANN-based HIF detection approach that is proposed for this work. This is needed for better understanding of the work performed for designing and testing the ANN, which will be detailed in Chapter 5.

### **3.1 Introduction to Artificial Neural Networks (ANNs)**

Research in the field of ANN has started since the early 1940's. The research was inspired by the ability of the biological brain to perform very complicated activities in a short time, though it is composed of simple processing elements called neurons [29, 30]. However, ANNs have received the most attention only during the last two decades, during which ANNs have been used in a variety of applications in various fields including aerospace, finance, medicine, robotics and engineering applications. Nowadays, ANNs can be trained to solve problems that are difficult, or impossible, for conventional computer algorithms or human beings [27].

There is no universal definition of an ANN. Many different definitions have been proposed by various researchers. Basically, an ANN consists of a group of connected nodes (or neurons) and a propagation rule. It can be either of two classes: supervised networks or unsupervised networks depending on the method of ANN training and the target information [31]. The following section describes briefly the ANN architectures (topologies). A detailed description of the ANN structures is available in references [7] and [32].

### **3.2 Architecture of the Feedforward ANN**

The ANN architecture or topology is the process that specifies the layout of the ANN and the method of interconnecting the processing elements. These processing elements are the neurons which are sometimes called nodes. Figure 3.1 shows a neuron model. The input elements ( $a_j$ ) to the model enter the unit after each element is multiplied by the weight ( $w_{j,i}$ ) of the link that connects the element to the unit. An activation function, usually a summation, is applied on the weighted input elements and a bias ( $b$ ) is then added. The result of the summation is acted upon by a transfer function ( $F$ ) that produces the output of the neuron. Figure 3.2 shows graphical illustrations of the most commonly used transfer functions [27]. The log-sigmoid and tan-sigmoid transfer functions are often applied for non-linear applications.

Two or more such neurons are connected to form a layer, and when two or more layers are connected together they form an ANN. The first layer is called the input layer and the last layer is called the output layer. All layers in between are called the hidden layers. The links (synapses) that connect the neurons and layers have varying weights. These weights represent the knowledge presented and stored in the ANN.

There is no rule for selecting the number of neurons in each layer except for the output layer where the number of neurons equals the number of targets for which the ANN is trained. For all other layers, the selection of the number of neurons depends on the experience of the designer and trial and error. It shall be noted that regardless of the

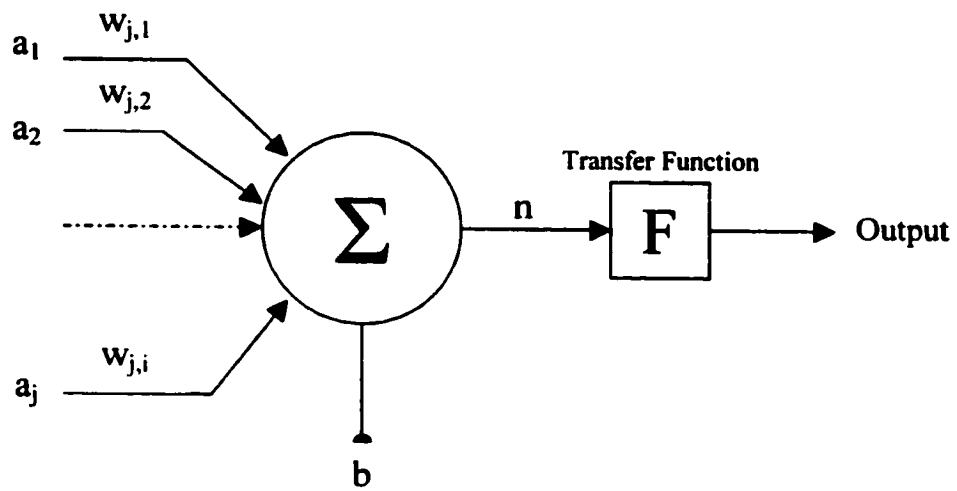
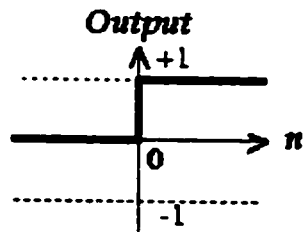
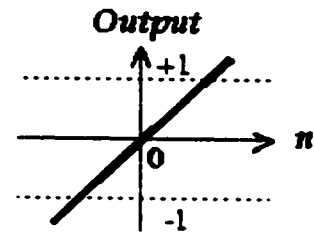


**Figure 3.1: Neuron Model**



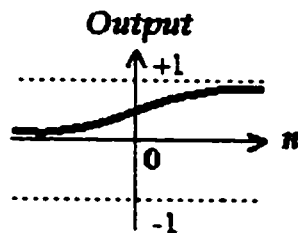
$$\text{Output} = \text{hardlim}(n)$$

Hard Limit (hardlim) Transfer Function



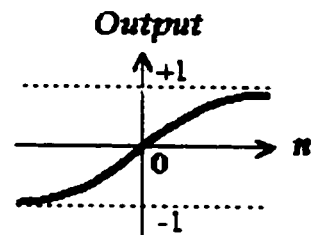
$$\text{Output} = \text{purelin}(n)$$

Linear (purelin) Transfer Function.



$$\text{Output} = \text{logsig}(n)$$

Log-sigmoid (logsig) Transfer Function



$$\text{Output} = \text{tansig}(n)$$

Hyperbolic Tangent-sigmoid (tansig)  
Transfer Function

**Figure 3.2: Commonly Used Transfer Functions For ANN**

number of input elements in the input vector and the number of neurons in the first hidden layer, each element in the input vector has to be connected to each of the neurons in the first hidden layer after the input element is multiplied by the corresponding weight. In other words, the number of neurons in the first hidden layer is independent of the number of input elements in the input vector.

Many types of ANNs exist, however, most of the ANN implementations for HIF detection are based on the multi-layer feed-forward ANN [31], which belongs to the supervised network class. Figure 3.3 shows a typical three-layer feedforward ANN (input layer is counted separately).

In feedforward ANNs, the inputs are all received at the input layer then they propagate forward from one layer to the next. The output signal is not fed back to the input of the ANN [11, 29]. For any ANN to perform a specific task, it has to be trained with a set of training inputs and expected targets or outputs. There are many methods that have been developed for training ANNs, however, the backpropagation (BP) training algorithm is the most popular technique which has shown very good success in many applications. BP algorithm is sometimes called the generalized delta rule [11].

### **3.3 Training with the Backpropagation (BP) Algorithm**

During the ANN training, the weight and biases are calculated so that they represent the relationship between the training set which consists of the inputs and their corresponding

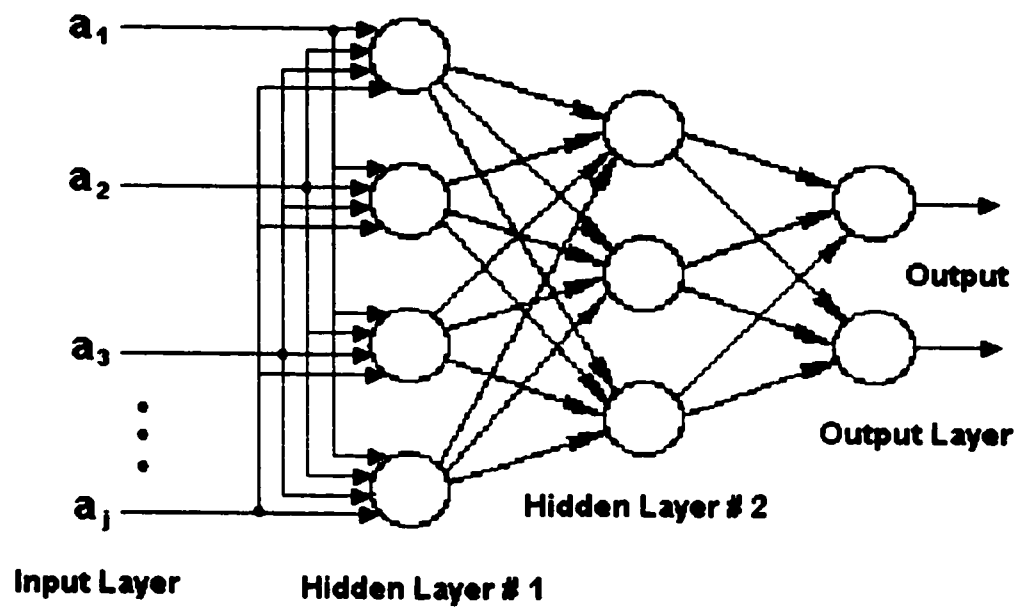


**Figure 3.3: A Typical Three-Layer Feedforward ANN**



desired outputs. In the backpropagation algorithm, preliminary weights and biases are assigned to all links in the ANN at the beginning of the training. This is called initialization of the network. Next, both the inputs and outputs in the training set are presented to the network and the error between the desired output and the actual output is calculated. The error is then used to modify the weights, which are then used with the same training set inputs and the error is recalculated. This process is repeated till the error is below a specified value or the number of iterations exceeds a preset maximum.

### **3.4 Description of the Proposed ANN**

For this thesis, a four-layer feedforward ANN is used. The ANN is trained using the improved faster versions of BP, namely the scaled conjugate gradient and the Fletcher-Reeves conjugate gradient. The number of neurons in each layer is varied and different combinations of these layers are tried till the appropriate architecture is obtained. Also, different transfer functions have been tried and the tangent-sigmoid has resulted in the most accurate and fastest convergence of the ANN. Details of the various designs that have been investigated together with their test results and accuracy analysis are presented in Chapter 5.

## **Chapter 4**

# **SIMULATION OF HIGH IMPEDANCE FAULTS (HIFs)**

The first step required for developing the proposed approach for HIF diagnosis is to simulate a typical 13.8 kV overhead distribution feeder to generate the voltage and current waveforms that are needed for training and testing the ANN designs. The following sections give description of the feeder model and details of the various components of the feeder model that have been used for the simulation. Review of the simulated cases is also presented in this chapter.

### **4.1 Description of Feeder Model**

The single line diagram of the 13.8 kV overhead distribution feeder used for the simulation is shown in Figure 4.1. Ratings and sizes of the different components shown in

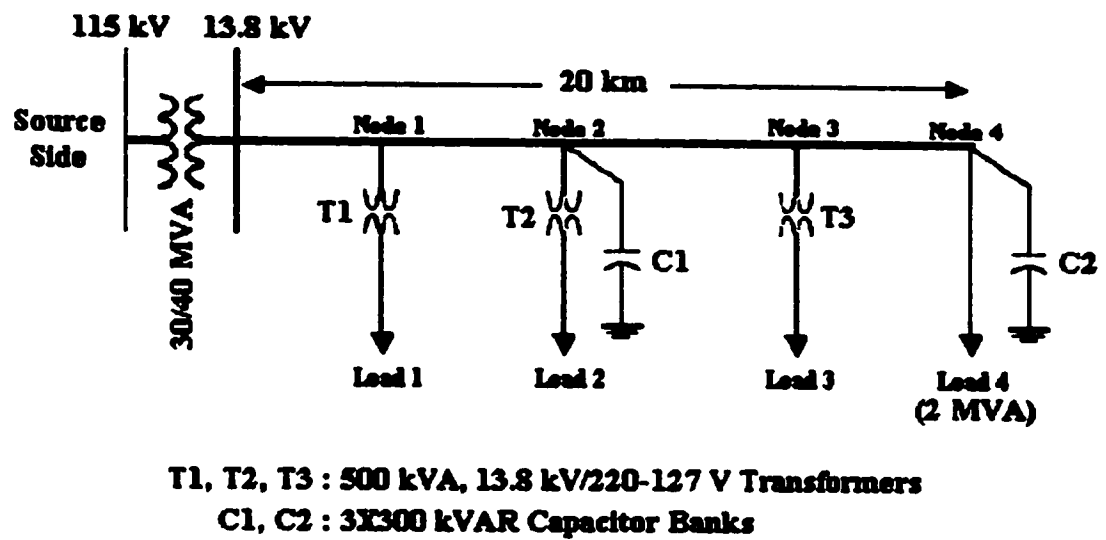


**Figure 4.1: Typical Feeder for HIF Simulation**

the figure are selected based on those typically used in the system of the Saudi Electricity Company-Eastern Region Branch (SEC-ERB). The feeder consists of a 20 km long overhead transmission line that is divided into four sections each of which is 5 km long. Three distribution transformers, each rated 500 kVA, are connected at Nodes-1, 2 and 3 to feed customers at the secondary side of the transformers with power supply at 220 V. A 2 MVA industrial load having a power factor (pf) of 0.9 is connected at Node-4. Two capacitor banks, each rated 3X300 kVAR, are connected at Nodes-2 and 4 to provide power factor correction and trap any fault signal, which might propagate back to the substation. The feeder is supplied from the secondary side of a 30/40 MVA, 115/13.8 kV, power transformer.

The following section details other parameters that have been used for the various components in the feeder model.

## **4.2 Simulation of the Base Case with EMTP**

Simulation of the feeder has been performed using the Electromagnetic Transients Program (EMTP) [33]. The capability of EMTP to handle switch closing and opening at specific or arbitrary times makes it ideal for applications involving transient analysis or fault simulation. Also, EMTP is capable to simulate unbalanced systems, such as the case of a single line to ground fault which is the case under study in this thesis. Throughout this work, three-phase simulation is used.

The feeder is simulated for a period of 5 cycles (83.33 ms) at a sampling rate of 0.2778ms, which results in 300 samples per phase for each case. In other words, for each case, there will be 1800 data points to represent the three phases of the current and voltage waveforms, as being measured by the potential and current transformers at the substation 13.8 kV bus. A flow chart and description of the EMTP input data structure, together with the three phase EMTP data file for the base case are included in Appendix A.

The 115 kV infinite bus is simulated using the Thevenin Equivalent of the system at the 115 kV bus. Table 4.1 lists the positive, negative and zero sequence impedances (in per unit) at a typical 115 kV bus in SEC-ERB system. For entry in EMTP, the per unit sequence impedances are converted into resistances (in ohms) and inductances (in millihenries). Only the positive and zero sequence resistances and inductances are entered in EMTP [34]. These are:

$$\begin{aligned} R_0 &= 0.156055 \, \Omega & L_0 &= 4.781458798 \, \text{mH} \\ R_1 &= 0.264500 \, \Omega & L_1 &= 5.609356286 \, \text{mH} \end{aligned}$$

The bases used in the calculations are: 100 MVA (3 $\Phi$ ) and 115 kV<sub>LL</sub>. The source is simulated with a conventional sinusoidal voltage source (type 14) which is connected to the source side terminal of the Thevenin equivalent.

The three phase saturable transformer model is used to simulate both the power (30/40 MVA) transformer and the distribution (500 kVA) transformers. The saturation

**Table 4.1: Typical Sequence Impedances at 115 kV Bus**

	<b>Resistance (pu)</b>	<b>Reactance (pu)</b>
<b>Positive Sequence</b>	0.00200	0.01599
<b>Negative Sequence</b>	0.00203	0.01597
<b>Zero Sequence</b>	0.00118	0.01363
<b>Base Quantities: 100 MVA (3<math>\Phi</math>) and 115 kV<sub>LL</sub></b>		

characteristics of these transformers have been taken from actual winding resistance measurements and no-load test reports for transformers installed in SEC-ERB substations. Other parameters of the transformers are given in Table 4.2.

All other components in the feeder are simulated using appropriate EMTP branch circuit cards, which are composed of combinations of resistances, inductances and capacitances. For instance, the feeder conductors are Merlin type, 179.7 mm<sup>2</sup> ACSR/AW, rated 412 A. The calculated resistance and inductance for each section of the feeder (5 km long) are:

$$R = 0.865285 \, \Omega \qquad L = 5.187535 \, \text{mH}$$

The capacitor bank is simulated with a shunt capacitance of 12.5358 uF per phase. To simulate HIFs, the ordinary switch card of EMTP is used to connect a pre-calculated impedance to the faulty node of the feeder at a specific time. The value of the impedance is selected so that the current at the 13.8 kV bus during the fault is less than 120 % of the normal load current. For the base case these switches are left open to simulate the normal feeder operation.

The next section discusses the different case and scenarios that have been simulated to cover the various single line to ground fault conditions.

**Table 4.2: Typical Transformer Parameters**

	<b>Power Transformer</b>	<b>Distribution Transformer</b>
Percentage Impedance (%)	12	5
Primary Winding Inductance (mH)	70.160799	25.25789
Secondary Winding Inductance (mH)	1.0103156	0.00641925



### **4.3 Simulation of HIFs with EMTP**

One of the key factors for a successful ANN design is the training set of the ANN , i.e. the input and output data that is used to train the network to perform the required task, which is HIF diagnosis in this work. As mentioned earlier, it is not difficult to produce an ANN design for HIF detection, but it is quite difficult to produce an ANN-based HIF detector that is capable of distinguishing HIFs from HIF-like events. Therefore, single line to ground HIFs as well as similar normal system operation events have been simulated.

#### **4.3.1 Types of Events**

A total number of 120 cases were simulated to cover the different possible fault and fault-like events. The following event types are simulated:

- a. Normal load switching
- b. Normal load and capacitor switching
- c. HIF with no load or capacitor switching
- d. HIF with load switching
- e. HIF with load and capacitor switching

##### **a. Normal Load Switching**

Cases were generated that simulate connecting Loads-1 to 4, as indicated in Figure 4.1, to the feeder. Voltage and current waveforms are recorded as measured by the potential and current transformers at the 13.8 kV substation bus. Sample waveforms are shown in Figures 4.2 and 4.3. While there is no appreciable change in bus voltage, the effect of

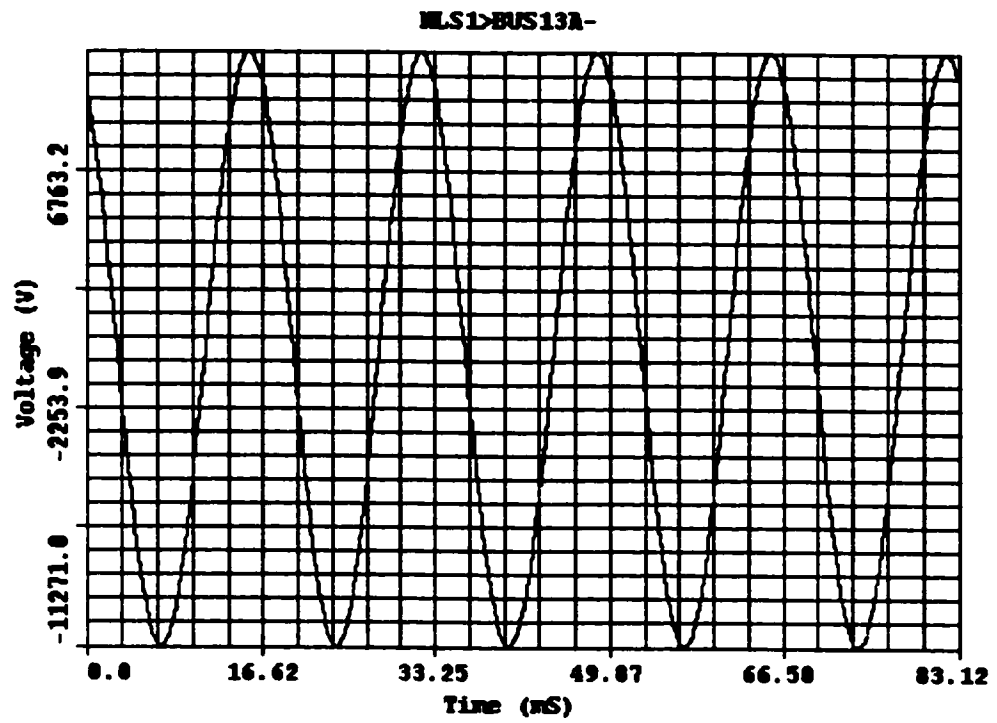


**Figure 4.2: Phase-A Voltage Waveform for Load-1 Switching**

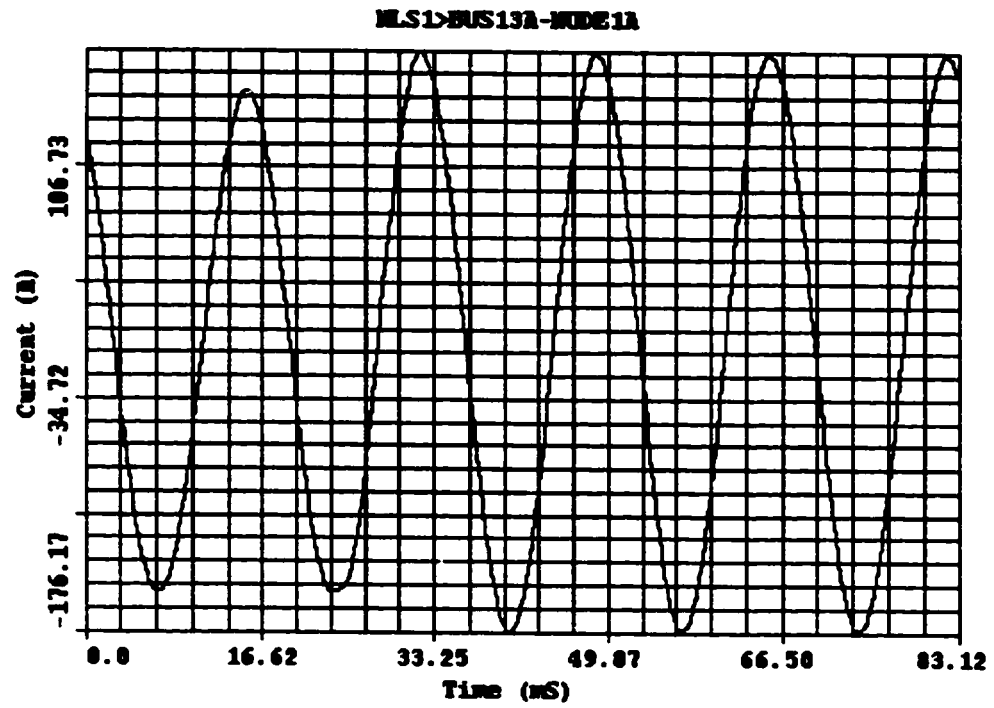


**Figure 4.3: Phase-A Current Waveform for Load-1 Switching**

connecting Load-1 can be clearly seen from Figure 4.3, where the current has increased from 152.39  $A_{(peak)}$  to 177.45  $A_{(peak)}$ , as a result of connecting the load at 23.38 ms. Similar waveforms have also been recorded for other phases, and for connecting other loads to distribution transformers at Nodes-1 to 4. Sketches of some of these waveforms are included in Appendix B.

**b. Normal Load and Capacitor Switching**

While normal load switching waveforms are associated with large increase in the current with small, rapidly disappearing transients, the transients that result from capacitor switching last longer and have larger amount of current increase as can be seen from Figures 4.4 to 4.7, which show sample waveforms for switching-in Load-4 and capacitor C1 at 23.38 ms. For instance, Figure 4.6 shows that the phase-B current magnitude has increased from 76.39  $A_{(peak)}$  to 199.97  $A_{(peak)}$  as a result of the switching. Figures of waveforms for other cases are given in Appendix B.

**c. HIF with No Load or Capacitor Switching**

Waveforms for a HIF on phase-A at Node-4 are shown in Figures 4.8 and 4.9. The figures show that the changes in the current waveforms are more significant than that of normal load switching. In this case, the current has increased from 175.63  $A_{(peak)}$  to 389.66  $A_{(peak)}$ . Also, there are only little distortions on the waveforms as there is no capacitor switching involved. Appendix B illustrates waveforms for some of the other simulated HIF cases.

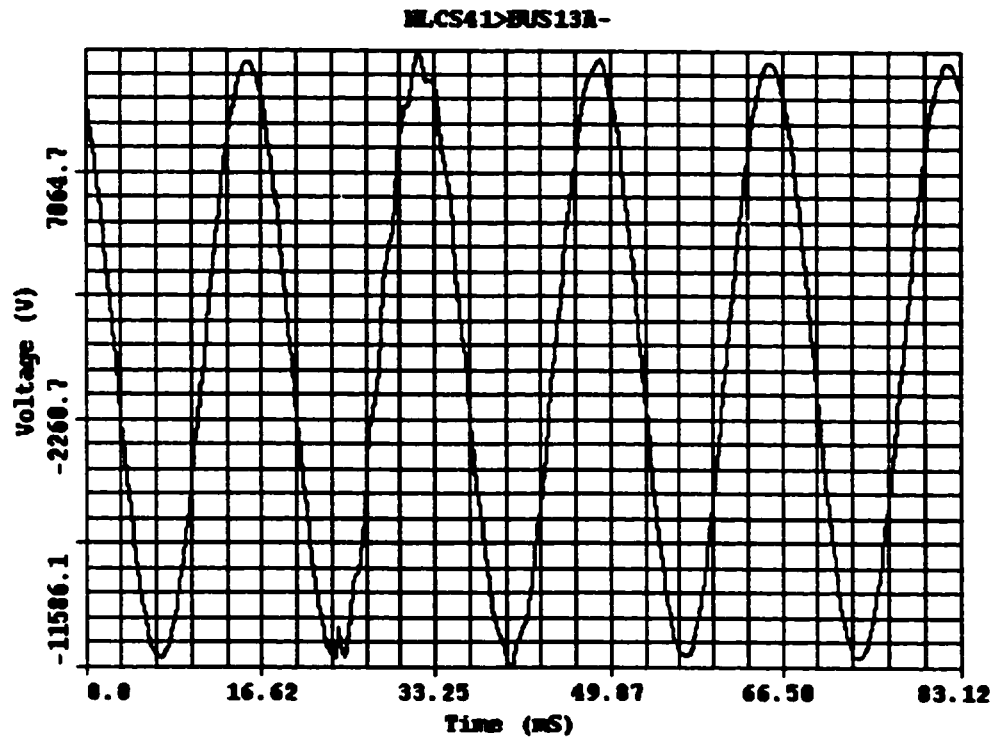


**Figure 4.4: Phase-A Voltage Waveform for Load-4 and C1 Switching**

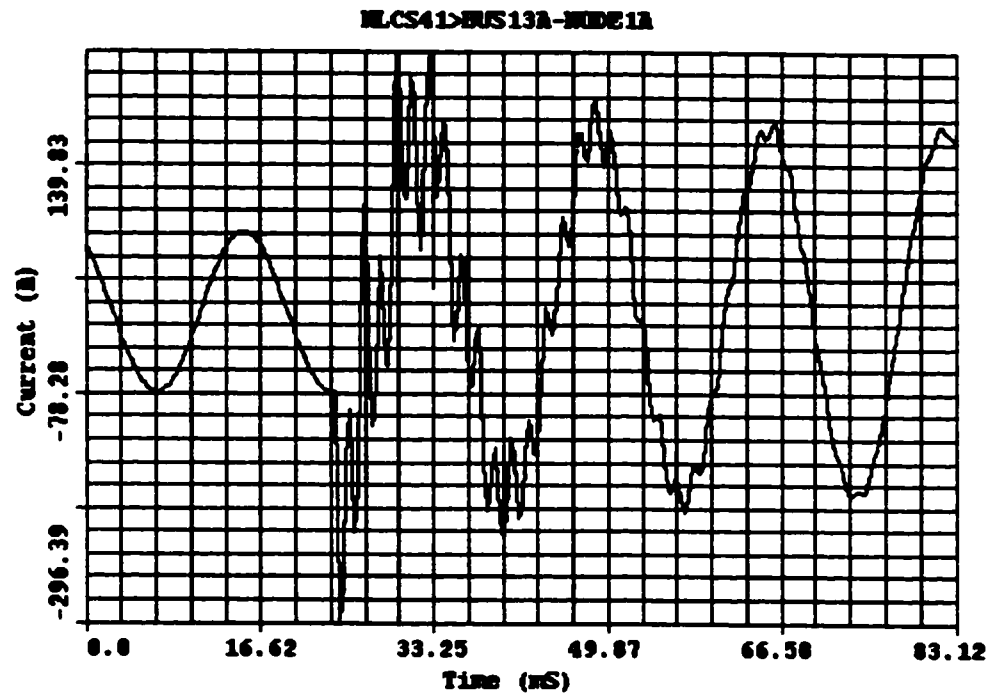


**Figure 4.5: Phase-A Current Waveform for Load-4 and C1 Switching**

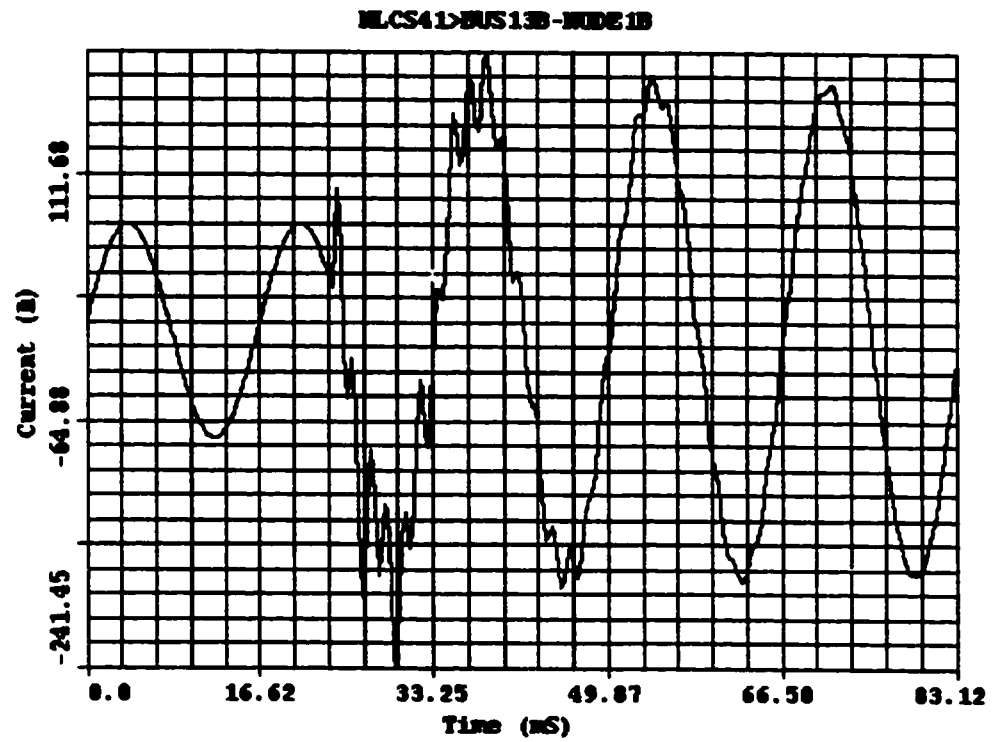


**Figure 4.6: Phase-B Current Waveform for Load-4 and C1 Switching**

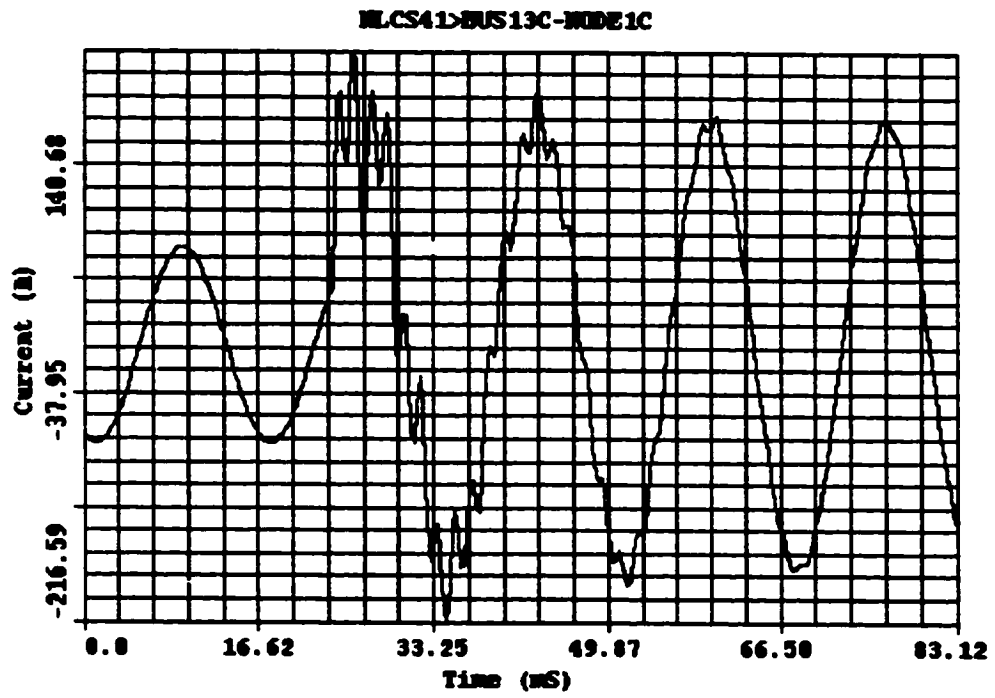


**Figure 4.7: Phase-C Current Waveform for Load-4 and C1 Switching**



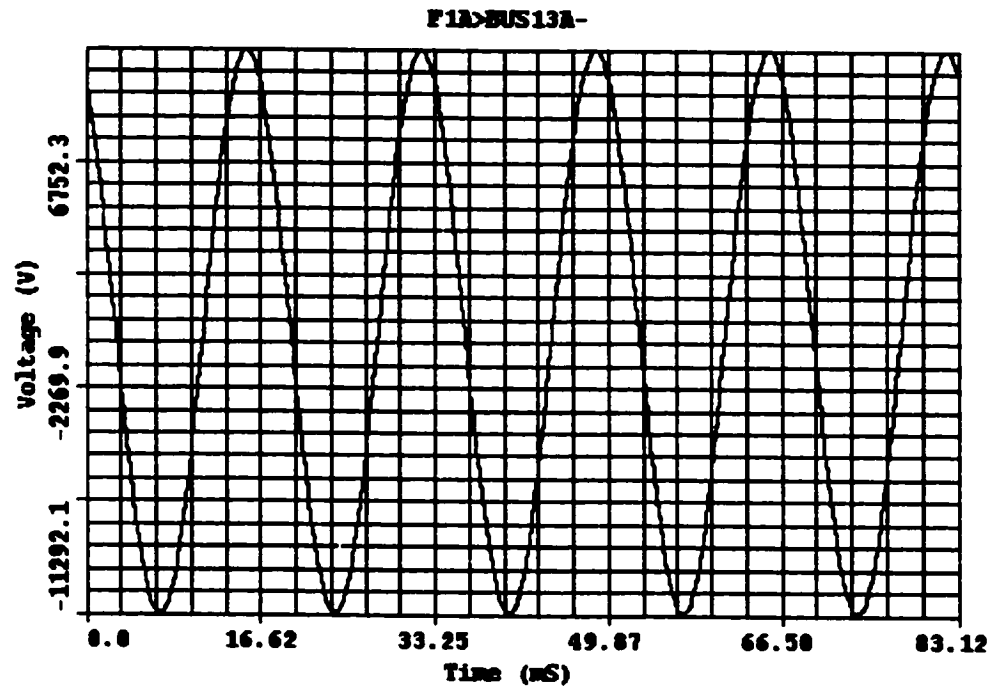


**Figure 4.8: Phase-A Voltage Waveform for HIF on Phase-A at Node-1**

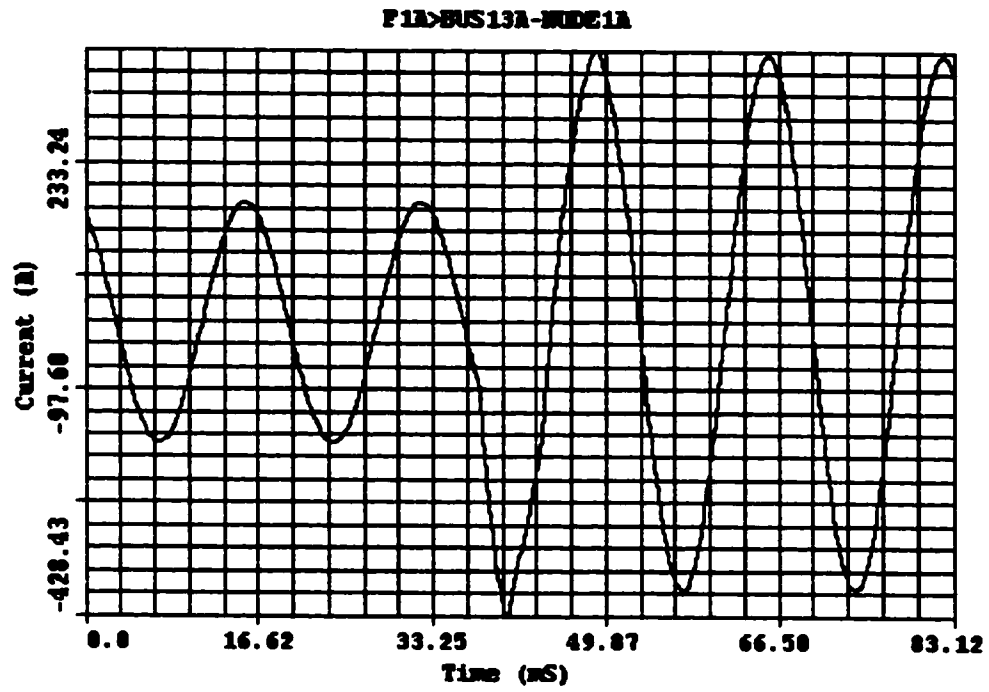


**Figure 4.9: Phase-A Current Waveform for HIF on Phase-A at Node-1**

**d. HIF with Load Switching**

Load switching results in little wave distortions, which extinguish quickly, on the faulty phase current as can be seen from Figures 4.10 to 4.13. While there is a large increase in current magnitude of the faulty phase (from 152.42  $A_{(peak)}$  to 398.81  $A_{(peak)}$ ), the only effect that is apparent on the other phases is a slight increase in current (from 152.42  $A_{(peak)}$  to 174.58  $A_{(peak)}$  on phase-B and from 152.41  $A_{(peak)}$  to 175.84  $A_{(peak)}$  on phase-C). Again there is no capacitor switching involved here. Other waveforms are included in Appendix B.4 for some of the simulations of HIF with load switching.

**e. HIF with Load and Capacitor Switching**

Figures 4.14 to 4.17 illustrate the waveforms for HIFs with load and capacitor switching. Capacitor switching has resulted in appreciable amount of transients on the current waveforms, particularly for the faulty phase, at 37.58 ms when the fault took place. For instance, Figure 4.17 show that the current on phase-C has increased from 100.40  $A_{(peak)}$  to 361.82  $A_{(peak)}$ . Appendix B gives waveforms of some other simulated cases.

### **4.3.2 Fault Scenarios**

All the fault simulations mentioned in the above section are for HIFs that take place at one of the nodes or branches of the feeder model illustrated in Figure 4.1. In addition to the fault location which was varied to cover all the four sections of the feeder (Nodes-1 to 4), the fault occurrence time was also varied.

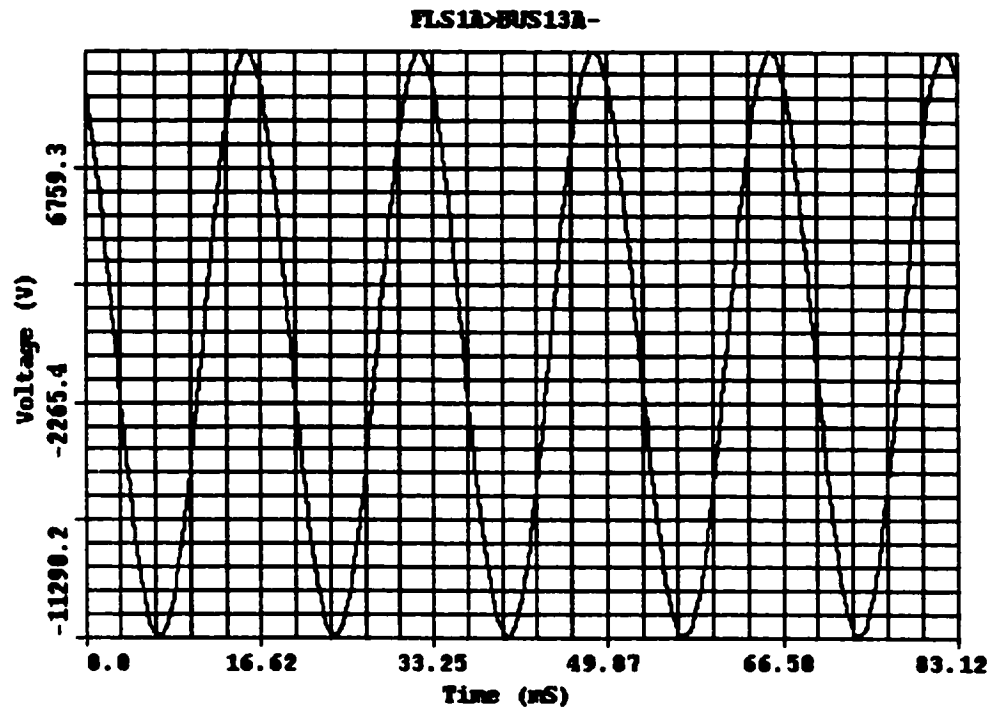


**Figure 4.10: Phase-A Voltage Waveform for HIF on Phase-A at Node-1  
with Load-1 Switching**

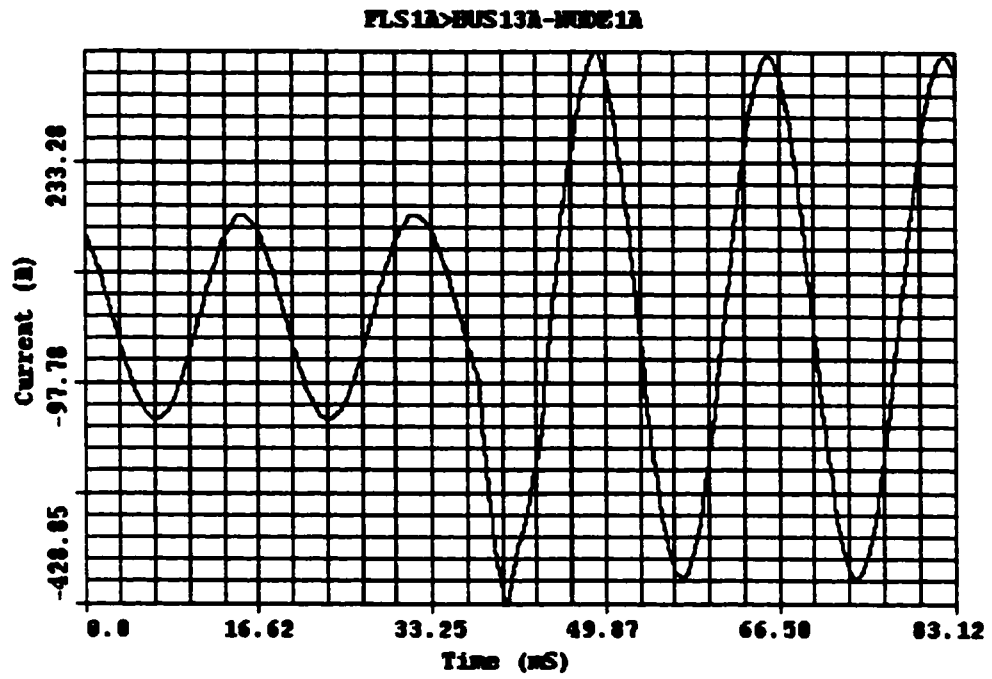


**Figure 4.11: Phase-A Current Waveform for HIF on Phase-A at Node-1  
with Load-1 Switching**

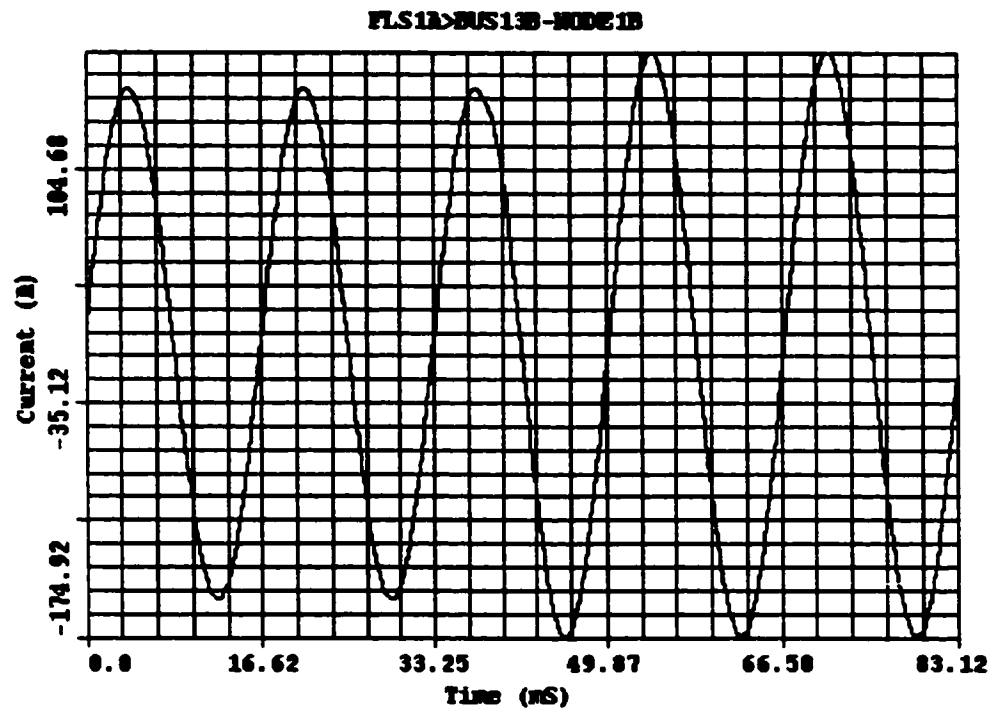


**Figure 4.12: Phase-B Current Waveform for HIF on Phase-A at Node-1  
with Load-1 Switching**

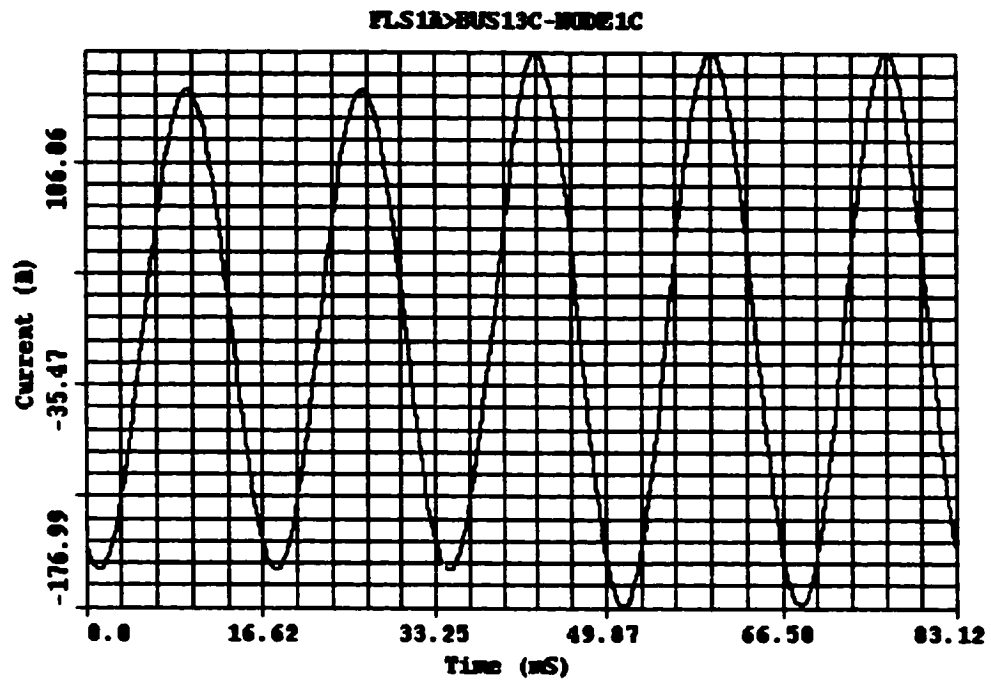


**Figure 4.13: Phase-C Current Waveform for HIF on Phase-A at Node-1  
with Load-1 Switching**

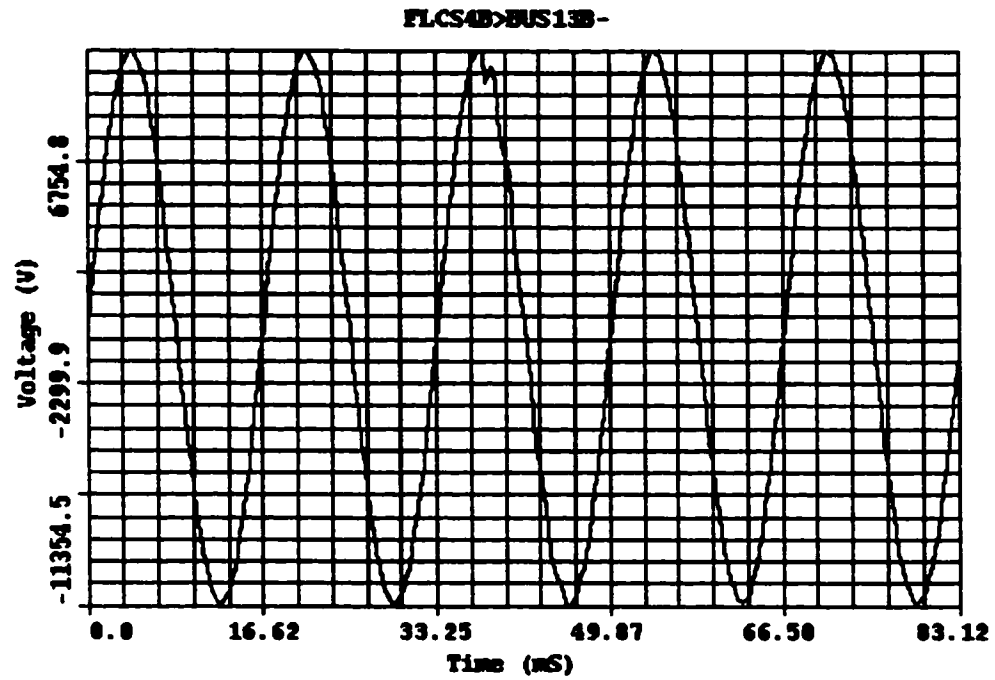


**Figure 4.14: Phase-B Voltage Waveform for HIF on Phase-B at Node-4  
with Load-4 and Capacitor C1 Switching**



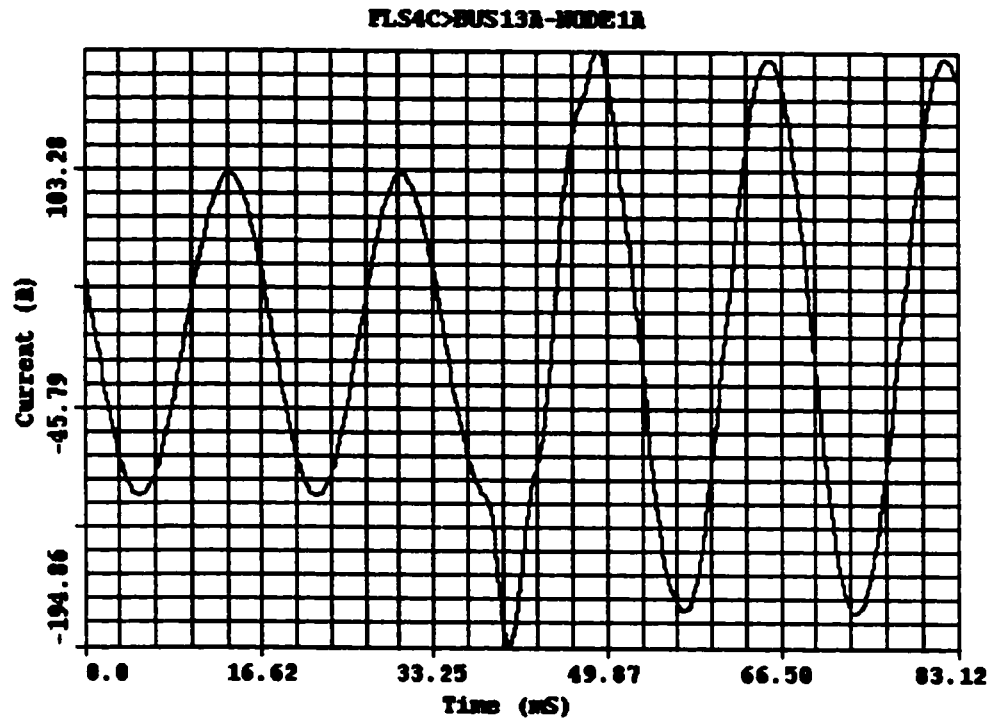


**Figure 4.15: Phase-A Current Waveform for HIF on Phase-B at Node-4  
with Load-4 and Capacitor C1 Switching**

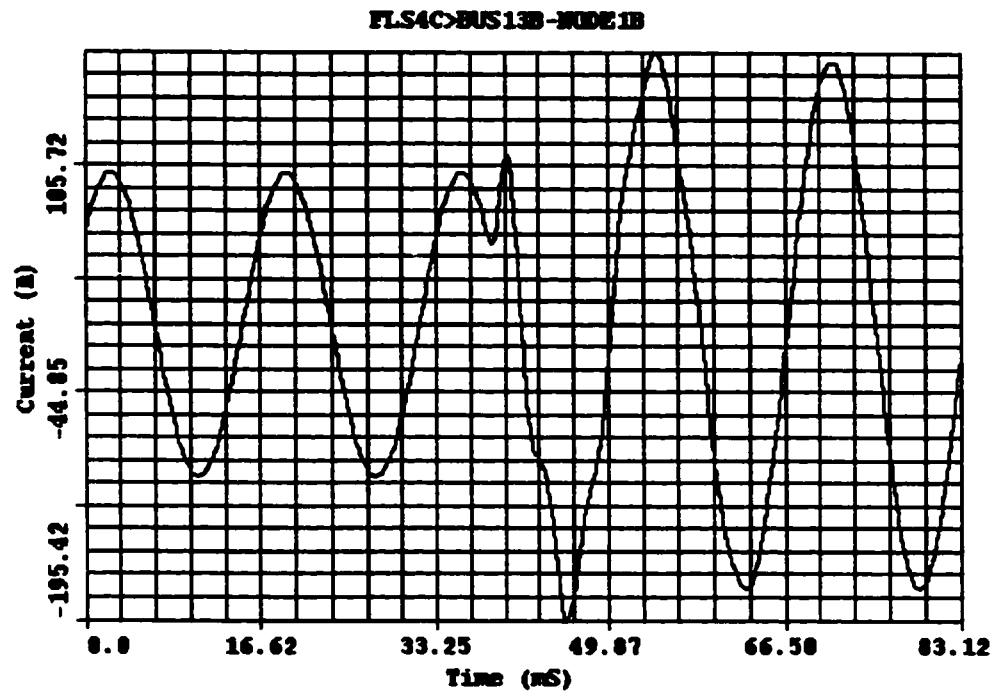


**Figure 4.16: Phase-B Current Waveform for HIF on Phase-B at Node-4  
with Load-4 and Capacitor C1 Switching**

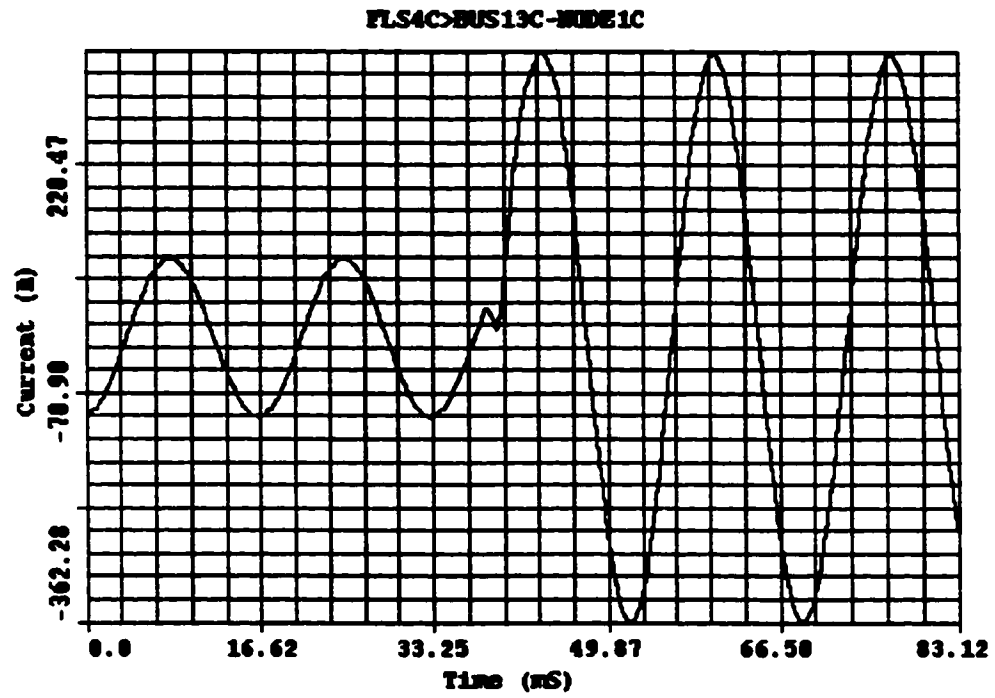


**Figure 4.17: Phase-C Current Waveform for HIF on Phase-B at Node-4  
with Load-4 and Capacitor C1 Switching**

This section discusses other fault scenarios that have been simulated to generate data for training the ANN to recognize the HIFs when different feeder parameters are used or when the ANN is used for totally new feeders. In other words, to improve the generalization of the ANN detector. The following fault scenarios are simulated:

- a. Mid-span HIFs
- b. HIF with varying fault impedance (or current)
- c. HIF with varying line impedance
- d. HIF for extended feeder
- e. HIF for lightly loaded feeder

**a. Mid-span HIFs**

In real life, HIFs most probably will result from a downed conductor, in which case the conductor may break somewhere along the span between the different branches of the distribution feeder. Therefore, several cases were generated to simulate a HIF that occurs at the middle of each of the feeder sections shown in Figure 4.1. These cases include faults between Nodes-1 and 2, Nodes-2 and 3, and Nodes-3 and 4. Figures 4.18 to 4.21 illustrate the voltage and current waveforms for a HIF on phase-A between Nodes-1 and 2. The perturbations on the current waveforms indicate that the fault has occurred at time 37.58 ms. The current magnitude has increased from 175.60  $A_{(peak)}$  to 391.36  $A_{(peak)}$  on phase-A, from 175.60  $A_{(peak)}$  to 388.25  $A_{(peak)}$  on phase-B and from 175.61  $A_{(peak)}$  to 386.85  $A_{(peak)}$  on phase-C. Waveforms for faults on other feeder sections are included in Appendix B.

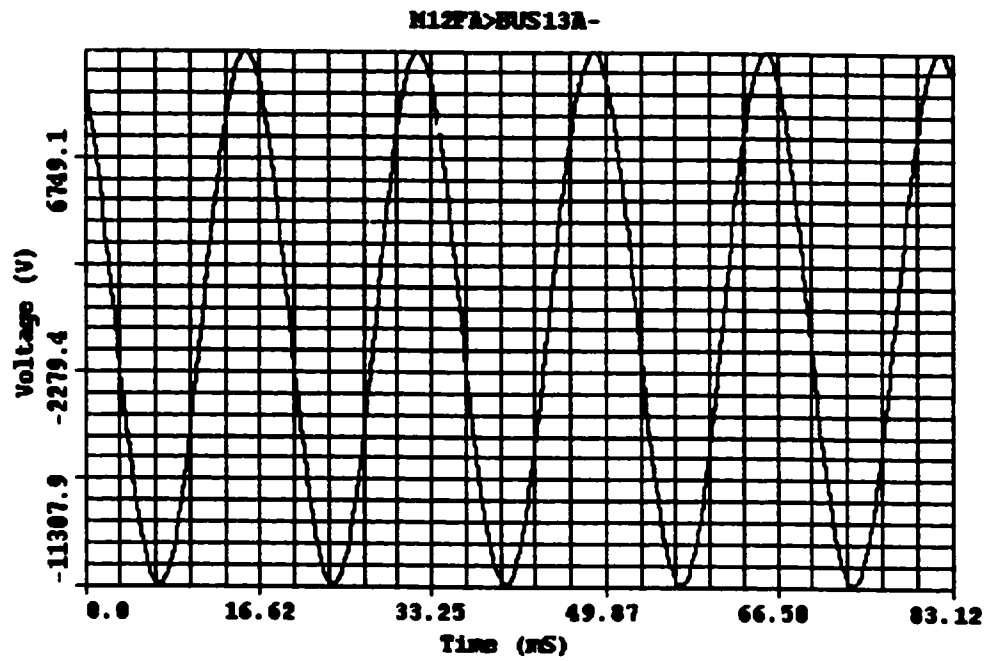


**Figure 4.18: Phase-A Voltage Waveform for HIF on Phase-A  
Between Nodes-1 and 2**

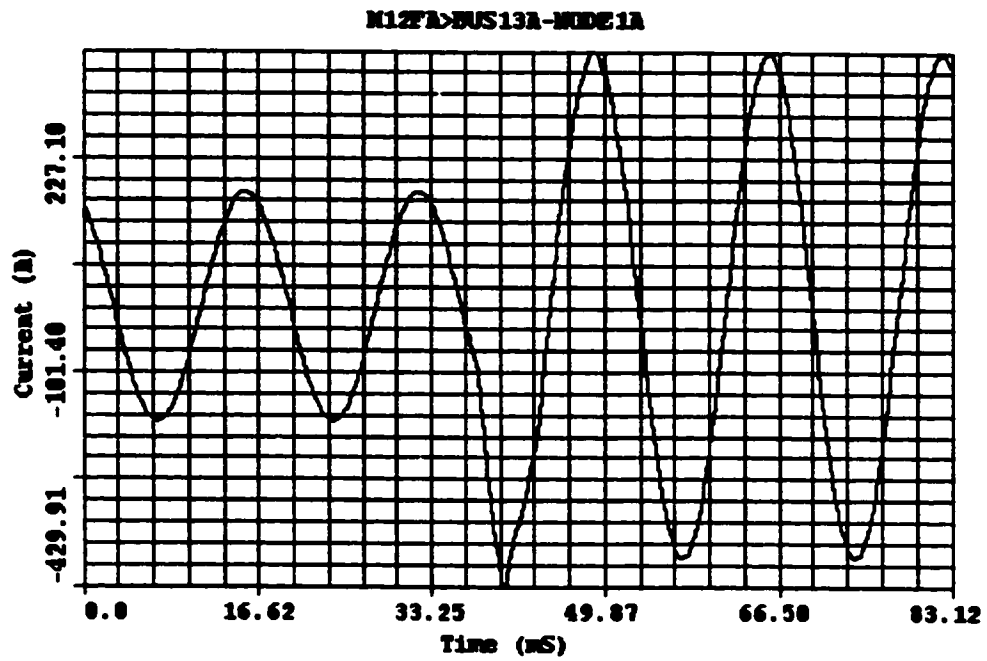


**Figure 4.19: Phase-A Current Waveform for HIF on Phase-A  
Between Nodes-1 and 2**

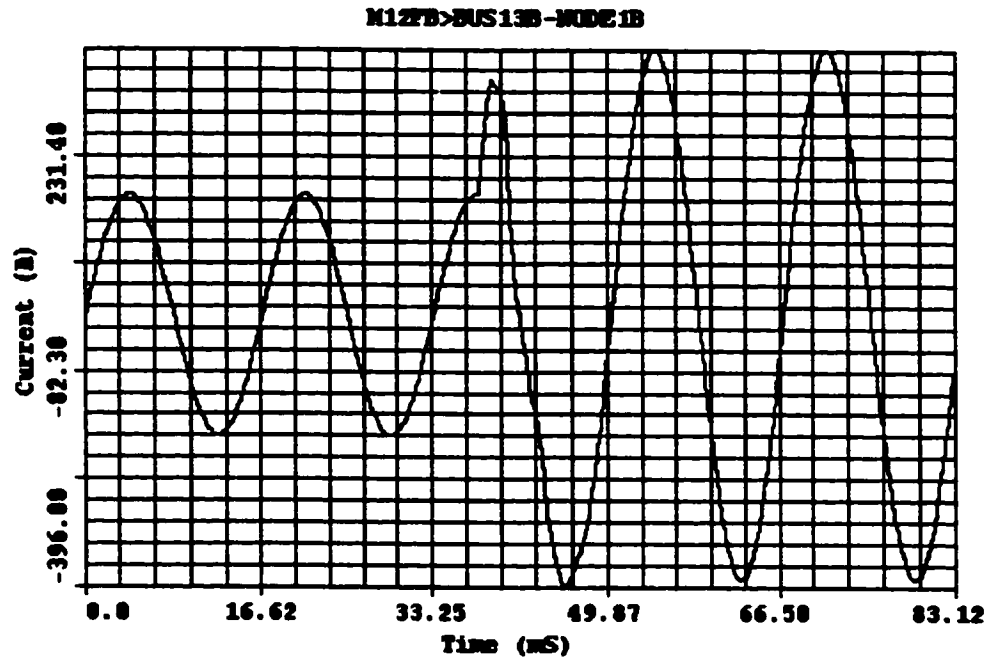


**Figure 4.20: Phase-B Current Waveform for HIF on Phase-B**

**Between Nodes-1 and 2**

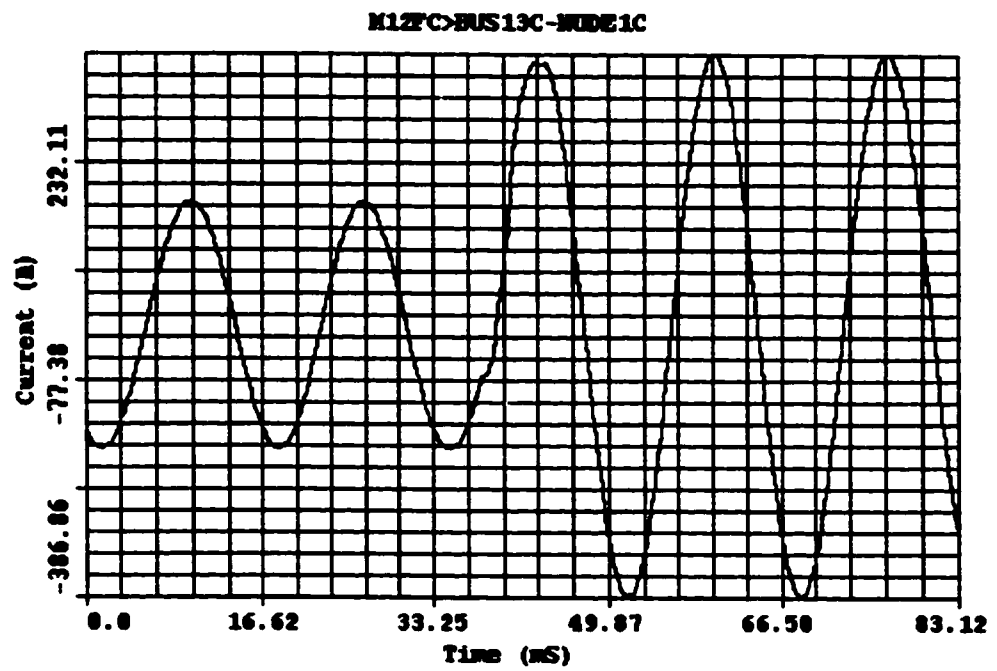


**Figure 4.21: Phase-C Current Waveform for HIF on Phase-C  
Between Nodes-1 and 2**



**b. HIF with Varying Fault Current**

Also, cases have been simulated for varying fault current or fault impedance. The fault current is varied between 50 % and 100 % of the fault current which will result in passing 120 % of the normal load current at the substation 13.8 kV bus. In addition, cases are simulated for HIFs with zero fault impedance (solidly grounded). The waveforms for such a fault at Node-1 and time 37.58 ms, are shown in Figures 4.22 and 4.23. Figures 4.24 and 4.25 show the waveforms recorded when the fault impedance passes only 70 % of the fault current to the ground. Comparison between Figure 4.23 and Figure 4.25 shows that the amount of change in the fault current is drastically reduced when the fault impedance is increased or the fault current is decreased. For the zero-fault impedance case, the current magnitude (on phase-A) has increased from 175.60 A<sub>(peak)</sub> to 1873.83 A<sub>(peak)</sub> as a result of the fault. On the other hand, the current magnitude has changed from 175.60 A<sub>(peak)</sub> to 292.55 A<sub>(peak)</sub> when the fault impedance is increased to pass only 70 % of the fault current to ground. Waveforms for other cases, including cases for 50 % fault current, are given in Appendix B.

**c. HIF with Varying Line Impedance**

The line impedance was varied between -20 % and +20 % of the impedance used for the base case. This will produce the data points required for training the proposed ANN so that it can be used with different line lengths from that of the typical feeder shown in Figure 4.1. The waveforms for HIFs on different phases, when the line impedance is reduced by 10 %, are shown in Figures 4.26 to 4.29. In this case, the current magnitude has increased from 176.90 A<sub>(peak)</sub> to 398.15 A<sub>(peak)</sub> on phase-A, from 176.91 A<sub>(peak)</sub> to

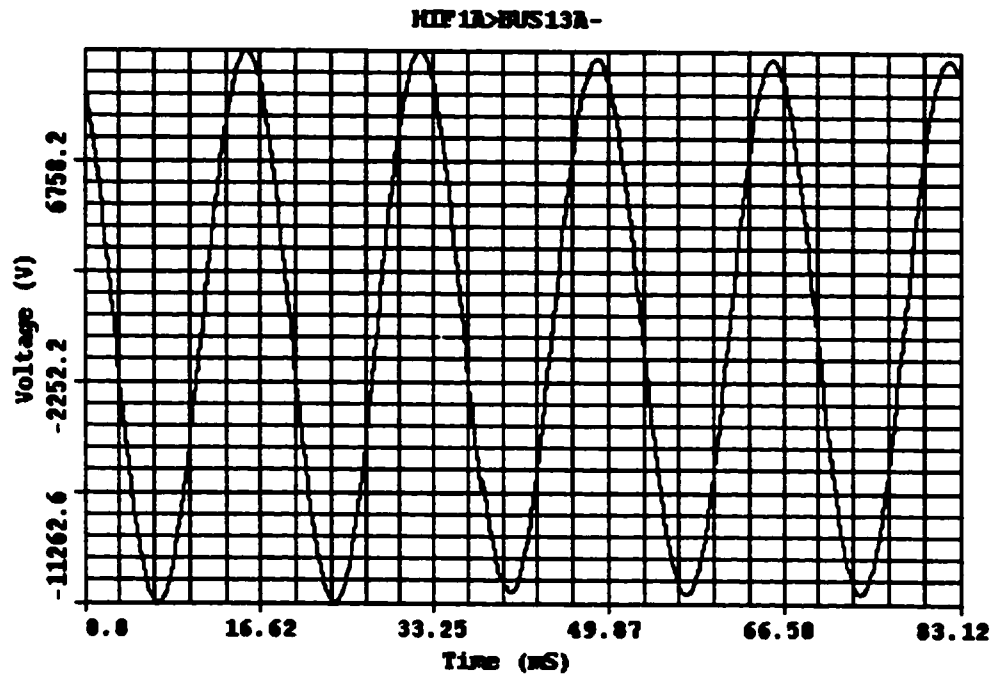


**Figure 4.22: Phase-A Voltage Waveform for HIF at Node-1  
with Zero Fault Impedance**

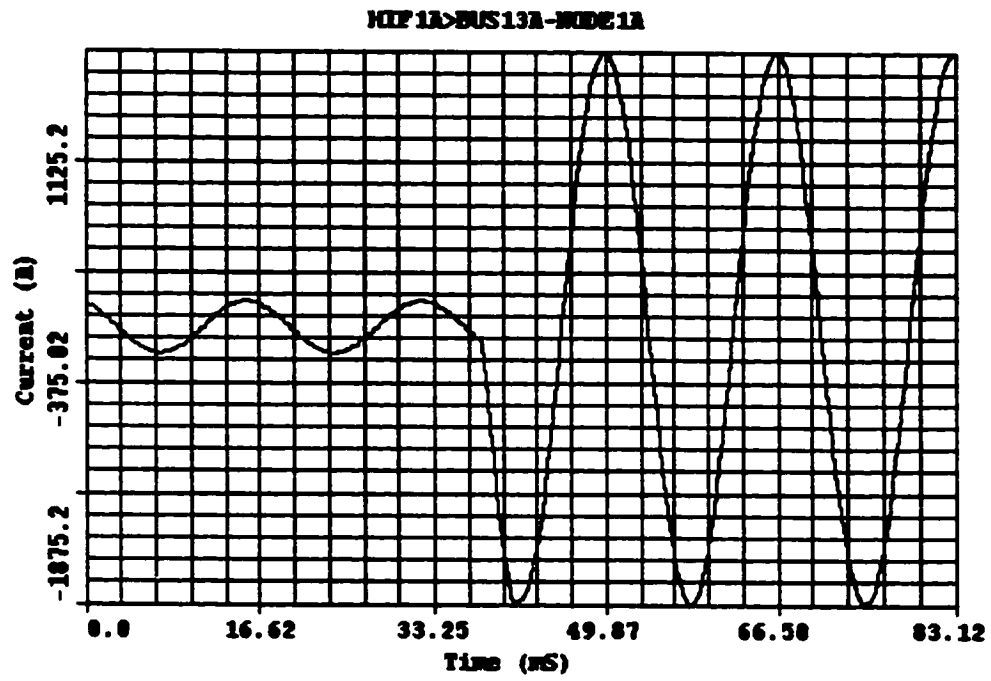


**Figure 4.23: Phase-A Current Waveform for HIF at Node-1  
with Zero Fault Impedance**

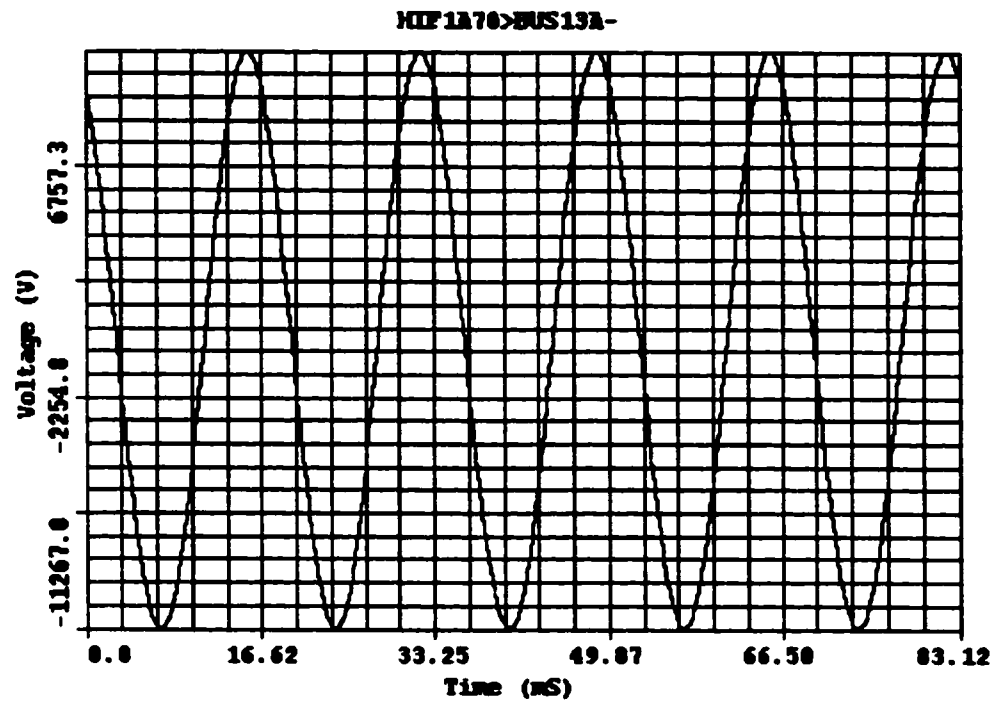


**Figure 4.24: Phase-A Voltage Waveform for HIF at Node-1  
with 70 % Fault Current**

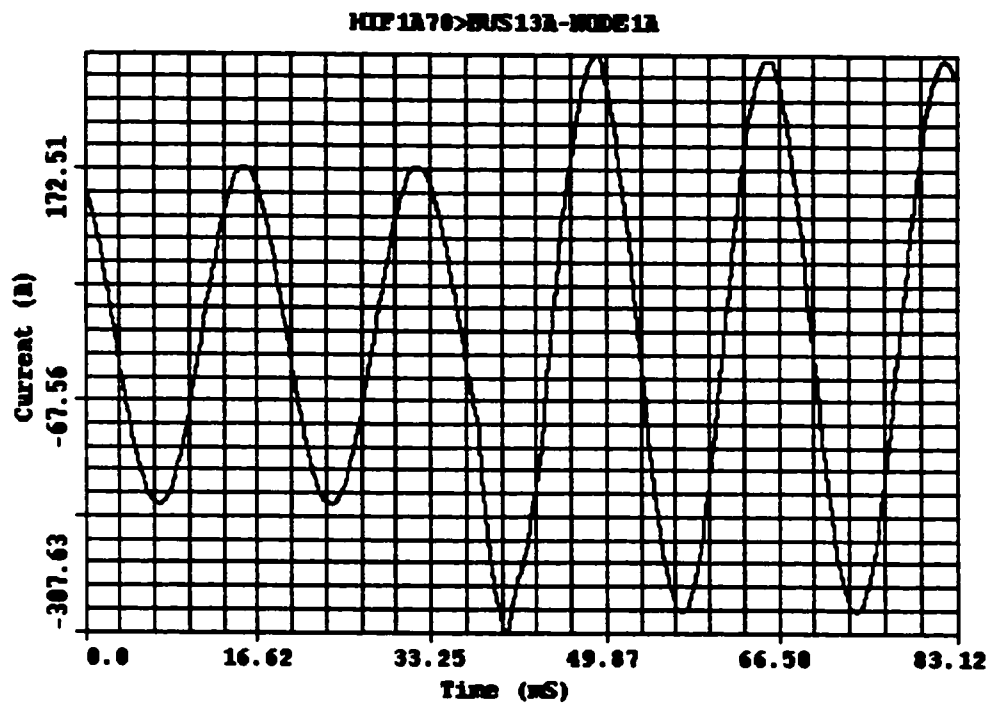


**Figure 4.25: Phase-A Current Waveform for HIF at Node-1  
with 70 % Fault Current**

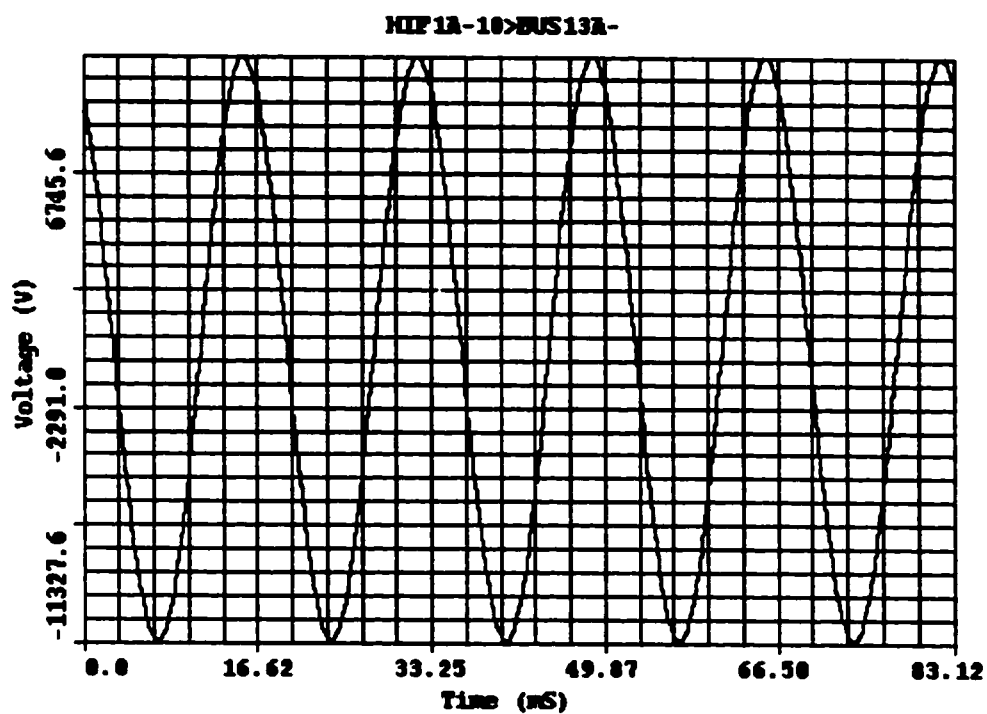


**Figure 4.26: Phase-A Voltage Waveform for HIF at Node-1 (Phase-A)  
with Line Impedance Reduced by 10 %**

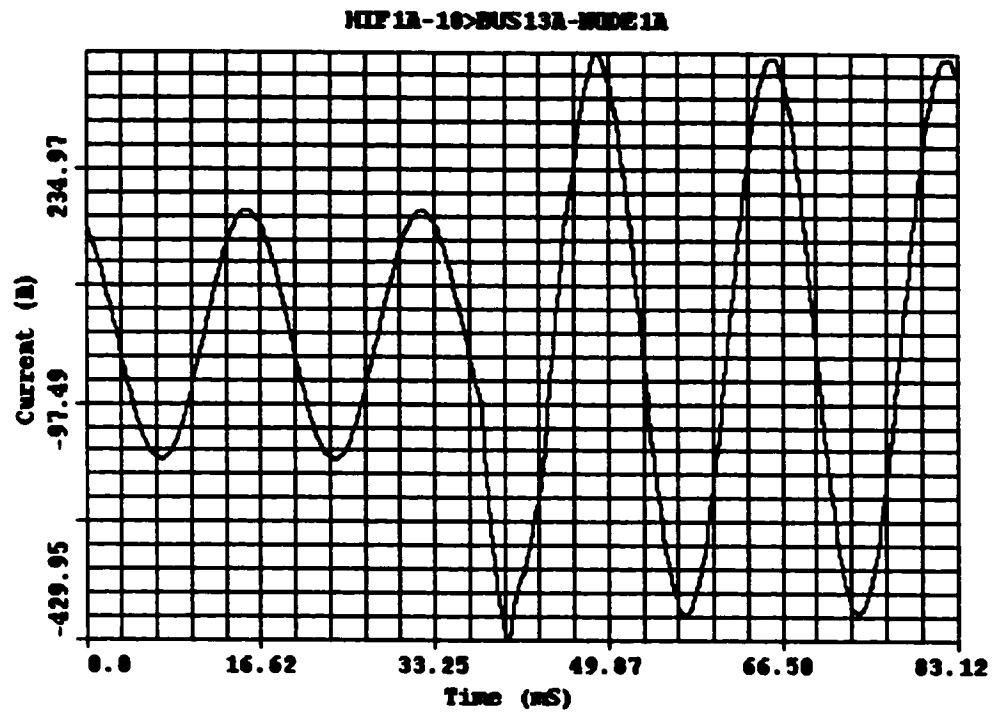


**Figure 4.27: Phase-A Current Waveform for HIF at Node-1 (Phase-A)  
with Line Impedance Reduced by 10 %**

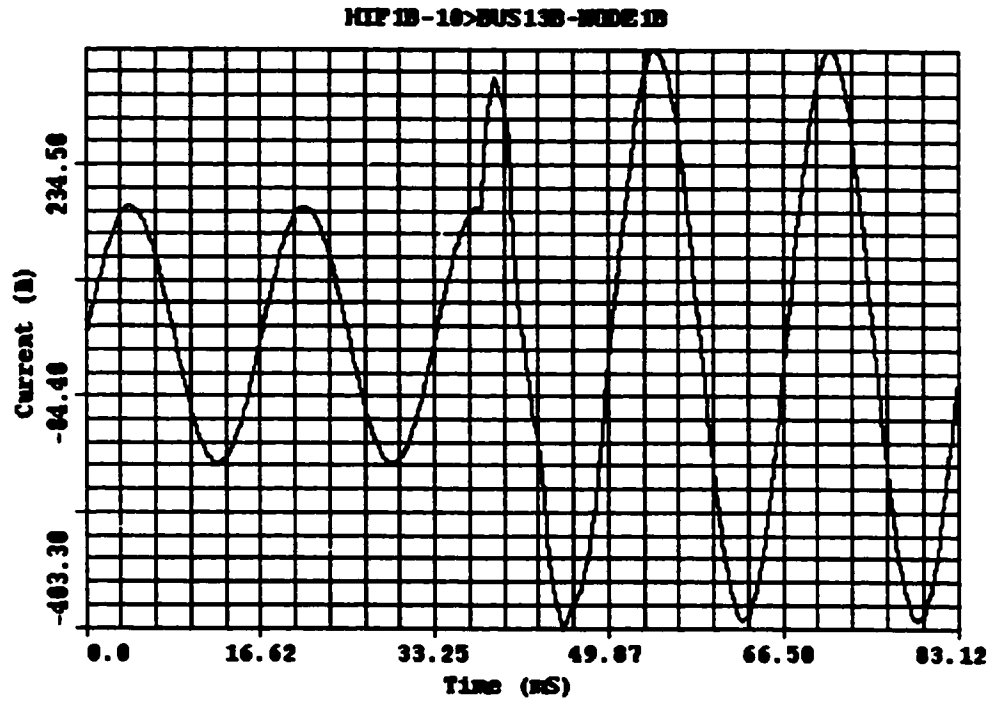


**Figure 4.28: Phase-B Current Waveform for HIF at Node-1 (Phase-B)  
with Line Impedance Reduced by 10 %**



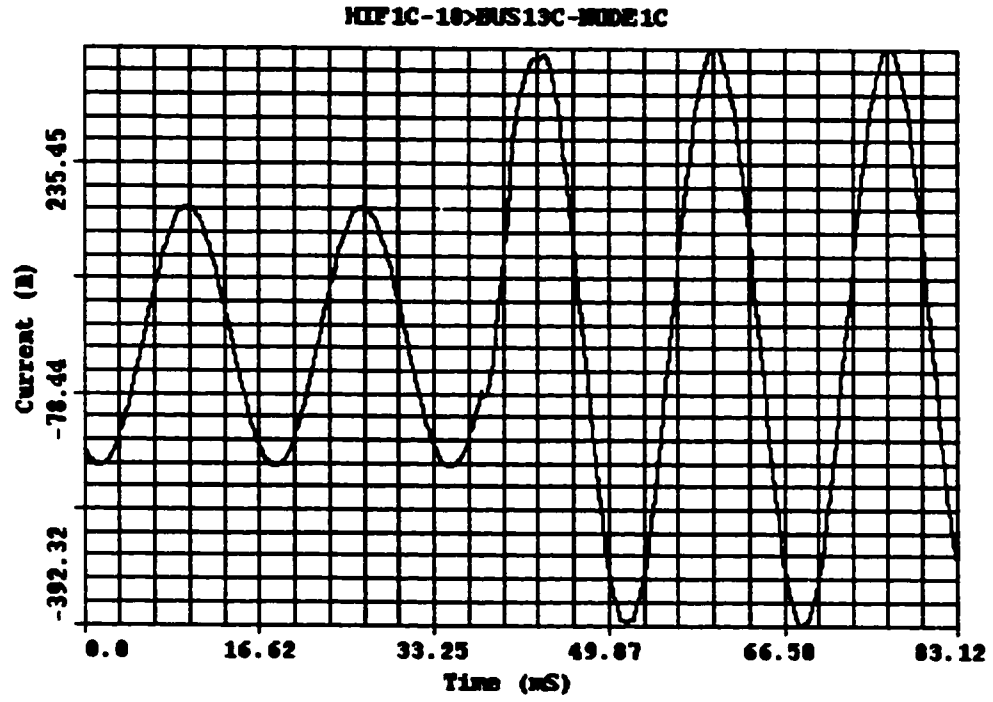


**Figure 4.29: Phase-C Current Waveform for HIF at Node-1 (Phase-C)  
with Line Impedance Reduced by 10 %**

391.21  $A_{(peak)}$  on phase-B and from 176.90  $A_{(peak)}$  to 393.97  $A_{(peak)}$  on phase-C. Waveforms for HIFs with a 20 % increase in line impedance are illustrated in Appendix B.

#### **d. HIF for Extended Feeder**

Cases have also been generated for a totally different feeder arrangement. A new branch is added at the end of the typical feeder shown in Figure 4.1. These cases are simulated to test the generalization or robustness of the proposed ANN design to recognize HIFs on different feeders for which the ANN is not trained. Figures 4.30 and 4.31 show the voltage and current waveforms for a phase-A HIF at Node-1 at 37.58 ms. The waveforms have the same pattern as of the original feeder design with the exception of some changes in the current and voltage magnitudes. For instance, the current magnitude has changed from 175.43  $A_{(peak)}$  to 398.87  $A_{(peak)}$ . Some other waveforms for HIFs with extended feeder are also included in Appendix B.

#### **e. HIF for Lightly Loaded Feeder**

In addition to simulating feeders of different lengths and configurations, cases were also simulated to cover feeder operation when it is lightly loaded. Different scenarios of load and capacitor switching have been simulated. For instance, Figures 4.32 to 4.35 illustrate the voltage and current waveforms for HIFs at Node-1 with transformer T3 and capacitor C2 disconnected at 37.58 ms. For these cases the current magnitude has changed from 153.61  $A_{(peak)}$  to 361.53  $A_{(peak)}$  on phase-A, from 153.62  $A_{(peak)}$  to 366.94  $A_{(peak)}$  on phase-B and from 153.64  $A_{(peak)}$  to 365.87  $A_{(peak)}$  on phase-C. Appendix B also shows

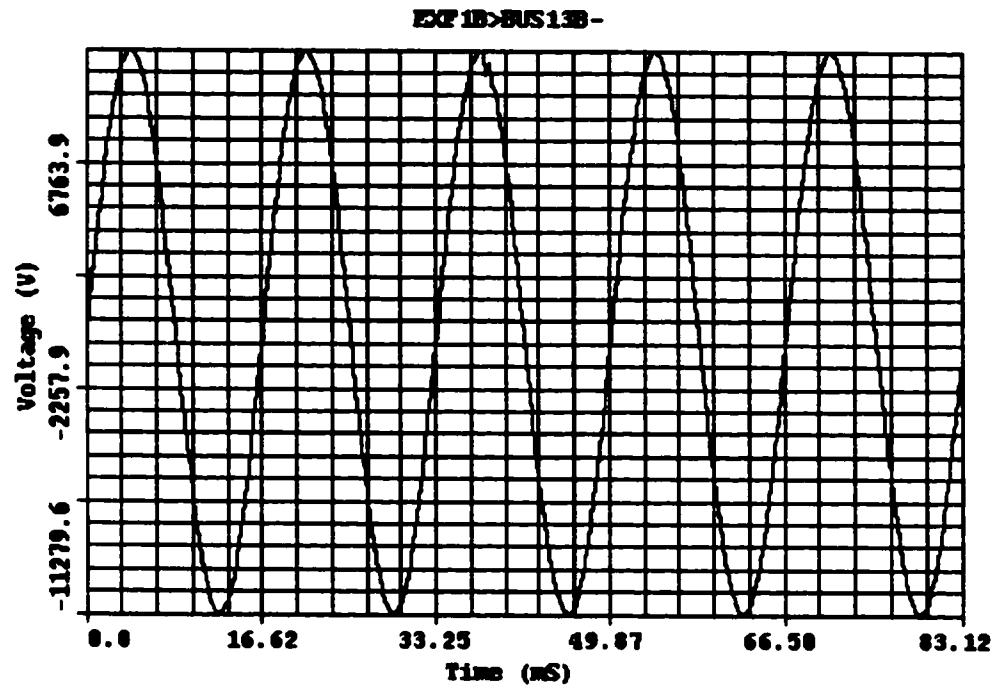


**Figure 4.30: Phase-B Voltage Waveform for HIF on Phase-A at Node-1  
with Extended Feeder**

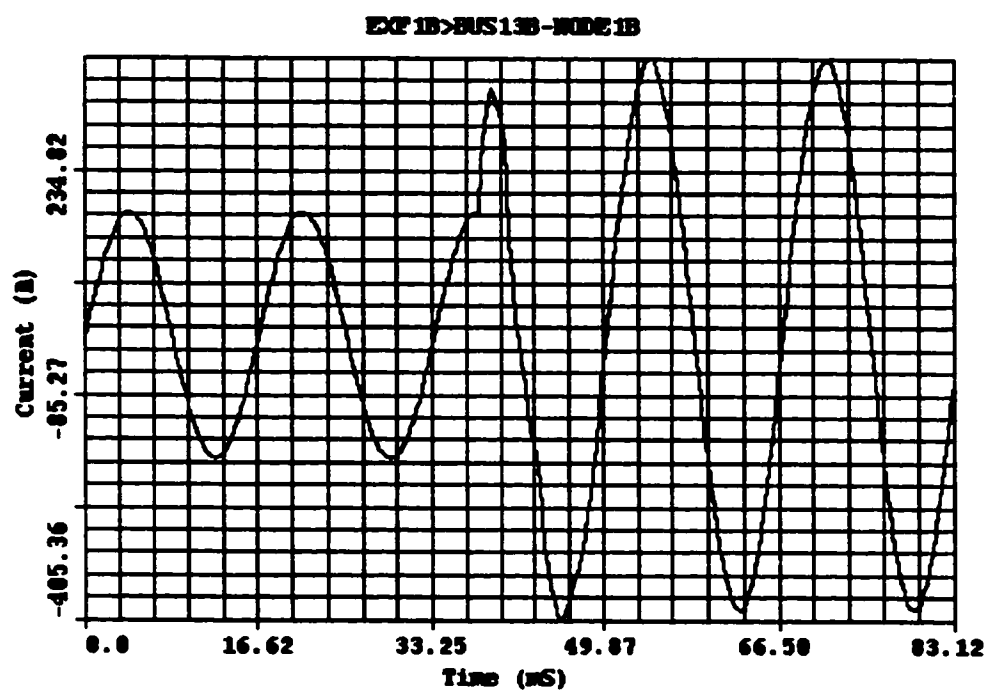


**Figure 4.31: Phase-B Current Waveform for HIF on Phase-A at Node-1  
with Extended Feeder**

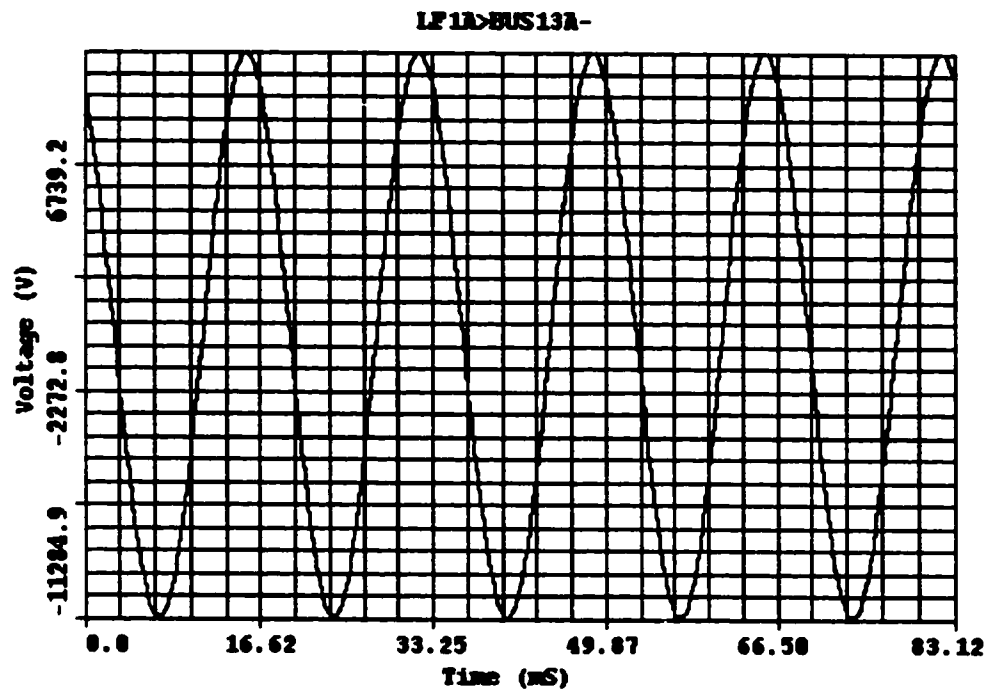


**Figure 4.32: Phase-A Voltage Waveform for HIF on Phase-A at Node-1  
with T3 and C2 Disconnected**

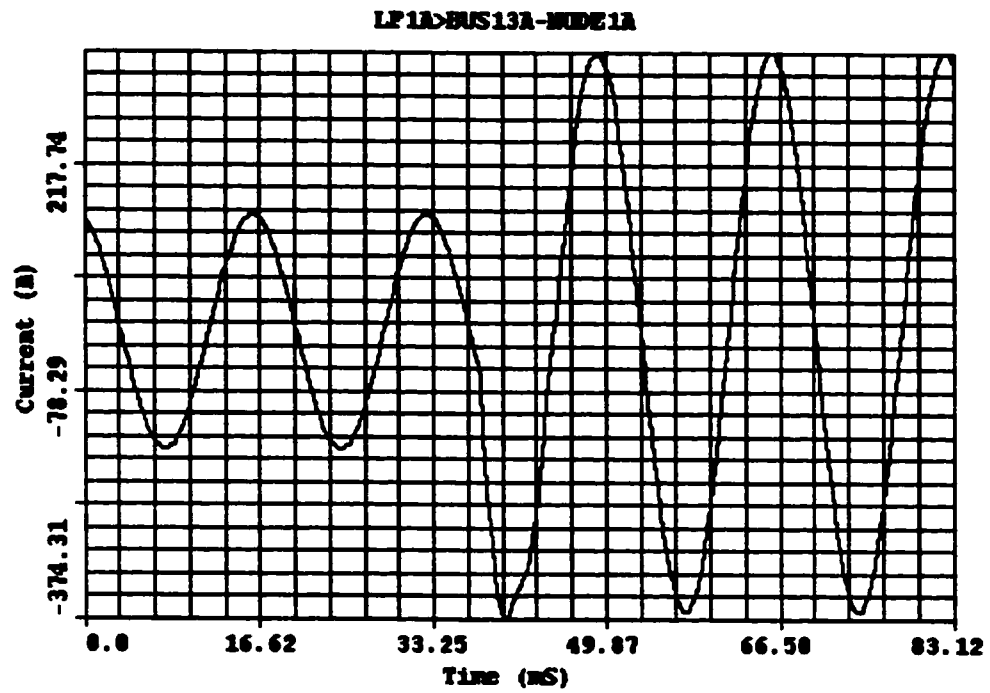


**Figure 4.33: Phase-A Current Waveform for HIF on Phase-A at Node-1  
with T3 and C2 Disconnected**

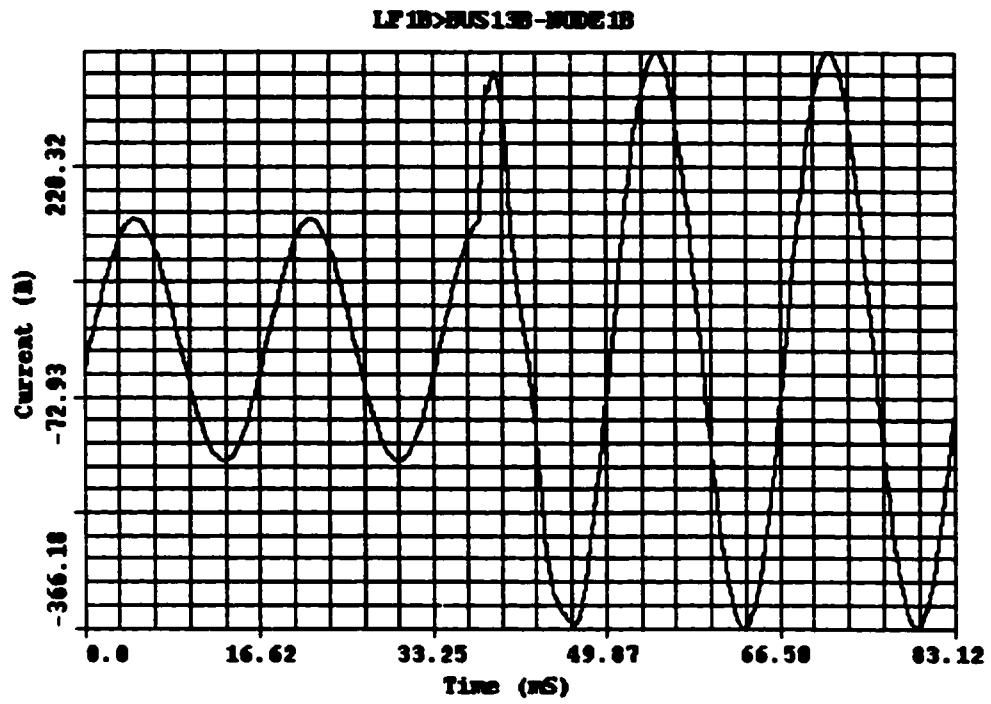


**Figure 4.34: Phase-B Current Waveform for HIF on Phase-B at Node-1  
with T3 and C2 Disconnected**

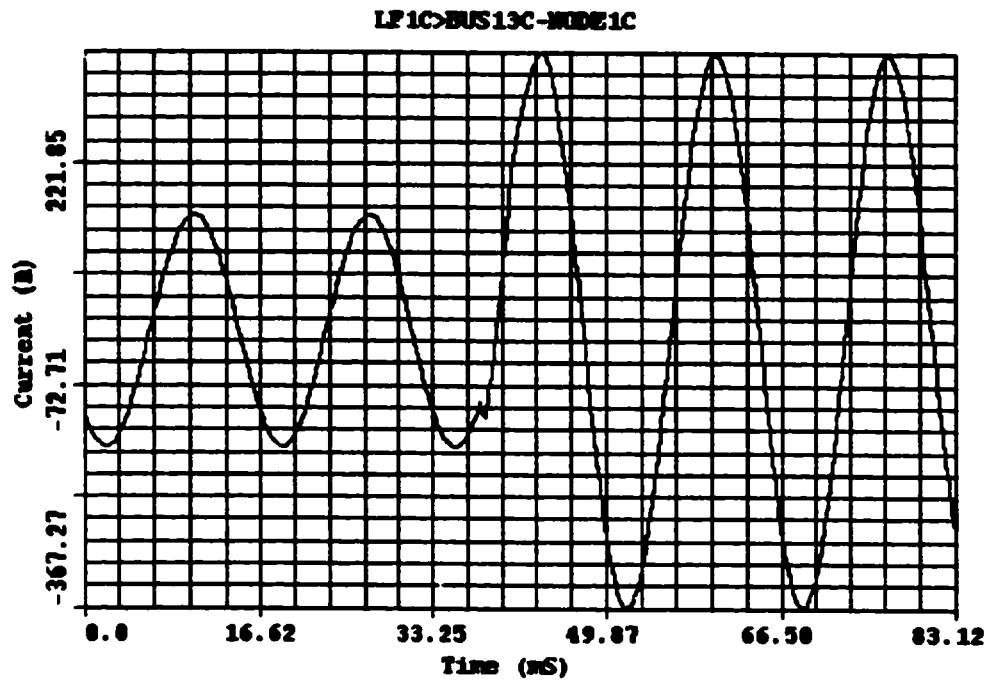


**Figure 4.35: Phase-C Current Waveform for HIF on Phase-C at Node-1  
with T3 and C2 Disconnected**



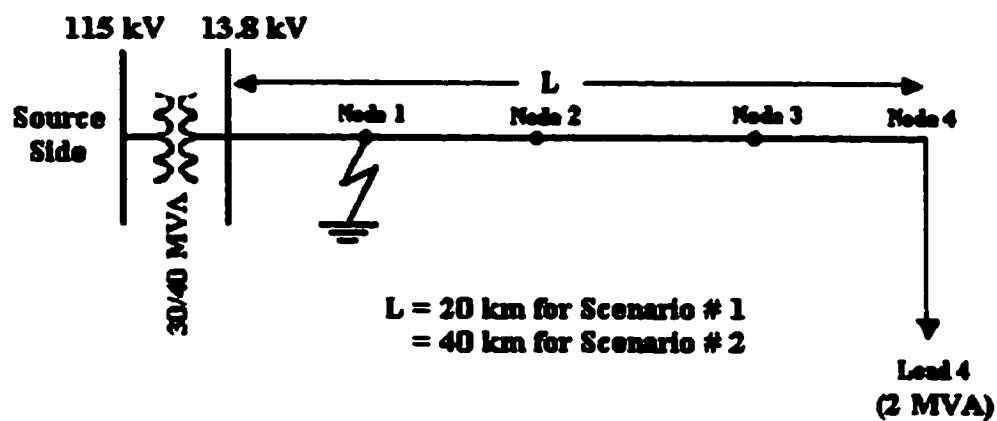
waveforms for HIFs at Node-1 with transformer T2 and capacitor C1 disconnected at 37.58 ms.

### **4.3.3 Additional EMTP Cases for ANN Validation**

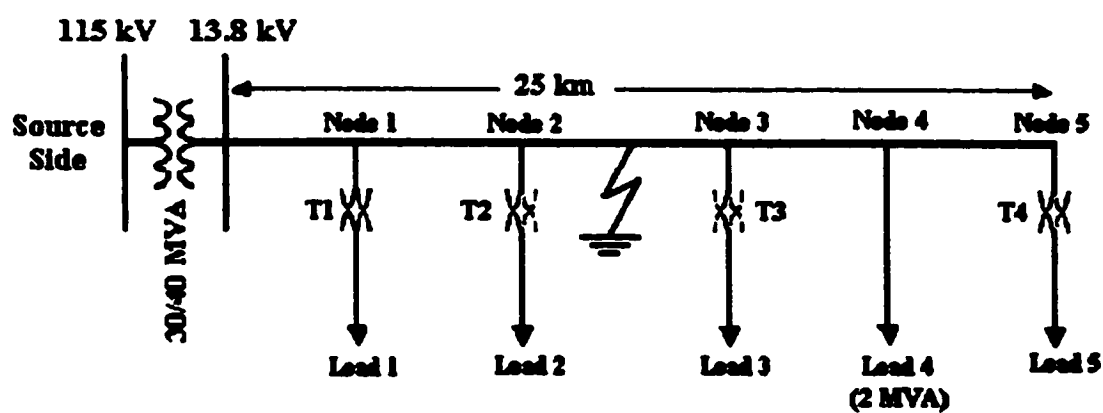
In addition to the EMTP cases that were simulated to cover the various feeder operations and fault scenarios, nine more EMTP cases were also generated to further validate the performance of the proposed ANN designs. These cases are as follows:

- Scenario # 1: three cases for single line HIF on each of the three phases at Node-1, with all the distribution transformers (T1, T2 and T3) and capacitor banks (C1 and C2) disconnected. That means the only load on the feeder is the 2 MVA industrial load connected at Node-4 of the feeder shown in Figure 4.1.
- Scenario # 2: three cases similar to the cases above but with the line impedance of the feeder doubled. In other words, the feeder length is doubled from 20 km to 40 km.
- Scenario # 3: three cases for Mid-span HIFs on each phase between Nodes-2 and 3. The fault impedance is increased so that only 5 % of the fault current passes to ground. Also, an additional node is connected at the end of the feeder and both capacitor C1 and capacitor C2 are disconnected.

Figure 4.36 show the single line diagram of the feeder for the simulation of these scenarios.



(A) For Scenarios # 1 and 2



T1, T2, T3, T4: 500 kVA, 13.8/220-127 Transformers

(B) For Scenario # 3

**Figure 4.36: Single Line Diagrams for Simulation of the Additional Validation Cases**

These cases represent feeder configurations and fault scenarios that are completely different from the types of fault events and scenarios discussed in the previous sections of this chapter. These cases will be used to validate the proposed ANN designs and check their robustness and performance.

#### **4.3.4 General Observations on the Waveforms**

Analysis of the waveforms presented above and those in Appendix B reveals that the most apparent effect on the voltage waveforms for the various cases simulated is the marginal change in voltage magnitude. This is due to the use of high impedance values for the simulation of all the HIF cases. The current waveforms, however, are quite different for each of the simulated cases depending on the event type. Transients are always present whenever capacitor switching is involved. The amount of the transients as well as the time it takes to extinguish these transients are varying for each case.

### **4.4 Data Preprocessing**

One of the critical elements that have to be properly selected for ANN training is the data set that will be used as inputs and outputs to the ANN during the learning phase. To examine the different possible input-output data sets, the proposed ANN has been trained with preprocessed training sets as well as training sets without preprocessing.

For training without preprocessing, each case is represented by 1800-point vector, which is the combination of the voltage and current waveform samples for the three phases, i.e. each phase is represented by 300 data points.

On the other hand, for the rest of the training cases, each case is represented by a preprocessed 600-point vector, i.e. each phase of the voltage and current waveforms is represented by 100 data points. To achieve this, the input data is preprocessed by applying the Fast Fourier Transform (FFT) to the training data set prior to using the data for training the ANN. For some of the cases the 600-point FFT is used, and for the other cases the FFT is applied first, then only the highest 100 frequency components are selected to represent each phase of the voltage and current waveforms.

The next chapter discusses in details the different data sets and ANN designs that have been investigated for this work with comparison of the accuracy achieved with each design.

## **Chapter 5**

# **ARTIFICIAL NEURAL NETWORK DESIGN AND TESTING**

Having generated the data required for training and testing the proposed ANN, this chapter discusses the various designs that have been investigated in this thesis. The objective of the ANN is to diagnose HIFs and distinguish them from normal system operation events, such as load switching. The input to the ANN consists of the voltage and current waveforms as measured at the 13.8 kV substation bus by potential and current transformers. The output of the ANN has four targets, namely

- Target # 1: Fault Detection
- Target # 2: Fault Location
- Target # 3: Event Type
- Target # 4: Faulty Phase

## **5.1 Overview**

ANN can be either of two classes, supervised networks or unsupervised networks. However, most of the ANN implementations for fault detection are based on the multi-layer feed-forward ANN, which belongs to the supervised network class. The latter class ANN with backpropagation learning algorithm is used for this work.

The “Neural Network Toolbox for MATLAB®” [27] is utilized to develop the ANN that will be used to diagnose HIF events.

Generally, there are five steps that have to be followed for designing an ANN to do a specific task. These steps are:

1. Select the ANN architecture or topology that is most appropriate for the required application.
2. Define the training data set (inputs and outputs) that represents the cases that the ANN has to learn.
3. Select the training algorithm and train the ANN.
4. Test the ANN using a set of test data until the ANN performance is satisfactory.
5. Check the robustness or generalization capabilities of the ANN by presenting to it a set of input data that is totally different from that used to train the ANN.

It shall be emphasized here that there are no guidelines for the selection of ANN architecture. It all depends on the experience of the user and trial and error approach. However, the more complex the ANN the longer the time required for its training, and the higher is the probability of error divergence.

For this work, the ANN consists of a four-layer feedforward network architecture with Tan-sigmoid (TANSIG) transfer functions. The best topology has been obtained with 35 neurons in the first hidden layer, 20 neurons in the second hidden layer, 30 neurons in the third hidden layer, and 4 neurons in the output layer. It shall be noted that most researchers count the input layer separately. Some of them, however, do not count it separately, in which case the proposed ANN is described as a five-layer network. The best topology has been reached after many trials with different combinations of number of hidden layers and the number of neurons in each layer.

A hundred and twenty (120) EMTP cases have been simulated to generate the data sets required for training and testing the ANN. Different combinations of training and testing sets are tried for the various ANN designs that will be detailed later in this chapter. Each design uses different sets of the EMTP cases for training and testing the ANN.

The ANN output set consists of four targets. The first target is for fault detection. It can have either of two values: zero (0) to indicate no fault and one (1) to indicate the presence of a fault. The second target is for locating the faulty section of the feeder. It can have one

out of five possible values: zero (0) for no fault, one (1) for a HIF at Node-1, two (2) for a HIF at Node-2 , three (3) for a HIF at Node-3 , and four (4) for a HIF at Node-4. The third target (event type) is used to distinguish HIFs from other similar events. Again this target may have any of the following five values: zero (0) for normal load switching, one (1) for normal load and capacitor switching, two (2) for a HIF with no load or capacitor switching, three (3) for a HIF with load switching, and four (4) for a HIF with load and capacitor switching. The last target (target # 4) is used to indicate the faulty phase. It can take one of four values: zero (0) for no fault, one (1) for a HIF on phase-A, two (2) for a HIF on phase-B, and three (3) for a HIF on phase-C. Table 5.1 presents a summary of the ANN targets.

For some of the ANN designs, binary output set consisting of 6 bits is used for ANN training. It was necessary to use 6 binary bits (instead of four decimal targets) to cover all possible output combinations, which are 38 for the problem under consideration.

Training data selection is very critical to the success of the ANN. If important data inputs are missing, the ANN performance may not meet the required accuracy. As will be discussed later, training of the ANN has been performed without preprocessing the data as well as after the data is preprocessed using the Fast Fourier Transform (FFT). But for all cases the input and output data sets are normalized (or scaled) to values in the range  $[-1,1]$  to improve the ANN performance and reduce the time needed for error convergence. This is achieved through the MATLAB function `PREMNMX`.



**Table 5.1: Summary of the ANN Targets**

<b>Target</b>	<b>Possible Values of the Targets (Decimal Output)</b>
<b>Target # 1 (Fault Detection)</b>	0: No fault
	1: Fault
<b>Target # 2 (Fault Location)</b>	0: No fault
	1: HIF at Node-1
	2: HIF at Node-2
	3: HIF at Node-3
	4: HIF at Node-4
<b>Target # 3 (Event Type)</b>	0: Normal load switching
	1: Normal load and capacitor switching
	2: HIF with no load or capacitor switching
	3: HIF with load switching
	4: HIF with load and capacitor switching
<b>Target # 4 (Faulty Phase)</b>	0: No fault
	1: HIF on phase-A
	2: HIF on phase-B
	3: HIF on phase-C

**Many training algorithms have been tried including the following:**

- **The reduced memory Levenberg-Marquardt Algorithm**
- **Resilient backpropagation Algorithm**
- **Quasi-Newton Algorithm**
- **One step secant Algorithm**

However, the best performance is achieved with the improved faster versions of backpropagation, namely the scaled conjugate gradient (TRAINSCG) and the Fletcher-Reeves conjugate gradient (TRAINCGF) algorithms. These algorithms can converge from 10 to 100 times faster than the standard backpropagation algorithm [27]. The former algorithm has been used for all the ANN designs described later in this chapter. For all the ANN designs the performance goal is set to be  $1 \times 10^{-5}$ .

A summary of the salient features that are common to the ANN designs is presented in Table 5.2. The ANN designs are different in terms of the number of cases used for training, testing and checking the generalization of the ANN. They also differ in the number of data points used in the input cases, as some of the designs use preprocessed training sets. In addition, some of the designs have been trained and tested for binary output.

**Table 5.2: Common Salient Features of the ANN Designs**

Architecture (Topology)	Feedforward ANN
Number of Layers	4
Transfer Function for all Layers	Tan-sigmoid (TANSIG)
Number of Neurons in Hidden Layer # 1	35
Number of Neurons in Hidden Layer # 2	20
Number of Neurons in Hidden Layer # 3	30
Number of Neurons in Output Layer	4 (for decimal output) 6 (for binary output)
Training Algorithm	Scaled Conjugate Gradient (TRAINSCG)
Performance Goal	$1 \times 10^{-5}$
Number of Input Data Points in Each Input Vector (for Each Case)	1800 (without preprocessing) 600 (after preprocessing)
Possible Values for Target # 1 (Fault Detection)	0, 1
Possible Values for Target # 2 (Fault Location)	0, 1, 2, 3, 4
Possible Values for Target # 3 (Event Type)	0, 1, 2, 3, 4
Possible Values for Target # 4 (Faulty Phase)	0, 1, 2, 3

## **5.2 Description of ANN Design # 1**

As mentioned earlier, an ANN design is only as good as the input data used to train it. Therefore, selection of the appropriate set of the input data and the corresponding desired output data (targets) is one of the most important factors that contribute to the success or failure of any ANN design. For Design # 1, thirty nine (39) cases (out of the 120 EMTP cases) have been used for training the ANN, 13 cases have been used for testing the ANN accuracy, and 48 cases have been used for checking the ANN generalization. These training and testing cases have been selected to represent the various HIF and HIF-like events, including normal load switching, normal load and capacitor switching, HIF without switching, HIF with load switching, and HIF with load and capacitor switching. The cases used to check the generalization represent HIF scenarios that are totally different from the cases used for training and testing the ANN. These scenarios include mid-span HIF cases, HIFs with varying fault impedance (or fault current), HIFs for lightly loaded feeder, and HIFs for extended feeder. The lightly loaded feeder cases and the extended feeder cases virtually represent totally different feeders from the typical feeder illustrated in Figure 4.1, which is used for generating the training data set.

The above mentioned work has been performed twice. Firstly, with each case represented by 1800-point vector, which is the combination of the voltage and current waveform samples for the three phases, i.e. each phase is represented by 300 data points. And secondly, with each case represented by a preprocessed 600-point vector, i.e. each phase

of the voltage and current waveforms is represented by 100 data points. The 600-point FFT has been used for data preprocessing.

To simplify the description, the 1800-point input cases will be referred to as **full data** cases, and the 600-point input cases will be called **reduced data** cases, throughout the subsequent text.

The full data design (Design D1F) took 414 epochs for the error to converge as can be seen from Figure 5.1. However, the reduced data design (Design D1R) reached the performance goal in 335 epochs, which is faster than the full data design. This is illustrated in Figure 5.2. It shall be noted that faster convergence does not necessarily imply better accuracy. This will be discussed in section 5.5 where the test results of the ANN designs are presented.

### **5.3 Description of ANN Design # 2**

Design # 2 uses 66 cases (out of the 120 EMTP cases) for training the ANN, 22 cases for testing the ANN and 24 cases for validating the generalization capabilities of this design. Cases used for training and testing the ANN include those used in Design # 1 in addition to cases for mid-span HIFs, HIFs with varying fault impedance, and HIFs with varying transmission line impedance. These cases are added to the training set to improve the ANN performance with respect to the fault scenarios covered by these additional cases,

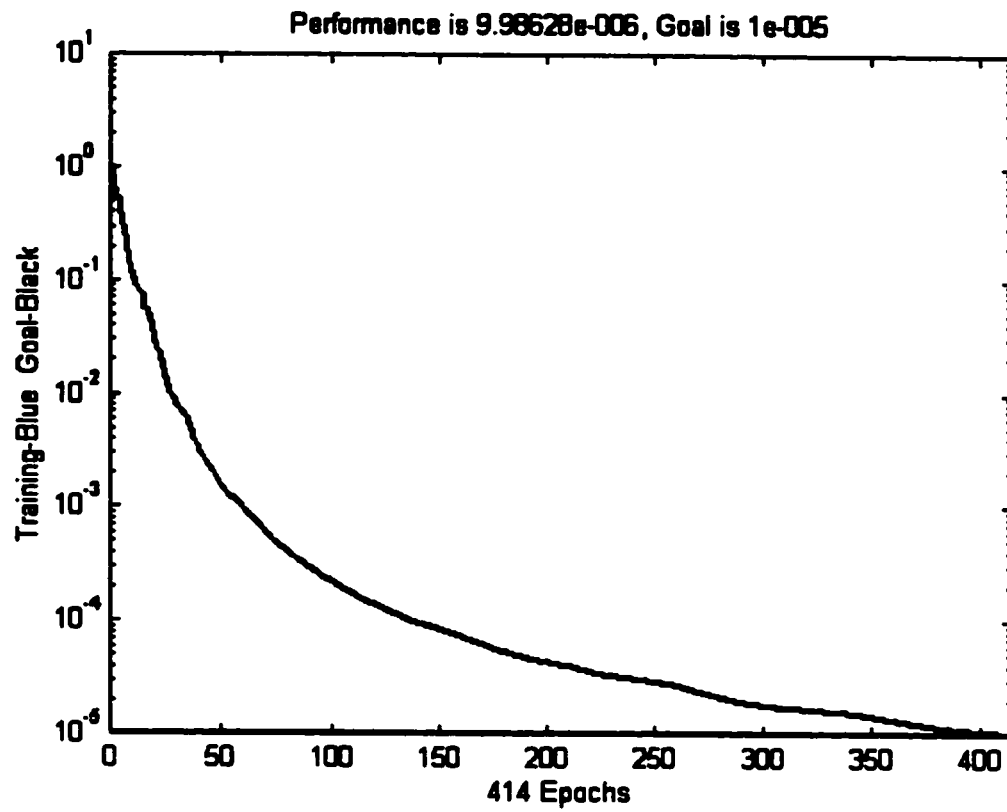


**Figure 5.1: Error Convergence for ANN Design D1F**

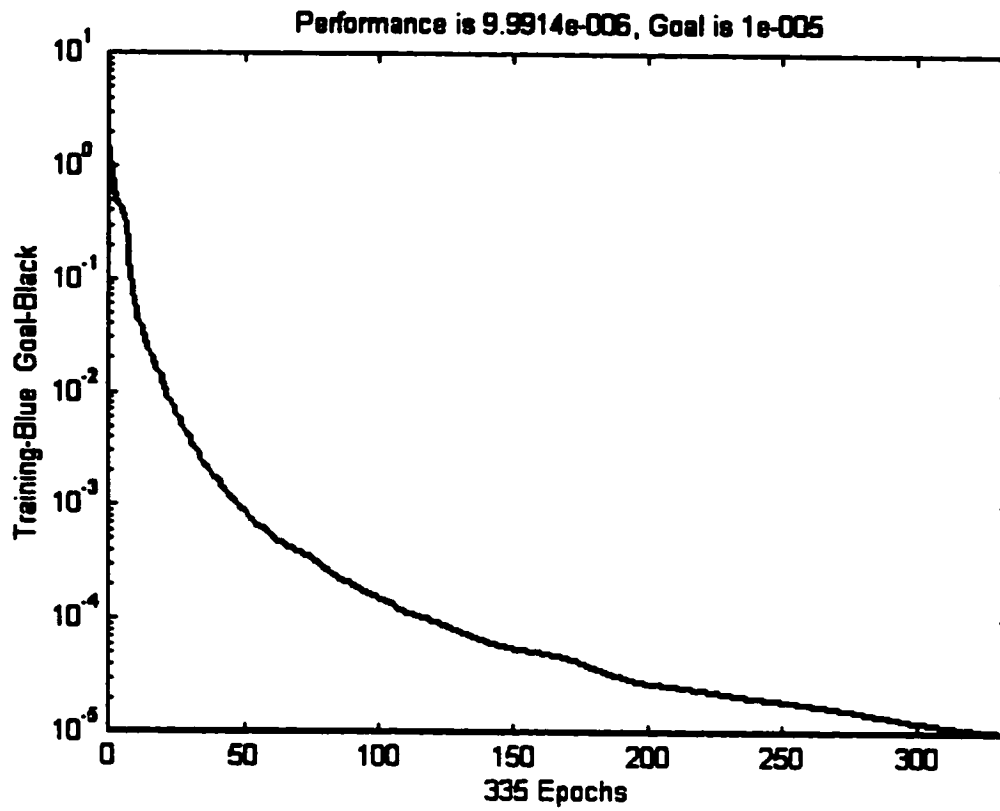


**Figure 5.2: Error Convergence for ANN Design D1R**

which have not been used for training the ANN in Design # 1. The generalization check cases include cases for extended feeder as well as cases for lightly loaded feeder.

There are three versions of Design # 2. The first version is for training and testing the ANN with full data (Design D2F). In the second version, the training and testing is performed with reduced data (Design D2R). For both of these versions, the target vector consists of four decimal digits to represent the various combinations of Targets # 1 to 4. However, the third version of this design is performed with reduced input and binary target vector consisting of six bits, which are the minimum bits needed to cover all the 38 possible combinations of Targets # 1 to 4. This version will be referred to as 'Design D2B' in the subsequent discussion.

Design D2F took 2872 epochs for the error to converge as can be seen from Figure 5.3. On the other hand, design D2R reached the performance goal in 844 epochs, and design D2B converged in 404 epochs. These are illustrated in Figures 5.4 and 5.5, respectively. Again, this shows that the reduced input designs converge faster than the full input designs as expected. Further, binary output design converges faster than the decimal output designs. However, accuracy of each of the designs will be discussed in section 5.5.



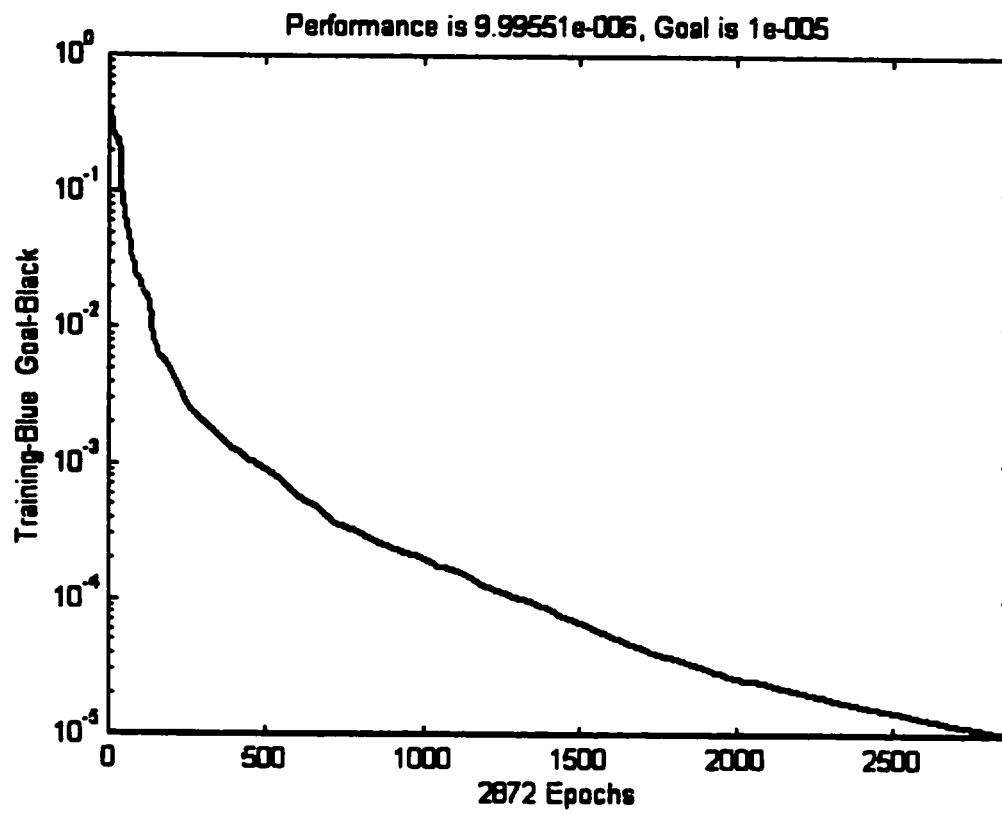


**Figure 5.3: Error Convergence for ANN Design D2F**

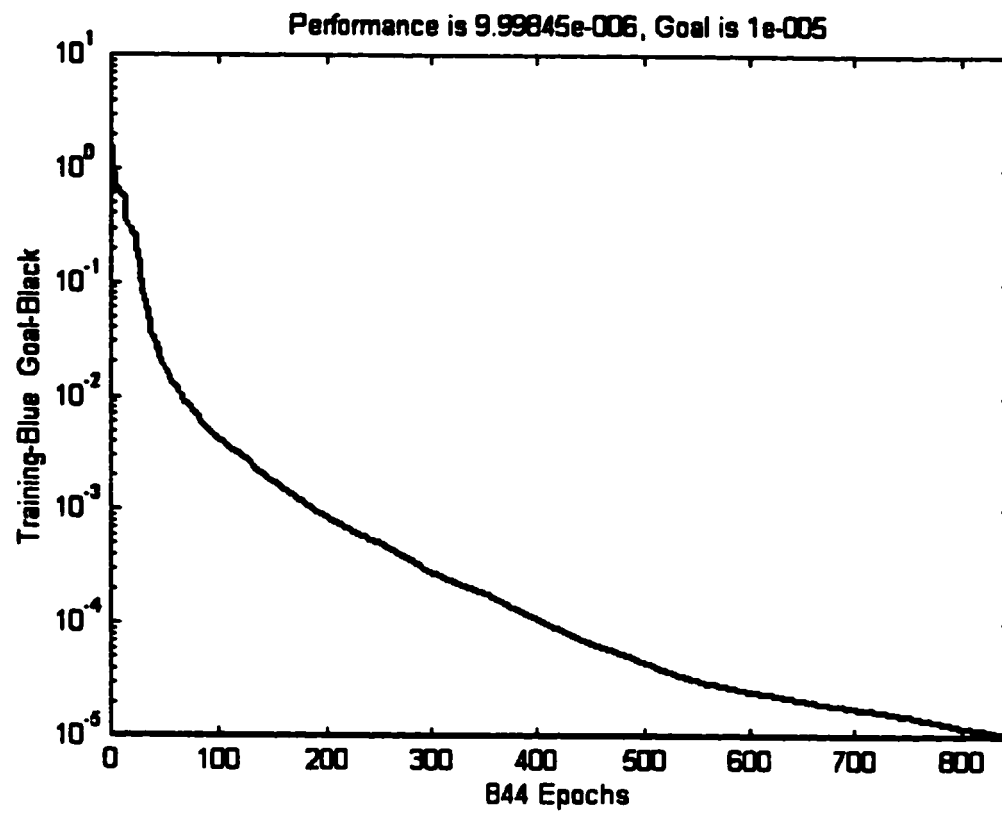


**Figure 5.4: Error Convergence for ANN Design D2R**

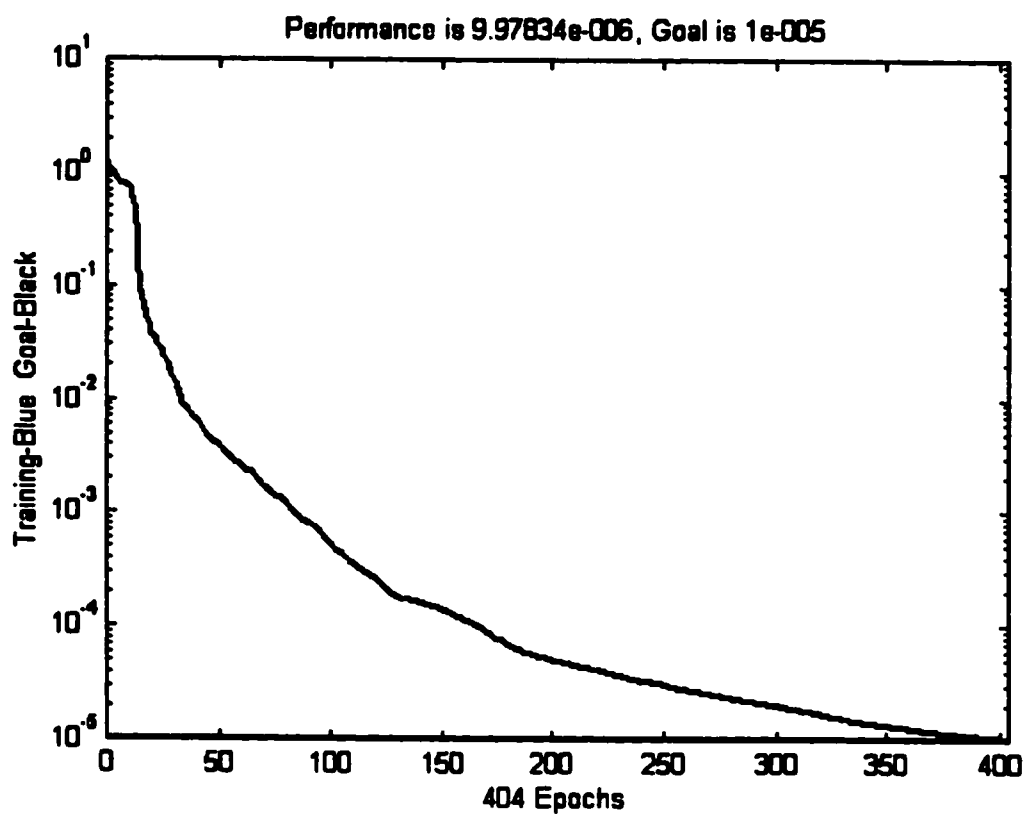


**Figure 5.5: Error Convergence for ANN Design D2B**

## **5.4 Description of ANN Design # 3**

In design # 3, fifty seven (57) EMTP cases are used to train the ANN, 20 cases are used to test it and 36 cases are used for checking the generalization capabilities of the design. The following cases are used in the training and testing set of the ANN:

- a. Normal load switching
- b. Normal load and capacitor switching
- c. HIF with no load or capacitor switching
- d. HIF with load switching
- e. HIF with load and capacitor switching
- f. HIF with varying fault impedance (60 % - 90 % fault current)
- g. HIF with varying transmission line impedance

The only difference between the training set for this design and design # 2 is that mid-span fault cases are not included in the training set of this design. This selection is made based on the comparison between the performance of designs # 1 and 2, which have performed excellently with respect to predicting the correct output for mid-span faults, though these faults have not been included in the training set of design # 1.

The generalization check cases, on the other hand, include mid-span fault cases, HIFs with extended feeder cases, HIFs with 50 % fault current and HIFs with lightly loaded feeder cases.

**This design is performed three times. First with full data (Design D3F), and then with reduced data (Design D3R). In both of these cases, decimal output vector is used. The third version of this design (Design D3B) is performed with reduced data and binary output vector. For designs D3R and D3B, FFT is used to preprocess the input data representing the voltage and current waveforms. As mentioned earlier, each phase of these waveforms is represented by 300 data points in the original input. After applying FFT, only the highest 100 frequency components are selected to represent each phase. This results in an input vector that is 600-point long instead of the original 1800-point vector.**

**Design D3F has converged after 1812 epochs, design D3R has converged in 1123 epochs, and design D3B has taken 457 epochs before it converges. Graphical illustrations of the error convergence for the three design versions are shown in Figures 5.6, 5.7 and 5.8, respectively.**

**Comparing the time it takes the different designs to converge, it can be seen clearly that the time required is directly proportional to the amount of data in the training set. The less points in the training set, the faster the convergence and the least time required to reach the performance goal. Also, cases of binary output vectors converge much faster than those with decimal output vectors. Table 5.3 summarizes the specific features used for each of the above mentioned designs.**

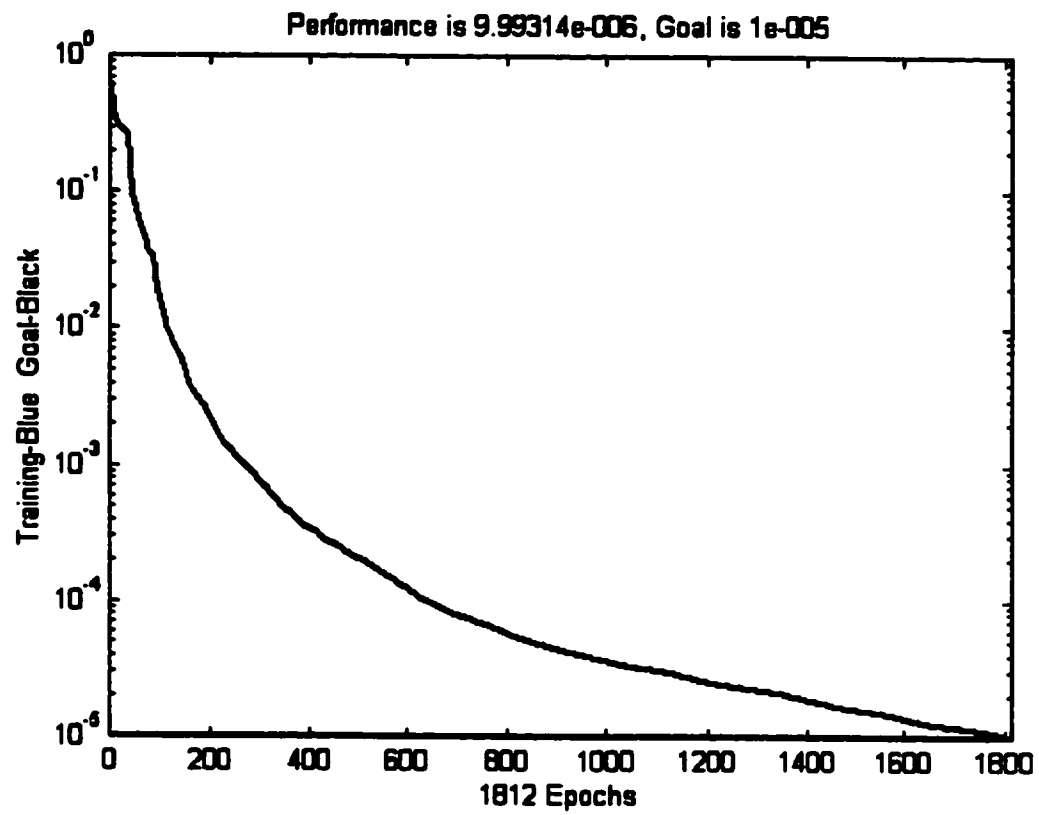


**Figure 5.6: Error Convergence for ANN Design D3F**

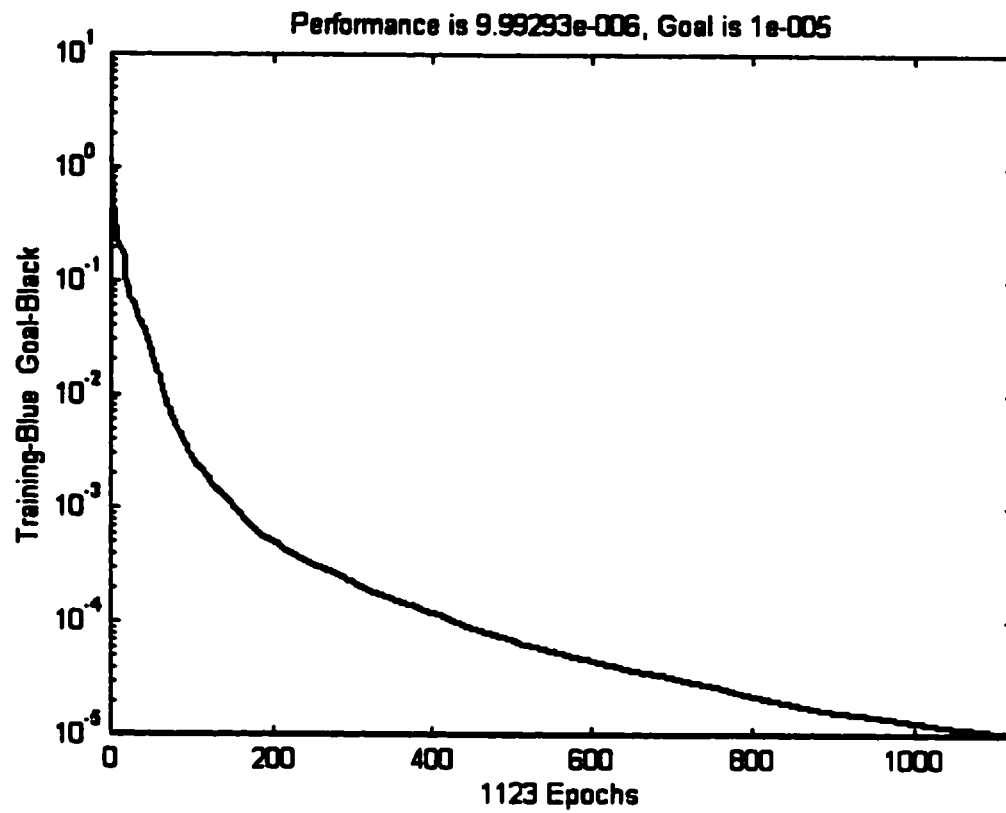


**Figure 5.7: Error Convergence for ANN Design D3R**

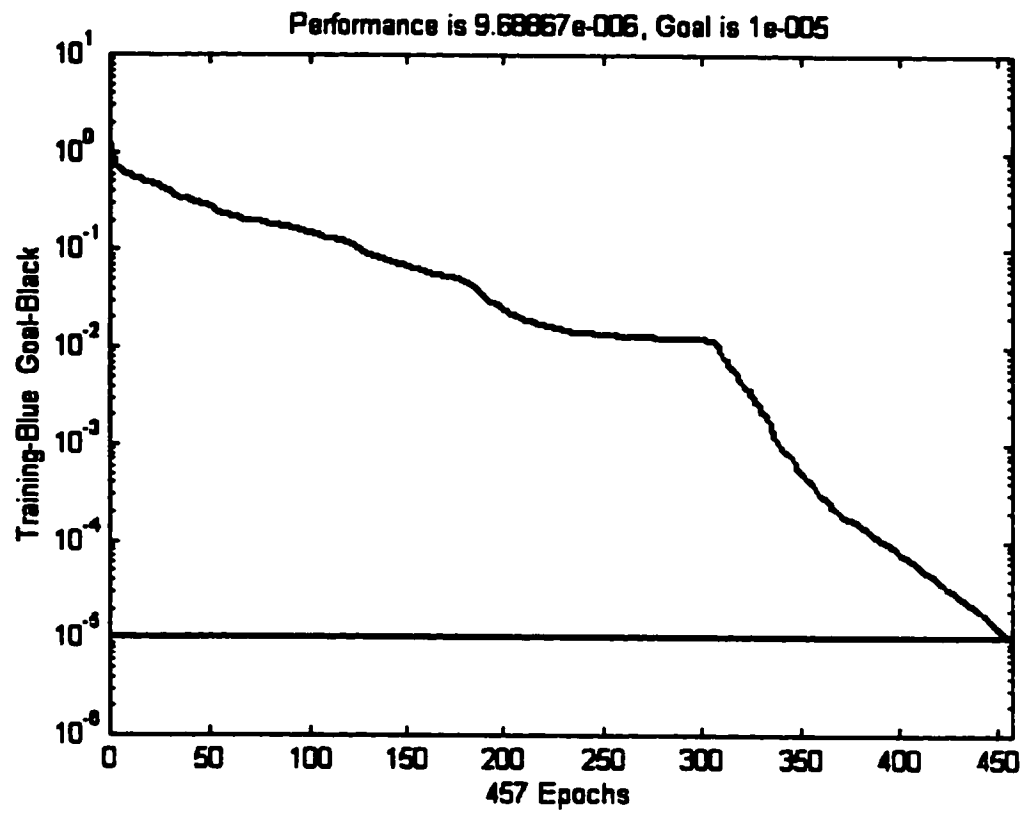


**Figure 5.8: Error Convergence for ANN Design D3B**



**Table 5.3: Specific Features of the Various ANN Designs**

Design No.		No. of EMTP Cases for ANN *			No. of Epochs
		Training	Testing	Generalization Check	
1	D1F	39	13	48	414
	D1R				335
2	D2F	66	22	24	2872
	D2R				844
	D2B				404
3	D3F	57	20	36	1812
	D3R				1123
	D3B				457

\* Each EMTP case is represented by a column in the input matrix to the ANN, i.e. the number of columns in the input matrix equals the number of EMTP cases. The number of data points in each column of the matrix is either 1800 points for full data cases or 600 points for reduced data cases.

## **5.5 Test Results**

This section presents analysis of the test and generalization check results for the various proposed designs of the ANN-based HIF diagnosis schemes. The accuracy of each design is discussed with respect to the various fault scenarios.

### **5.5.1 Design # 1**

For design # 1, thirteen (13) cases have been used for testing the design. This means the ANN has to recognize 52 targets (13 cases each having four targets). As far as generalization check is concerned, 48 cases have been used. This corresponds to 192 targets that the ANN is expected to recognize.

#### **a. Design D1F**

Design # D1F has recognized 51 out of the 52 targets, i.e. it has had only one error. The error was in identifying the faulty node (Target # 2) for HIF with no load or capacitor switching. This works out to an overall accuracy of 98.1 % and an accuracy of 92.3 % as far as the fault location is concerned.

When the ANN generalization is checked for mid-span HIFs and HIFs on extended feeder, the output of the ANN shows clearly that the network is capable of identifying whether the feeder is faulty or not (Target # 1), the type of event (Target # 3), and faulted phase (Target # 4) with 100 % accuracy. For faults in between nodes, the second output

of the ANN is always somewhere between the node numbers where the fault took place. This is expected since the original ANN was trained to recognize the faulty node and no target was reserved for faults between any two nodes on the feeder. Again, this indicates that the ANN is giving the expected output with 100 % accuracy for faults midway between the nodes. There is only one error in identifying the fault location (Target # 2) for the extended feeder case, which results in an overall accuracy of 98.8 % or an accuracy of 95.2 % with regard to recognizing the fault location (one error out of 21 cases used to represent mid-span HIFs and HIFs on extended feeder).

For the rest of the generalization check cases (27 cases), the test results of design D1F for varying fault impedance shows the following:

- a. ANN detected the fault (Target # 1) for zero-fault impedance cases, and for fault currents of 70 % and above.
- b. ANN identified the faulty phase (Target # 4) for fault currents of 80 % and above.
- c. ANN identified the fault location and type of event (Targets # 2 and 3) for fault currents of 90 % and above.

Further, for lightly loaded feeder cases, the test results shows that design D1F is able to detect whether the feeder is faulty or not (Target # 1) with 100 % accuracy. It can also identity the event type (Target # 3) for HIFs on Phase-A, and identify the faulty phase

(Target # 4) for faults on Phase-C. However, this design cannot detect the fault location (Target # 2) for all cases. This is not unexpected since lightly loaded feeder represents a totally different feeder. Also, it shall be emphasized that all the cases used to check the generalization are new to the ANN and are not presented to the ANN during its training.

**b. Design D1R**

On the other hand, the reduced input design D1R has achieved an overall accuracy of 94.23 % when tested with the 13 test cases. Three errors have resulted from the test; one error in locating the fault, one in detecting the event type, and one in identifying the faulty phase. This design also detected the fault with 100 % accuracy.

For the generalization check cases, design D1R achieved the following results:

- a. For mid-span HIFs, the overall accuracy is 94.4 %, with two errors. The first error is in detecting the event type and the other in identifying the faulty phase. This design has no errors as far as detecting the HIF occurrence and locating the fault (Targets # 1 and 2) are concerned.
- b. For extended feeder cases, the accuracy is 100 % with no errors.
- c. For varying fault impedance cases, the ANN has been able to detect the HIF for zero-fault impedance cases and for faults with 70 % and above fault currents. It identifies the faulty phase with 50 % accuracy. The performance of this design, however, is poor with an accuracy of around 30 % with regard to locating the fault and detecting

the type of event. This has been improved in Design # 2 by introducing the varying fault impedance cases in the training set of the ANN.

- d. For lightly loaded feeder cases, the accuracy of the design is 100 % for Target # 1 (fault location) and Target # 4 (faulty phase). For identifying the event type (Target # 3) the accuracy is 50 %, but the design has the poorest accuracy in locating the fault (Target # 2).

### **5.5.2 Design # 2**

Design # 2 uses 22 cases for testing the design, which means that the ANN shall predict 88 targets for cases with decimal output (design D2F and D2R) and 132 targets for the binary output case (design D2B). Twenty four (24) cases are used to check the generalization of this design for which the ANN is expected to predict 96 targets or 144 targets for decimal and binary output cases, respectively.

#### **a. Design D2F**

The overall accuracy of this design, when tested with the 22 test cases, is 97.7 %. There are only two errors in locating the fault (Target # 2). However, the error is only one feeder-section different from the actual fault location. It may be noted that there has been no error for mid-span HIFs, HIFs with varying fault impedance, and HIFs with varying line impedance. This demonstrates the improved performance of the ANN with regard to these fault scenarios as a result of including these fault cases in the training set of the

**ANN.** One of the two errors has occurred in cases of HIF with no load or capacitor switching and the other in cases of HIF with load and capacitor switching.

On the other hand, the overall accuracy of this design when presented with the generalization check cases, is 63.5 %. Most of the errors have been in predicting Targets # 2, 3 and 4 (fault location, event type and faulty phase) for lightly loaded feeder cases. For fault detection (Target # 1), there are only two errors. There is only one error in predicting the fault location for extended feeder cases, which works out to an accuracy of 97.9 %. This design also shows poor performance with regard to lightly loaded feeder cases. But, it may be emphasized here that the performance of this design with respect to fault detection is 91.7 %. Needless to say that fault detection is the most important output of the HIF detector. The following designs have better performance than this design as far as the generalization check cases are concerned.

**b. Design D2R**

This design has an overall test accuracy of 96.6 %. There have been only three errors all of which have occurred in fault location (Target # 2) with one feeder-section difference from the correct fault location. One error is in cases of HIF with no load or capacitor switching and two are in cases of HIF with load and capacitor switching. This is similar to the above design D2F.

On the other hand the overall generalization check accuracy of this design is 77.1 %. There are no errors for the extended feeder cases (100 % accuracy). In other words, all the errors occur for cases of lightly loaded feeder. For fault detection (Target # 1) the accuracy is 100 %. Four (4) errors have been in locating the fault (Target # 2), with a difference of one feeder-section from the correct fault location. Most of the errors have occurred in detecting the event type (Target # 4) and identifying the faulty phase. This shows the improved performance of this design as compared to design D2F.

**c. Design D2B**

This design has binary output consisting of 6 bits. Except for Target # 1, which takes binary values (either one (1) for fault cases or zero (0) for no-fault cases), all other targets cannot be represented by single binary bit. This makes it difficult to measure the accuracy of this design with respect to the different targets.

The overall accuracy of this design, when tested with the 22 test cases, is 86.4 %. This is worse than the performance of the previous designs. However, the generalization check accuracy of this design is 86.1 %, which is better than the accuracy of the previous designs. As is the case with the above designs, most of the errors are for cases of lightly loaded feeder.

### **5.5.3 Design # 3**

Twenty (20) cases are used to test this design and thirty six (36) cases are used for generalization capability check. This means that for design # 3, the ANN is expected to predict 80 targets during testing and 144 targets during generalization check.

#### **a. Design D3F**

The overall accuracy of the test cases for this design is 96.3 %. There are three errors in locating the fault (Target # 2), one error for cases of HIF with no load or capacitor switching, one for cases of HIF with load switching, and the third error is for cases with HIF with load and capacitor switching. It may be noted that the error is only one feeder-section apart from the actual fault location on the feeder.

For the generalization check cases, the overall accuracy is 79.2 %. This design has no errors with respect to fault detection (Target # 1). Also, the design has predicted all other targets for mid-span fault cases with 100 % accuracy. For extended feeder cases, there are 2 errors in locating the fault (Target # 2), but no errors for all other targets. The most difficult fault scenario is the case of HIF with lightly loaded feeder. For this cases, the design has an accuracy of 33.3% with respect to fault location (Target # 2) and identification of faulty phase (Target # 4). As far as event type detection, the design has predicted all HIF cases as HIF with load and capacitor switching. For HIF with 50 % fault



current, the design predicted all targets accurately except for one error in detecting the fault location.

**b. Design D3R**

The overall accuracy of the test cases for this design is 100 %. This design predicted all the 80 targets as desired.

For the generalization check cases, the overall accuracy is 81.9 %, which is the best result obtained for the generalization check. There are no errors with respect to fault detection (Target # 1). Also, the design has predicted all other targets for mid-span fault cases, for extended feeder cases and for HIF with 50 % fault current, with 100 % accuracy. Similar to design D3F, for cases of HIF with lightly loaded feeder, this design has an accuracy of 33.3 % with respect to fault location and identification of faulty phase (Targets # 2 and 4). Also, this design has predicted all HIF cases as HIF with load and capacitor switching (Target # 3).

**c. Design D3B**

Similar to design D2B, this design has binary output consisting of 6 bits. Except for Target # 1, which takes binary values (either one (1) for fault cases or zero (0) for no-fault cases), all other targets cannot be represented by single binary bit. This makes it difficult to measure the accuracy of this design with respect to the different targets.

The overall accuracy of this design, when tested with the 36 test cases, is 80 %. However, the generalization check accuracy of this design is 81 %. As is the case with the above designs, most of the errors are for cases of lightly loaded feeder.

Table 5.4 presents a summary of the test results for all the ANN designs with respect to the targets, and Table 5.5 gives similar comparison but with respect to the applicable fault scenarios. It may be noticed that for cases with binary output, accuracy is not measured against the targets as six bits are used to represent the various possible output combinations. Comparisons and discussions of the test results are covered in the next section.

## **5.6 Comparison of the Test Results**

A quick look into Table 5.3 will reveal that the best design, in terms of the overall accuracy of the results of the test cases and generalization check cases, is design D1F. Though, it has a 100 % overall accuracy in the test cases, design D3R comes next to design D1F as its accuracy for the generalization check cases is only 81.9 %, which is much below that of design D1F. Design D2B comes in the third place with an overall accuracy of 86.4 % for the test cases and 86.1 % for the generalization check cases.

Comparing the performance of the various designs with respect to the designated targets of the ANN, it is clear that the designs have performed best in detecting the HIF

**Table 5.4: ANN Designs Test Results with Respect to Targets**

Design No.		Overall Accuracy (%)	Accuracy (%) w.r.t. Target #			
			1	2	3	4
Test Cases	D1F	98.1	100	92.3	100	100
	D1R	94.2	100	92.3	92.3	92.3
	D2F	97.7	100	90.9	100	100
	D2R	96.6	100	86.4	100	100
	D2B	86.4	NA	NA	NA	NA
	D3F	96.3	100	85	100	100
	D3R	100	100	100	100	100
	D3B	80	NA	NA	NA	NA
Generalization Check Cases	D1F	99.3	100	95.2	100	100
	D1R	70.3	87.5	52.1	58.3	85.4
	D2F	63.5	91.7	45.8	58.3	58.3
	D2R	77.1	100	83.3	58.3	75
	D2B	86.1	NA	NA	NA	NA
	D3F	79.2	100	75	75	83.3
	D3R	81.9	100	83.3	66.7	77.8
	D3B	81	NA	NA	NA	NA

**Legend:**

- w.r.t.: with respect to
- NA: not applicable

**Table 5.5: ANN Designs Test Results with Respect to Fault Scenarios**

Design No.	Overall Accuracy (%)	Accuracy (%) w.r.t. Fault Scenario				
		1	2	3	4	5
D1F	60.9	100	26.7	NA	98.8	41.7
D1R	70.8	94.4	36.7	NA	100	66.7
D2F	73.5	100	100	100	97.9	29.2
D2R	83.3	100	100	100	100	54.2
D2B	89.4	94.4	100	100	93.1	79.2
D3F	82.6	100	96.4	100	97.2	41.7
D3R	84.9	100	100	100	100	45.8
D3B	84.1	87	100	100	88.9	63.9

**Legend:**

- w.r.t.: with respect to
- NA: not applicable

**Fault Scenarios:**

1. Mid-span HIFs
2. HIF with varying fault impedance (or current)
3. HIF with varying line impedance
4. HIF for extended feeder
5. HIF for lightly loaded feeder

occurrence (Target # 1). The next best performance is in identifying the faulty phase (Target # 4). Then comes detecting the fault location (Target # 2), and distinguishing the event type (Target # 3) as the least performance.

On the other hand, design D2B has the best accuracy (89.4 %) with respect to the various fault scenarios simulated in this work, as indicated in Table 5.5. The second and third best designs, with respect to fault scenarios, are design D3R and design D3B with overall accuracies of 84.9 % and 84.1 %, respectively.

If we compare the performance of the various designs with respect to the various fault scenarios indicated in Table 5.5, we can see that the best performance is achieved in detecting HIFs with varying transmission line impedance, HIFs with extended feeder and mid-span HIFs. The performance with respect to HIFs with varying fault impedance (or current) is a little less. But the least performance is for lightly loaded feeder cases.

The above comparisons shall be read in conjunction with the analysis of the test results as presented in Section 5.5. If read separately, these comparisons could be misleading.

Considering the discussions of Section 5.5 together with the test result summaries presented in Tables 5.4 and 5.5, the best design for the HIF diagnosis system proposed in this thesis is design D3R. This is because of the following:

1. This design has an overall accuracy of 100 % for the test cases (for all targets).
2. This design has an accuracy of 100 % for mid-span HIF cases.
3. This design has an accuracy of 100 % for extended feeder cases.
4. This design has an accuracy of 100 % for varying fault impedance cases.
5. This design has an accuracy of 100 % for varying transmission line impedance cases.
6. All errors in predicting the correct targets for this design occur for lightly loaded feeder cases. There are six errors in locating the fault (Target # 2) all of which are only one-feeder section apart from the correct fault location. Also, there are 8 errors in identifying the faulty phase (Target # 4) for faults on Phase-A and Phase-B. The remaining 12 errors are in distinguishing the event type (Target # 3) as being 'a HIF with load and capacitor switching' instead of the correct event type which is 'a HIF with no load or capacitor switching'.

Needless to say that the most important function of any HIF diagnosis system is fault detection for which design D3R has achieved a 100 % accuracy independent from the fault scenario. The second most important function of the HIF diagnosis system is to distinguish between HIFs and HIF-like events. In other words, the system shall not give a false indication of the presence of a HIF when the real system event is a normal operating condition, like load or capacitor switching. This function is also achieved by design D3R as it mistakenly gives an indication of 'a HIF with load and capacitor switching' for the case of 'a HIF with no load or capacitor switching', but it never indicates a normal system operation for a HIF case or vice versa. That is to say that design D3R fails to distinguish

between two HIF conditions but succeeds in not indicating a normal operating condition for cases of HIFs.

It shall also be remembered that all errors of design D3R occur for lightly loaded feeder cases, which are used for checking the generalization of the design. These cases have never been presented to the ANN during the training phase of this design. Eventually, these cases represent a totally new feeder configuration with different components from the feeder model of Figure 4.1. Nevertheless, design D3R has performed very well with respect to the various targets and fault scenarios, which demonstrates the strong capabilities of the design to generalize for different distribution feeder arrangements.

## **5.7 Validation Results of the ANN Designs**

To check the accuracy of the ANN designs when the proposed ANN-based HIF diagnosis systems are applied to a completely new feeder under a set of totally different operating conditions, the full data designs D1F, D2F and D3F are tested with the data that resulted from the EMTP simulation of the additional nine cases described under section 4.3.3. Table 5.6 summarizes the test results for these validation cases with respect to the various targets.

This table indicates that the overall accuracy of designs D1F and D3F is 50 % while that of design D2F is only 33.3 %. As far as the performance of each of these designs with

**Table 5.6: Test Results for Validation Cases with Respect to Targets**

Design No.	Scenario No.	Overall Accuracy of the Designs (%)	Accuracy (%) w.r.t. Target #			
			1	2	3	4
D1F	1	50	100	0	66.7	33.3
	2		100	0	66.7	33.3
	3		100	0	66.7	33.3
D2F	1	33.3	100	0	0	100
	2		100	0	0	100
	3		0	0	0	0
D3F	1	50	100	0	0	100
	2		100	0	0	100
	3		100	100	0	0
Overall Accuracy (%) w.r.t. Targets			88.9	11.1	22.23	55.6

**Notes:**

- Each scenario has three cases for HIFs on each of the three phases.
- Scenario # 1: HIF at Node-1 of the feeder of Figure 4.1 with T1, T2, T3, C1 and C2 disconnected.
- Scenario # 2: Similar to Scenario # 1 but with the feeder length doubled (to 40 km).
- Scenario # 3: Mid-span HIF between Nodes-2 and 3. The fault impedance is increased so that only 5 % of the fault current passes to ground. Also, an additional node is connected at the end of the feeder and both C1 and C2 are disconnected.



respect to the four targets, it can be seen that the best accuracy is achieved with target # 1 (HIF detection), which is the most important target. Design D2F did not detect the HIF occurrence for scenario # 3 cases. The least accuracy was in locating the fault.

It is expected that the performance of the ANN designs will drop due to the fact that not only the feeder configuration is changed for the validation cases but also the fault scenarios. Nevertheless, designs D1F and D3F detected the HIF occurrence for all the validation cases. Also, design D2F detected the HIF occurrence for all the cases of both scenarios # 1 and 2.

Furthermore, the results here may not be realistic because the number of the validation cases is so small for concluding about the performance of each of the ANN designs.

## **Chapter 6**

# **CONCLUSIONS AND RECOMMENDATIONS FOR FUTURE WORK**

This chapter presents a summary of the work performed in this thesis. It also gives some recommendations for future work.

### **6.1 Conclusions**

One of the challenges that face electricity utilities, up till today, is the detection of HIFs on electric power distribution feeders. Most HIFs draw a little current, which makes them difficult to detect by conventional overcurrent relays. If HIFs are not detected, they create

a public hazard and threaten the lives of the public. It is the desire to improve public safety which has been the primary motivator for the development of HIF detectors.

Many HIF detection techniques have been developed over the last three decades. However, till the present there is no detection technique that can detect all HIFs with a high degree of security or dependability. In other words, it is relatively easy to develop a HIF detector, but it is extremely difficult to make this detector able to distinguish HIFs from HIF-like events, such as normal load switching. Another difficulty that faces the researchers in HIF detection field is the scarcity of data about HIF events due to the legal implications associated with injuries or damages that might result from an undetected HIF.

Some of the HIF detection techniques which are developed based on expert systems (ES) are already available these days but there are no reports about their field performance. On the other hand, there are no commercially available ANN-based detectors so far. This fact, among other reasons, such as the advantages of ANN over ES, has motivated this work. This work is also motivated by the fact that approximately 50 % of the primary distribution circuits in the system of SEC-ERB are overhead lines [8], and that around 95% of all faults occur on overhead lines [9].

The objective of this work is to develop an ANN-based HIF diagnosis system that can reliably detect the HIF, indicate its location, distinguish it from HIF-like normal system operating conditions, such as load or capacitor switching, and finally identify the faulty

phase. This objective is achieved through performing the following activities (details are presented in Chapter 2):

1. Simulation of a typical 13.8 kV overhead distribution feeder using EMTP. Single line to ground fault is simulated at different times and locations along the feeder. The following cases are simulated:
  - a. Normal load switching
  - b. Normal load and capacitor switching
  - c. High impedance fault with no load or capacitor switching
  - d. High impedance fault with load switching
  - e. High impedance fault with load and capacitor switching
2. Developing an ANN-based design and training it with some of the voltage and current waveforms that are generated from the EMTP simulation. Some of the waveforms are used for training, and the rest are used for testing the ANN design and checking its robustness or generalization capabilities.

The feeder used for the simulation represents a typical 13.8 kV overhead distribution feeder in the network of SEC-ERB. All the parameters of the components used in the feeder are based on SEC-ERB standards and specifications for components that are already installed in the SEC-ERB network. This makes the thesis more practical and

realistic. For instance, the power and distribution transformers are modeled for EMTP simulation based on actual test reports of transformers installed in SEC-ERB substations.

The total number of cases simulated with EMTP is 120 cases that cover all the cases mentioned above in addition to the following fault scenarios:

- a. Mid-span HIFs
- b. HIF with varying fault impedance or current (50 – 100 %)
- c. HIF with varying line impedance (-20 % to +20 %)
- d. HIF for extended feeder
- e. HIF for lightly loaded feeder

Each case is represented by its voltage and current waveforms for the three phases. A total number of 1800 data points is used for each case, which means that each phase is described by 300 data points. To improve the performance of the ANN, these data points are scaled or normalized prior to training the ANN. Further, some of the ANN designs that are tried in this work are trained with preprocessed input data. The FFT is used for preprocessing the input data so that 600 data points are used instead of the original 1800 data points.

The “ Neural Network Toolbox for MATLAB® ” [27] is utilized to develop the ANN-based HIF diagnosis system. The following work is performed for ANN training:

1. The ANN architecture or topology is selected to have three feedforward layers with tan-sigmoid transfer functions. The optimum topology has 35 neurons in the first hidden layer, 20 neurons in the second hidden layer, 30 neurons in the third hidden layer, and 4 neurons in the output layer.
2. Different training data sets (inputs and outputs) are selected for the different ANN designs as explained in Chapter 5.
3. The scaled conjugate gradient (TRAINSCG) algorithm, which is basically an improved faster version of the standard backpropagation algorithm, is used for training the ANN.
4. The ANN is then tested using a set of test data until the ANN performance meets the error target which is set to be  $1 \times 10^{-5}$ .
5. The robustness or generalization capabilities of the ANN is checked then by presenting to it a new set of input data which is totally different from that used to train the ANN.

Three designs are performed. These designs differ in the number of EMTP cases that are used for training the ANN, testing it and checking its generalization. Design # 1 has two versions, namely design D1F and design D1R. Design # 2 has three versions: design D2F, design D2R and design D2B. Finally, design # 3 has also three versions, which are: D3F, design D3R and design D3B. These eight design versions differ in the input and output sets used for ANN training. Details of these design versions are available in Chapter 5.

Out of these eight design versions, four are very promising for the intended application of HIF diagnosis. These are designs D1F, D2B, D3R and D3B. However, the best performance is achieved with design D3R.

Design D3R uses 57 of the 120 EMTP cases for ANN training, 20 cases for ANN testing and 36 cases for generalization check of the ANN. The input data to the ANN for this design is preprocessed with FFT and only the highest 100 frequency components are selected to represent each phase of the voltage and current waveforms. This means, only 600 data points are used for training the ANN instead of the original 1800 data points. This has helped in improving the ANN performance and reducing the time needed for error convergence (only 457 epochs). This design is selected to be the best design because of the following:

1. It has an overall accuracy of 100 % for the test cases (for all targets).
2. This design has an accuracy of 100 % for mid-span HIF cases, for extended feeder cases, for varying fault impedance cases and for varying transmission line impedance cases.
3. All errors in predicting the correct targets for this design occur for lightly loaded feeder cases. Nevertheless, the design has no errors in detecting the HIF (Target # 1). Though this design is not able to distinguish between 'a HIF with load and capacitor switching' and 'a HIF with no load or capacitor switching', it succeeds in not false indicating a HIF for normal system operation event or vice versa.

It shall be emphasized that lightly loaded feeder cases eventually represent a totally new feeder that is completely different from the feeder model of Figure 4.1 which is used to generate the training cases of the ANN. The high accuracy achieved by design D3R (and other designs also tried in this work) demonstrates clearly the great potential for real life application of this design for HIF diagnosis on overhead distribution feeders.

## **6.2 Recommendations for Future Work**

This section highlights some of the interesting investigation areas or subjects that may be taken for future study and research. A brief description of each of these study areas is given in the following paragraphs.

1. As concluded in EPRI's survey of faults on primary distribution systems, 95 % of the faults on primary distribution feeders occur on overhead lines [9]. Around 5-20 % of these faults are HIFs [2]. Though only about 5 % of the faults are occurring on underground distribution cable circuits, it may be worth investigating if the proposed ANN-based HIF diagnosis system works adequately well for these rare eventualities. It is well known that most HIFs do not present any adverse effects on power system stability and the main motivator for developing HIF detectors is public safety. Despite the fact that HIFs on underground distribution cables do not result in public hazard, detecting HIFs on underground distribution circuits is advantageous to save the power losses that are unavoidable if HIFs remain undetected.



2. Only single line to ground HIFs are simulated in this work because the majority of faults on overhead distribution lines are single line to ground type. It would be advantageous if this work can be extended to consider other fault types, such as double line to ground faults, three line to ground faults, and line to line faults.
3. The simulation of the distribution feeder in this thesis is performed using EMTP. The output of the simulation is then converted into M-file format before it can be used for ANN training. This could be avoided if the “ Power System Blockset for Use with SIMULINK® ” [35] is used for the feeder simulation. This blockset is recently developed by Hydro-Quebec Research Institute (IREC), Teqsim International Inc., Ecole de Technologie Superieure and Universite Laval. With this blockset the data needed for ANN training using the “ Neural Network Toolbox for MATLAB® ” will be readily available. This will save time and effort and will allow more variations of the components of the feeder model. Examples of possible variations that have not been considered in this work is to add voltage regulators along the feeder model and to use nonlinear fault impedances.
4. It may be worthwhile to repeat this work using the “ Wavelet Toolbox for MATLAB® ” [36]. One of the most important advantages of using wavelet analysis for signal processing over other techniques, such as FFT, is its capability to reveal some features of the signal which are missed by other signal analysis techniques. These features include trends, breakdown points, discontinuities in higher derivatives and self similarity. In addition, wavelet analysis detects and retains the exact instance at which signal change takes place.

5. **Research shall be done to develop the optimum approach for realization and actual implementation of the proposed design. Two types of feedforward ANN implementation may be investigated. These are software implementation and hardware implementation. Each of these approaches has its own advantages and drawbacks. Discussions of the merits and demerits of these approaches together with detailed description of the different ways used to implement these approaches are presented by Anne-Johan Annema [29].**

# **APPENDICES**

## **Appendix A**

### **EMTP INPUT DATA STRUCTURE**

This appendix describes the Input Data Structure for EMTP simulation. The single-phase data file for the base case of this work is also included for illustration purpose.

#### **A.1 Input Data Structure**

Basically, the EMTP input data file consists of eight sections separated by a blank card to terminate each of the sections. These are:

1. **BEGIN NEW DATA CASE** card, which is a mandatory statement that precedes the input deck.
2. The fixed point miscellaneous data card. This card contains real-number parameters that specify the time step for the simulation, the maximum time for the simulation, the power frequencies for specifying inductances and capacitances, etc.

3. **The integer miscellaneous data card.** This card contains several integer numbers that control printing or plotting of the desired outputs.
4. **The branch (or circuit) data cards.** These cards are used to model all branch circuits, such as transmission lines, loads, inductances, capacitances, transformers, etc.
5. **The switch data cards,** which are used to simulate switching action of the various components of the model being simulated.
6. **The source card.** This is used to specify the type of source (voltage or current) used for the simulation and the amplitude of the source signal.
7. **The output data card,** which specifies the variables to be printed or plotted.
8. **The blank cards** that are used to end the EMTP simulation.

These eight sections are illustrated graphically in Figure A.1.1 as well as in the EMTP data file of the base case which is presented in Section A.2. It may be noted that this file was not used for the simulations needed for this thesis. The three-phase version of the data file has been used instead as this work concentrates on single-line to ground fault cases which are unbalanced cases and can only be simulated with the three-phase version of the EMTP data file.

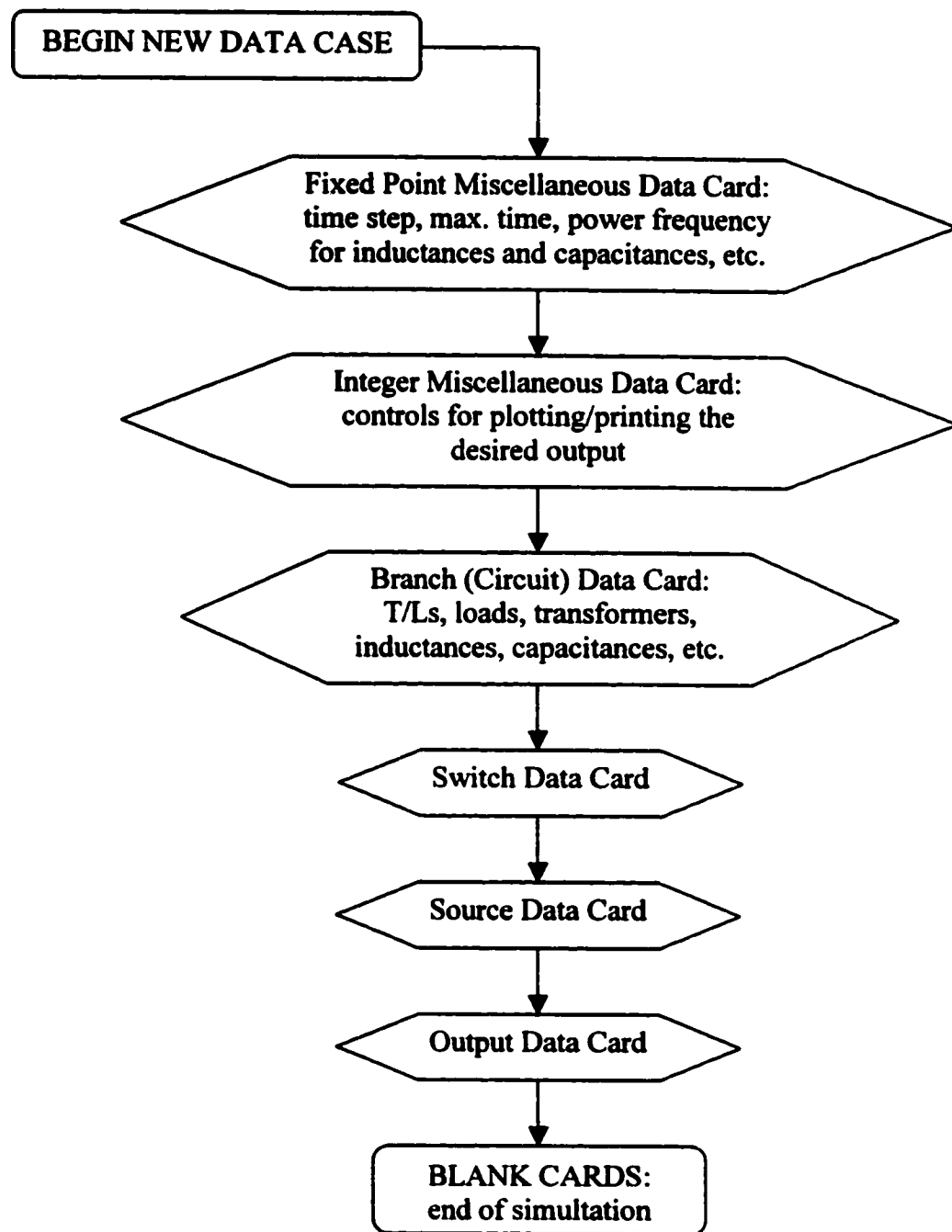


**Figure A.1.1: EMTP Input Data Structure**

## A.2 Three Phase EMTP Data File for the Base Case

```

C
BEGIN NEW DATA CASE
C      1      2      3      4      5      6      7      8
C 3456789012345678901234567890123456789012345678901234567890
C
C ----dt<---Tmax<---Xopt<---Copt<---Epsiln<---Tolmat<---Tstart
.521E-3  0.167  0.0  0.0  0
C -Iprnt<---Iplot<---Idoubl<---Kssout<---Maxout<---Ipun<---Memsav<---Icat<---Nenerg<---Iprsup
      1      3      0      0
C
C .....CIRCUIT DATA.....
C      1      2      3      4      5      6      7      8
C 3456789012345678901234567890123456789012345678901234567890
C Bus1->Bus2-><-----><-----R<-----L<-----
51STHEVABUSTHA      .15606  4.7814588
52STHEVBBUSTHB      .26450  5.6093563
53STHEVCBUSTHC
C Bus1->Bus2->Bus3->Bus4-><-----R<-----L<-----C<-----
BUS13ANODE1A      .865285.1875 1
BUS13BNODE1B      .865285.1875 1
BUS13CNODE1C      .865285.1875 1
NODE1ANODE2A      .865285.1875 1
NODE1BNODE2B      .865285.1875 1
NODE1CNODE2C      .865285.1875 1
NODE2ANODE3A      .865285.1875 1
NODE2BNODE3B      .865285.1875 1
NODE2CNODE3C      .865285.1875 1
NODE3ANODE4A      .865285.1875 1
NODE3BNODE4B      .865285.1875 1
NODE3CNODE4C      .865285.1875 1
LOAD1A      .08712.11923 0
LOAD1B      .08712.11923 0
LOAD1C      .08712.11923 0
LOAD2A      .08712.11923 0
LOAD2B      .08712.11923 0
LOAD2C      .08712.11923 0
LOAD3A      .08712.11923 0
LOAD3B      .08712.11923 0
LOAD3C      .08712.11923 0
CAP1A      12.536 0
CAP1B      12.536 0
CAP1C      12.536 0
CAP2A      12.536 0
CAP2B      12.536 0
CAP2C      12.536 0
FALT1A      1.E6 0
FALT1B      1.E6 0
FALT1C      1.E6 0
FALT2A      1.E6 0
FALT2B      1.E6 0
FALT2C      1.E6 0
FALT3A      1.E6 0
FALT3B      1.E6 0
FALT3C      1.E6 0
FALT4A      1.E6 0
FALT4B      1.E6 0
FALT4C      1.E6 0

```

```

LOAD4A                85.698110.10                0
LOAD4B                85.698110.10                0
LOAD4C                85.698110.10                0
C      1      2      3      4      5      6      7      8
C 34567890123456789012345678901234567890123456789012345678901234567890
C <---XFMR---><--REF>-----<--I--><FLUX><BX>---<Rmag>-----
TRANSFORMER          2.064246.816T15A                1
  0.9177016269      36.3652766343
  1.3346219362      41.5646032251
  2.0642166320      46.8164486427
  4.3604564783      51.9182434493
  9.0726977662      54.4691364523
 18.4749039349      56.7574404975
      9999
1BUSTHABUSTHB          1.221576.007115.00
2BUS13A                .014005.26597.9674
TRANSFORMER T15A                T15B
1BUSTHBBUSTHC
2BUS13B
TRANSFORMER T15A                T15C
1BUSTHCBUSTHA
2BUS13C
C
TRANSFORMER          .93214.25918T31A                1
  0.4425072187      0.1155510978
  0.5579938682      0.1522670097
  0.7377335408      0.2127417446
  0.9321305774      0.2591817107
  1.0229571916      0.2807801867
  1.6732749920      0.3390945746
  2.3369609291      0.3930932589
  3.9114862391      0.4287314927
  6.4413949082      0.4913665737
      9999
1NODE1ANODE1B          5.273543.78013.800
2XBUS1A                .00043.40291.12701
TRANSFORMER T31A                T31B
1NODE1BNODE1C
2XBUS1B
TRANSFORMER T31A                T31C
1NODE1CNODE1A
2XBUS1C
C
TRANSFORMER          .93214.25918T32A                1
  0.4425072187      0.1155510978
  0.5579938682      0.1522670097
  0.7377335408      0.2127417446
  0.9321305774      0.2591817107
  1.0229571916      0.2807801867
  1.6732749920      0.3390945746
  2.3369609291      0.3930932589
  3.9114862391      0.4287314927
  6.4413949082      0.4913665737
      9999
1NODE2ANODE2B          5.273543.78013.800
2XBUS2A                .00043.40291.12701

TRANSFORMER T32A                T32B
1NODE2BNODE2C
2XBUS2B

```



```

TRANSFORMER T32A
1NODE2CNODE2A
2XBUS2C
C
TRANSFORMER .93214.25918T33A
0.4425072187 0.1155510978
0.5579938682 0.1522670097
0.7377335408 0.2127417446
0.9321305774 0.2591817107
1.0229571916 0.2807801867
1.6732749920 0.3390945746
2.3369609291 0.3930932589
3.9114862391 0.4287314927
6.4413949082 0.4913665737
9999
1NODE3ANODE3B 5.273543.78013.800
2XBUS3A .00043.40291.12701
TRANSFORMER T33A T33B
1NODE3BNODE3C
2XBUS3B
TRANSFORMER T33A T33C
1NODE3CNODE3A
2XBUS3C
C
BLANK END OF CIRCUIT DATA
C
C .....SWITCH DATA.....
C 1 2 3 4 5 6 7 8
C 34567890123456789012345678901234567890123456789012345678901234567890
C Bus-->Bus--><---Tclose<---Topen<-----Ie
NODE1AFALT1A 9990. 9999. 0.0 0
NODE1BFALT1B 9990. 9999. 0.0 0
NODE1CFALT1C 9990. 9999. 0.0 0
NODE2AFALT2A 9990. 9999. 0.0 0
NODE2BFALT2B 9990. 9999. 0.0 0
NODE2CFALT2C 9990. 9999. 0.0 0
NODE3AFALT3A 9990. 9999. 0.0 0
NODE3BFALT3B 9990. 9999. 0.0 0
NODE3CFALT3C 9990. 9999. 0.0 0
NODE4AFALT4A 9990. 9999. 0.0 0
NODE4BFALT4B 9990. 9999. 0.0 0
NODE4CFALT4C 9990. 9999. 0.0 0
NODE2ACAP1A -1. 9999. 0.0 0
NODE2BCAP1B -1. 9999. 0.0 0
NODE2CCAP1C -1. 9999. 0.0 0
NODE4ACAP2A -1. 9999. 0.0 0
NODE4BCAP2B -1. 9999. 0.0 0
NODE4CCAP2C -1. 9999. 0.0 0
NODE4ALOAD4A -1. 9999. 0.0 0
NODE4BLOAD4B -1. 9999. 0.0 0
NODE4CLOAD4C -1. 9999. 0.0 0
XBUS1ALOAD1A -1. 9999. 0.0 0
XBUS1BLOAD1B -1. 9999. 0.0 0
XBUS1CLOAD1C -1. 9999. 0.0 0
XBUS2ALOAD2A -1. 9999. 0.0 0
XBUS2BLOAD2B -1. 9999. 0.0 0
XBUS2CLOAD2C -1. 9999. 0.0 0
XBUS3ALOAD3A -1. 9999. 0.0 0
XBUS3BLOAD3B -1. 9999. 0.0 0
XBUS3CLOAD3C -1. 9999. 0.0 0

```

```

C
BLANK END OF SWITCH DATA
C .....SOURCE DATA.....
C      1      2      3      4      5      6      7      8
C 3456789012345678901234567890123456789012345678901234567890
C Bus--><I<Amplitude<Frequency<--Phase--<-----<-----Tstart<-----Tstop
14STHEVA      93897      60.0      0.0      0.0      -1.0      9999.
14STHEVB      93897      60.0     -120.0      0.0      -1.0      9999.
14STHEVC      93897      60.0      120.0      0.0      -1.0      9999.
C
BLANK END OF SOURCE DATA
C .....OUTPUT REQUEST DATA.....
C Bus-->Bus-->Bus-->Bus-->Bus-->Bus-->Bus-->Bus-->Bus-->Bus-->Bus-->
  NODE1ANODE1BNODE1CNODE2ANODE2BNODE2CNODE3ANODE3BNODE3CNODE4ANODE4BNODE4C
  STHEVASTHEVBSTHEVCBUSTHABUSTHBBUSTHCBUS13ABUS13BBUS13C
C
BLANK END OF OUTPUT REQUESTS
BLANK END OF ALL CASES

```

## **Appendix B**

# **VOLTAGE AND CURRENT WAVEFORMS FOR SIMULATED CASES**

This appendix includes graphical illustrations of some of the voltage and current waveforms, for the various event types and fault scenarios simulated in this work, other than those covered in Chapter 4.

As mentioned earlier, analysis of these waveforms show that the most apparent effect on the voltage waveforms for the various cases simulated is the small change in voltage magnitude. The current waveforms, however, are quite different for each of the simulated cases depending on the event type. Transients are always present whenever capacitor switching is involved. The amount of the transients as well as the time it takes to extinguish these transients are varying for each case.

Descriptions of the figures included in this appendix are similar to the corresponding descriptions for the figures presented in Sections 4.3.1 and 4.3.2.

## **B.1 Normal Load Switching**

Figures B.1.1 to B.1.6 show the voltage and current waveforms for switching of Load-2 and Load-4 of the feeder model of Figure 4.1.

## **B.2 Normal Load and Capacitor Switching**

Voltage and current waveforms resulting from switching Load-1 and capacitors C1 and C2 are shown in Figures B.2.1 to B.2.4. Figures B.2.5 and B.2.6, however, illustrate the waveforms for switching Load-2 and capacitor C2.

## **B.3 HIF with No Load or Capacitor Switching**

Figures B.3.1 to B.3.6 show the waveforms for HIFs on different phases at Node-1, Node-2 and Node-4.

## **B.4 HIF with Load Switching**

Graphical illustrations for waveforms due to HIFs on Phase-B at Node-2 with Load-2 switching, are given in Figures B.4.1 to B.4.4.

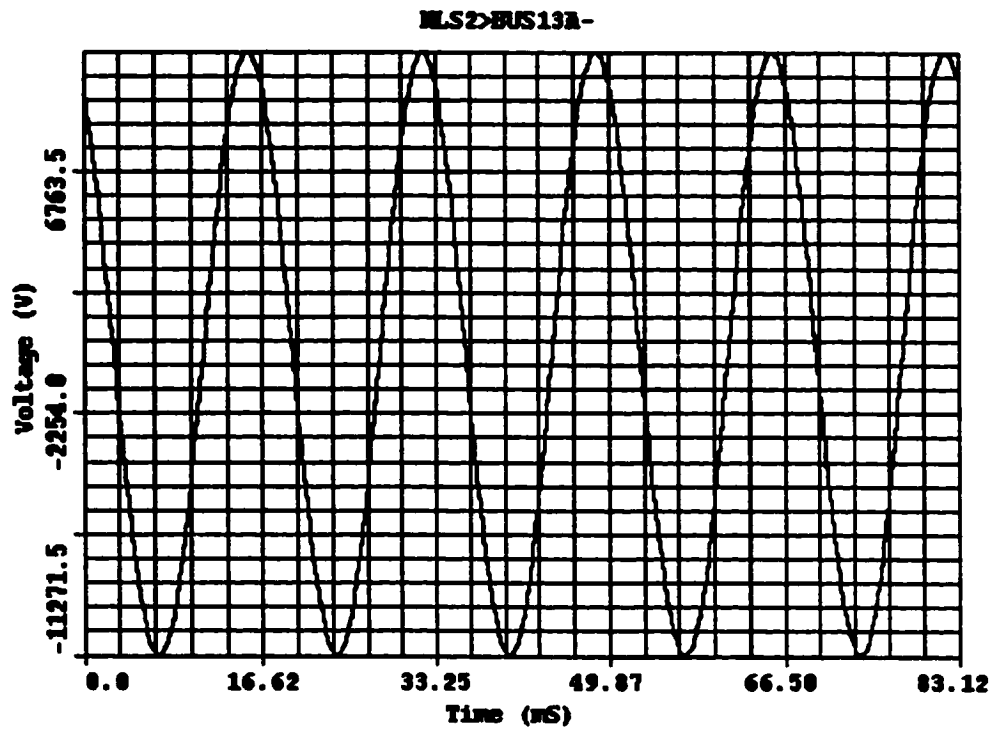


**Figure B.1.1: Phase-A Voltage Waveform for Load-2 Switching**

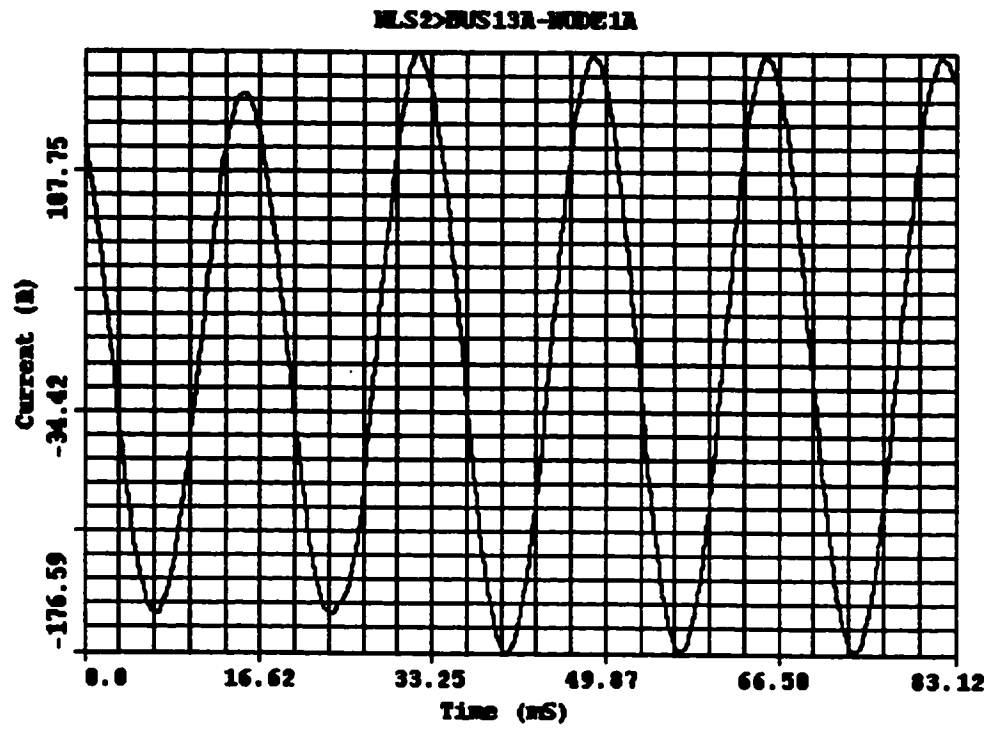


**Figure B.1.2: Phase-A Current Waveform for Load-2 Switching**

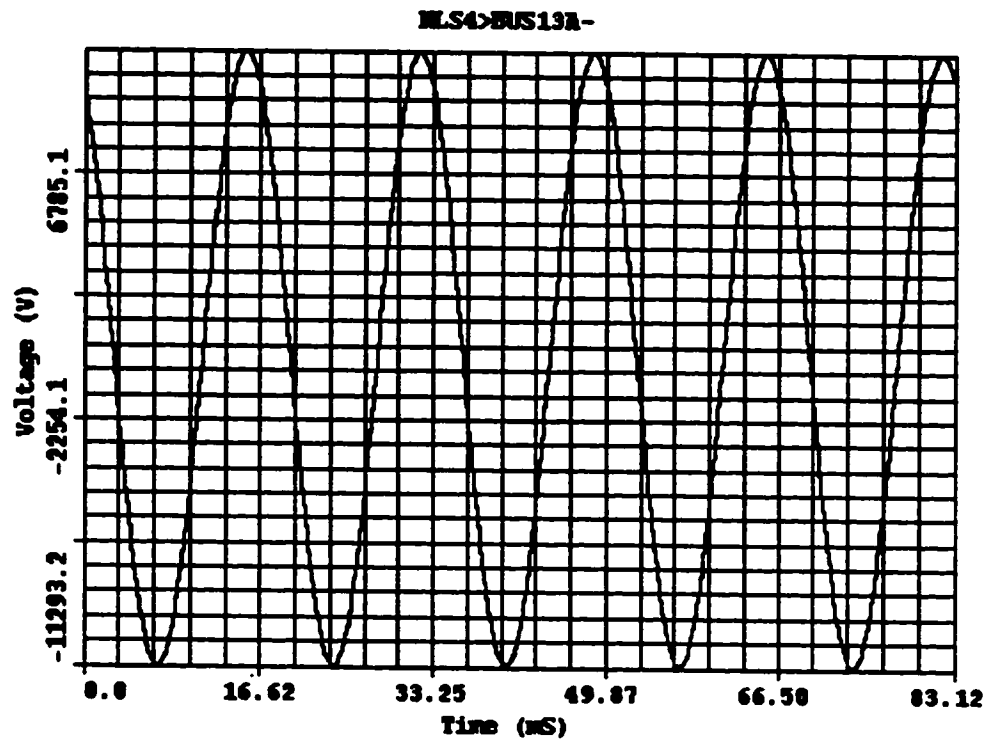


**Figure B.1.3: Phase-A Voltage Waveform for Load-4 Switching**

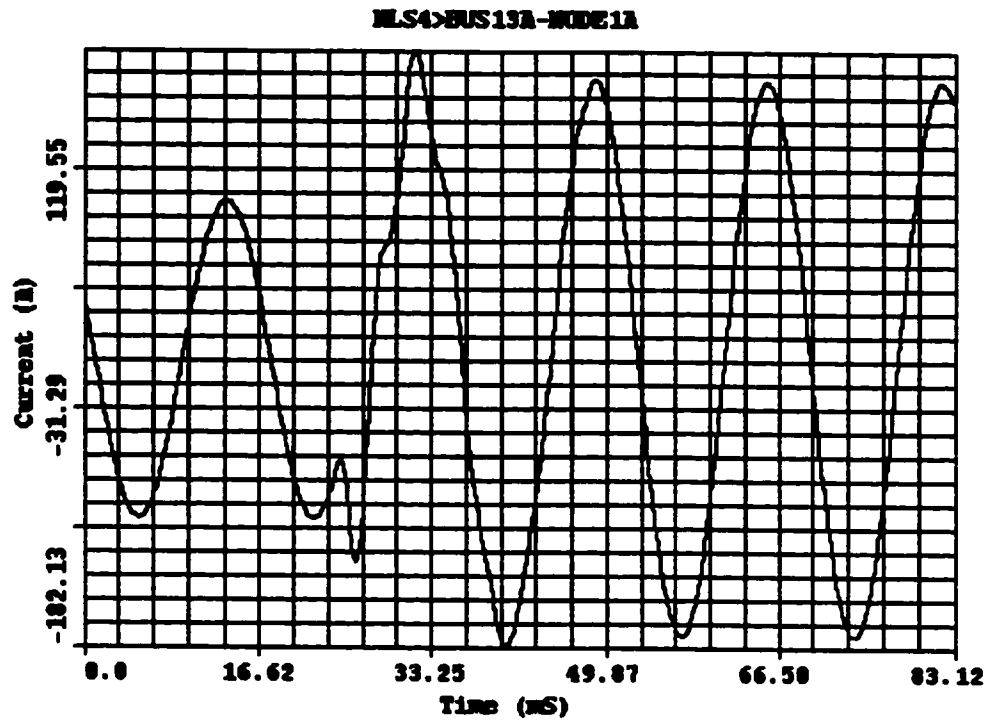


**Figure B.1.4: Phase-A Current Waveform for Load-4 Switching**



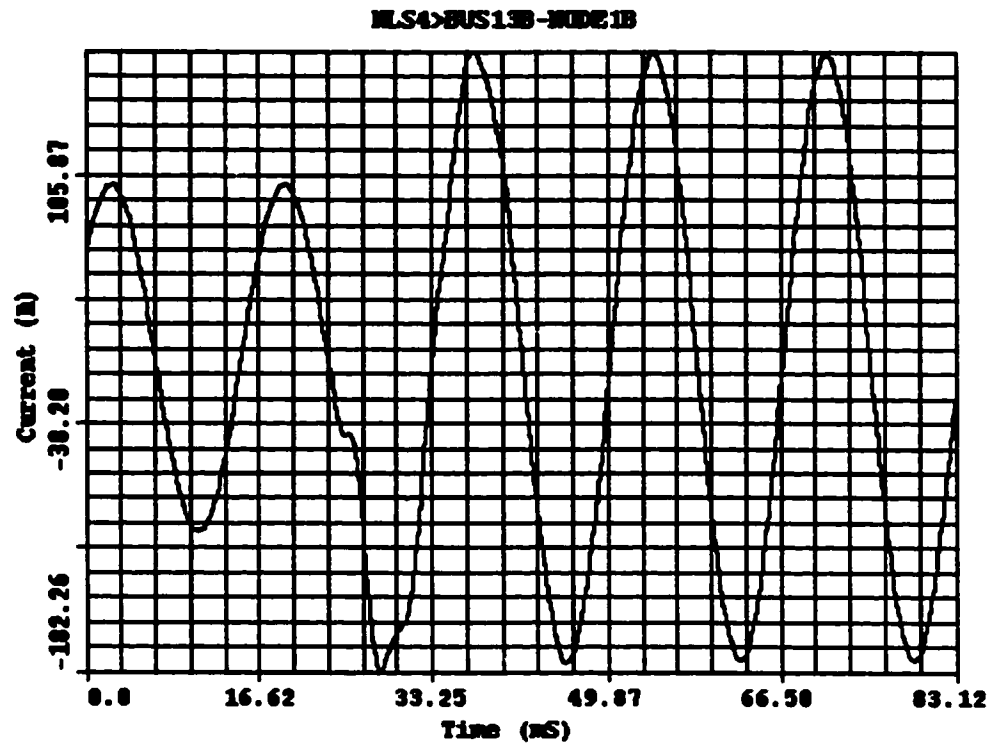


**Figure B.1.5: Phase-B Current Waveform for Load-4 Switching**

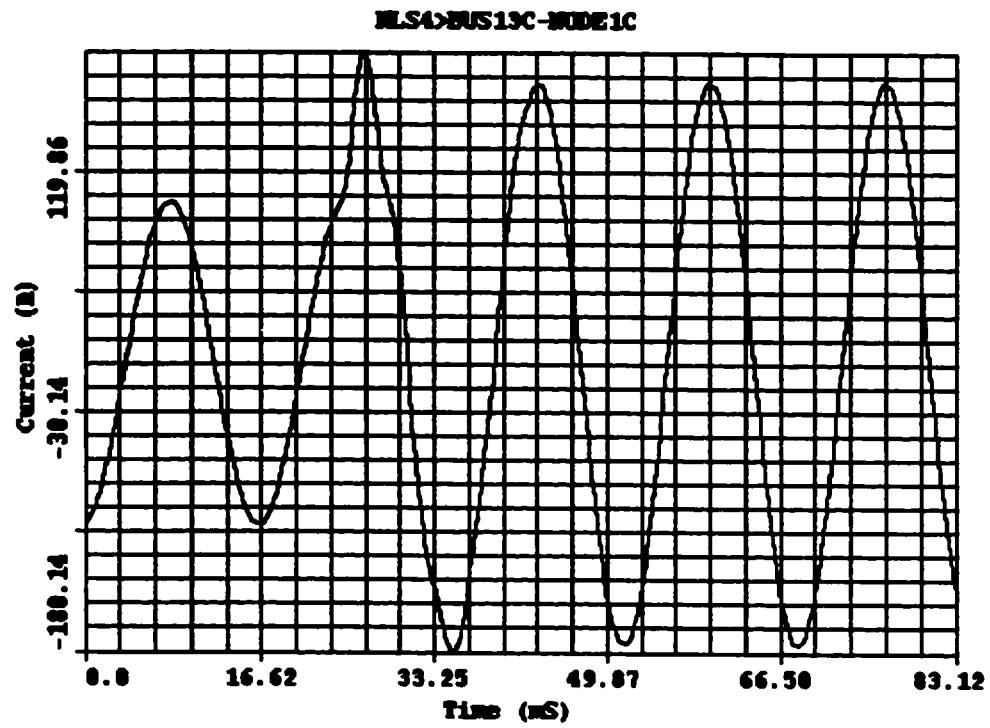


**Figure B.1.6: Phase-C Current Waveform for Load-4 Switching**

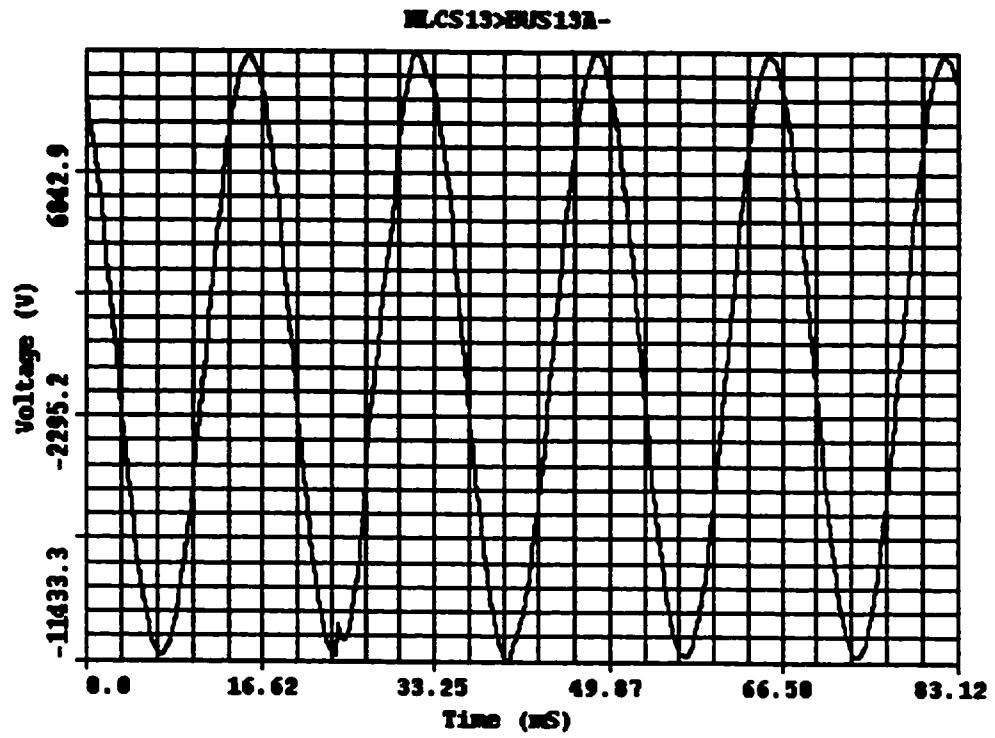


**Figure B.2.1: Phase-A Voltage Waveform for Load-1 and C1 & C2 Switching**

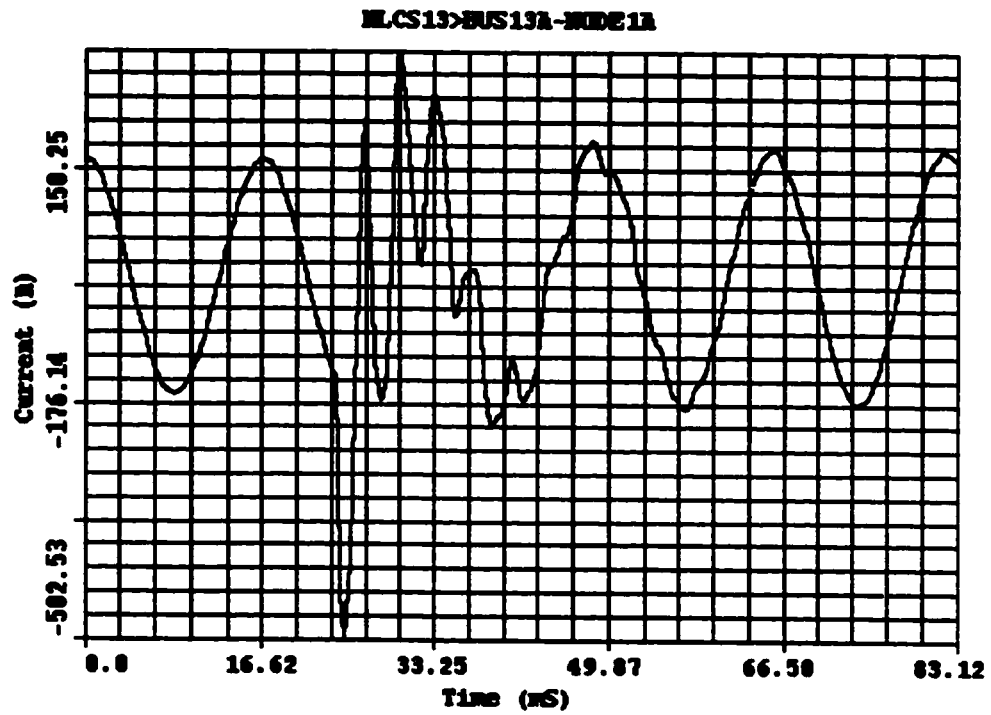


**Figure B.2.2: Phase-A Current Waveform for Load-1 and C1 & C2 Switching**

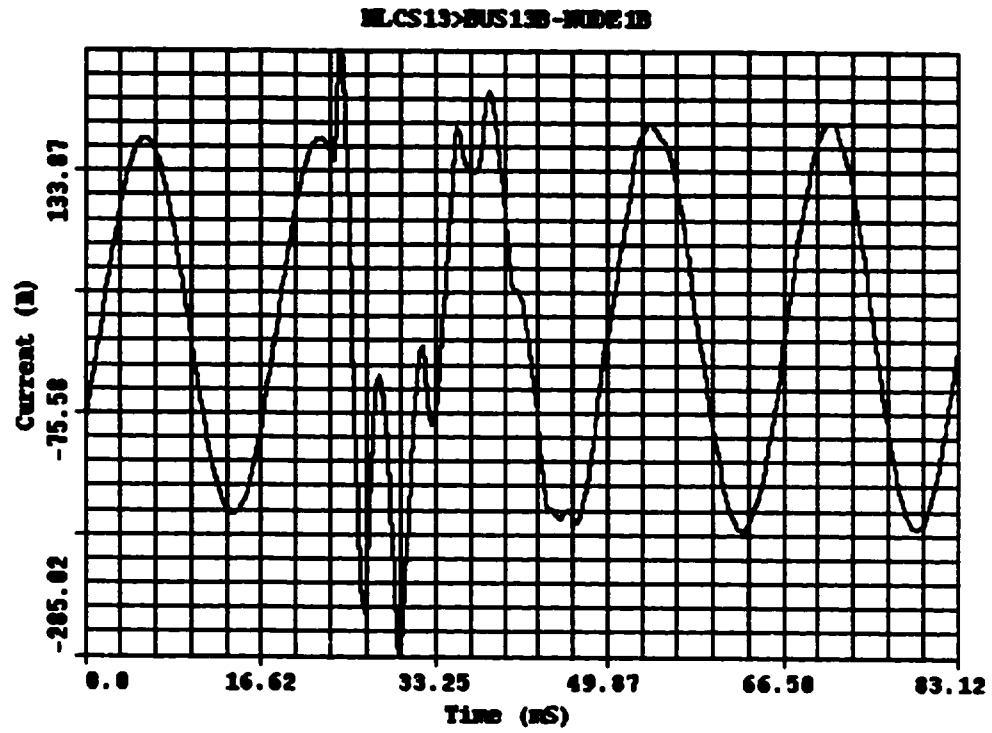


**Figure B.2.3: Phase-B Current Waveform for Load-1 and C1 & C2 Switching**

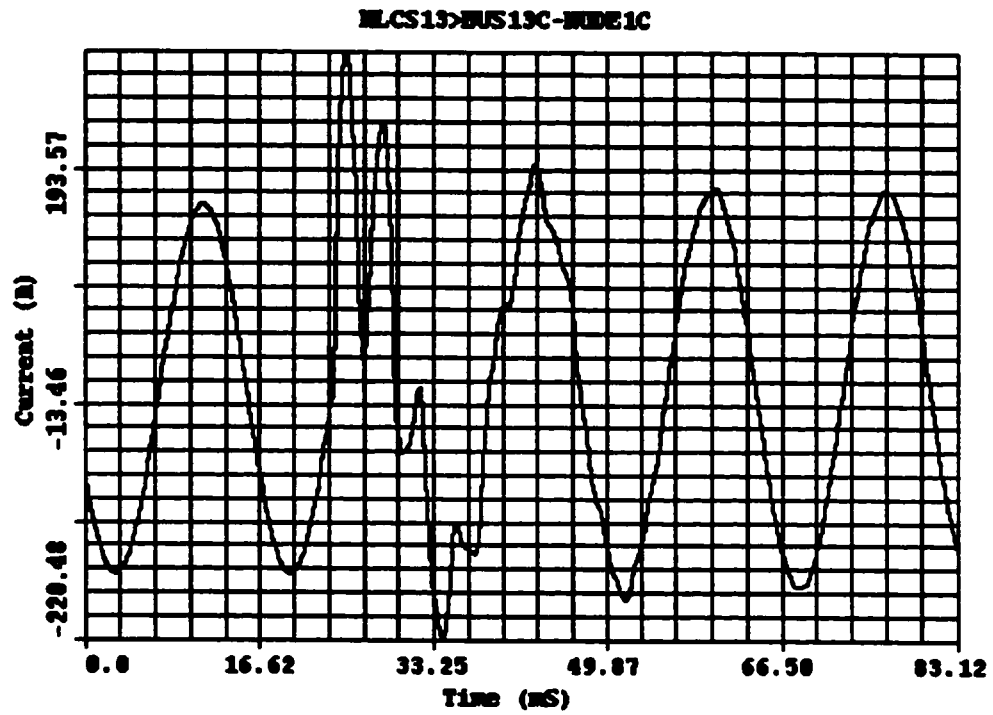


**Figure B.2.4: Phase-C Current Waveform for Load-1 and C1 & C2 Switching**

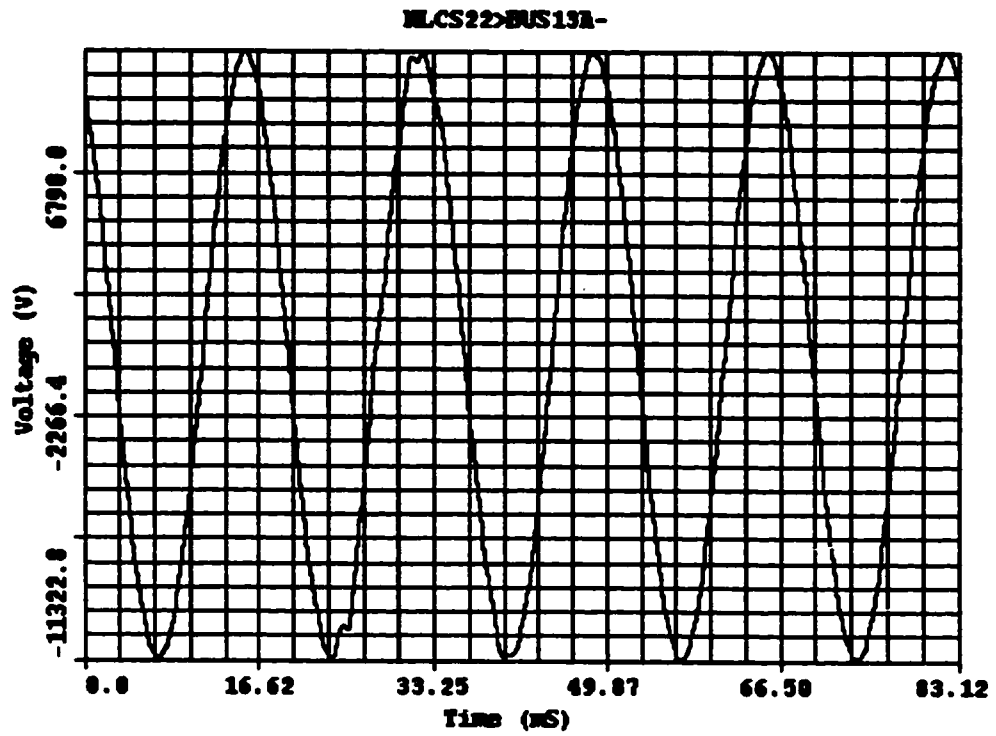


**Figure B.2.5: Phase-A Voltage Waveform for Load-2 and C2 Switching**

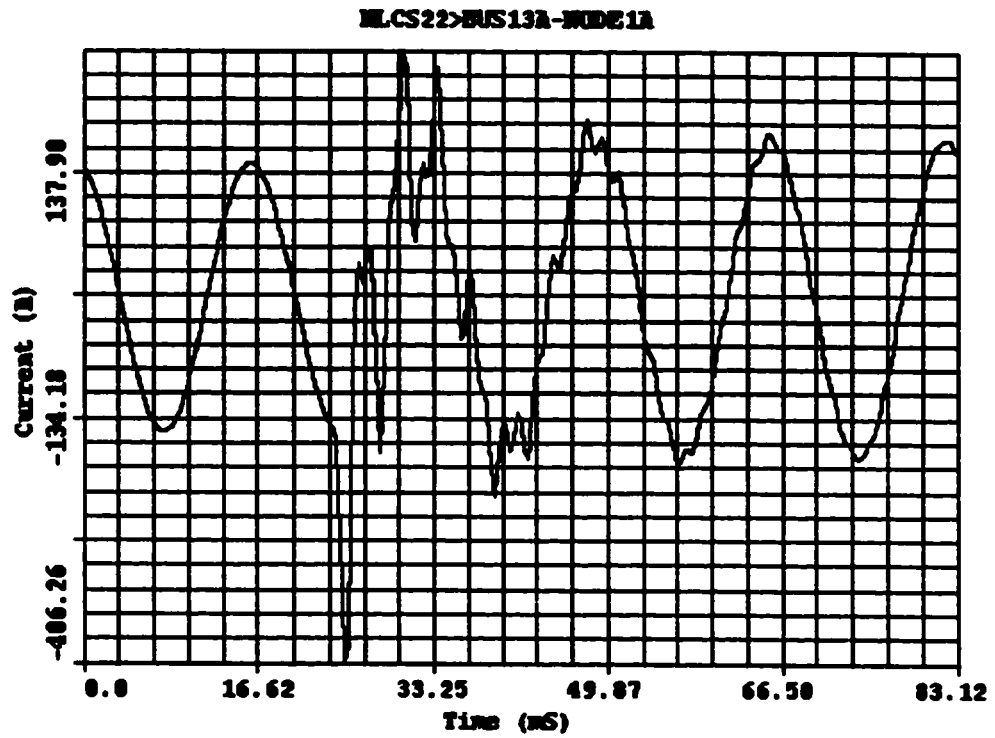


**Figure B.2.6: Phase-A Current Waveform for Load-2 and C2 Switching**



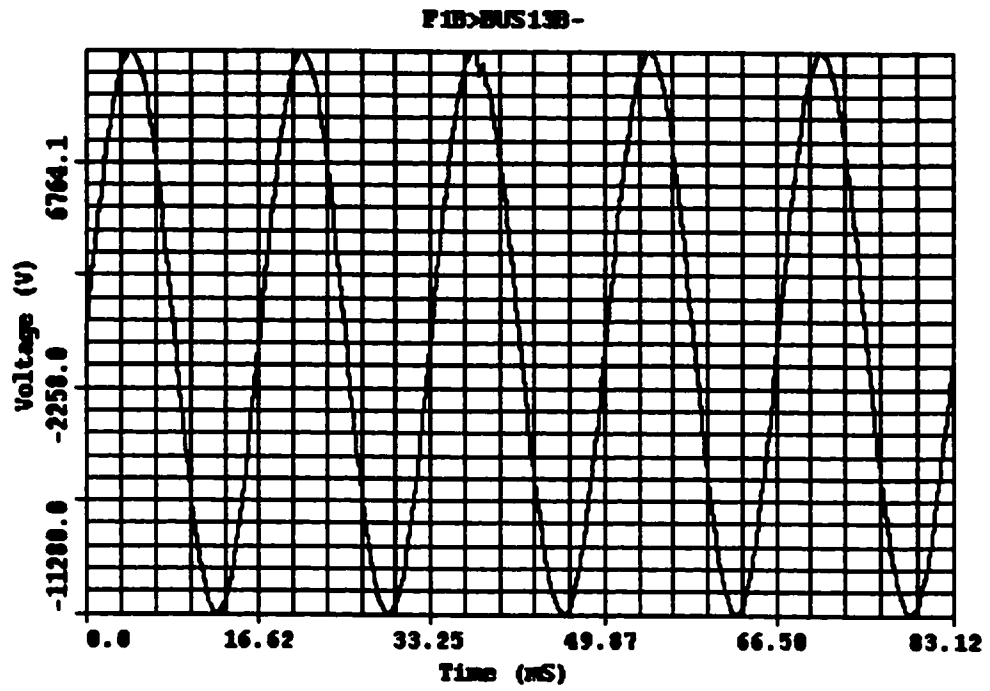


**Figure B.3.1: Phase-B Voltage Waveform for HIF on Phase-B at Node-1**

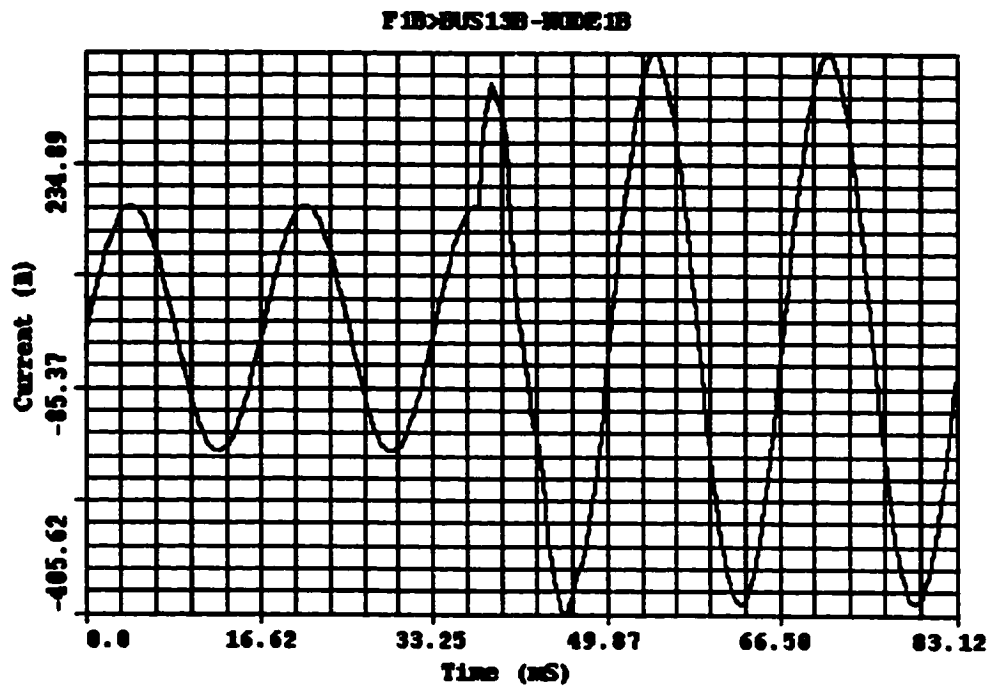


**Figure B.3.2: Phase-B Current Waveform for HIF on Phase-B at Node-1**

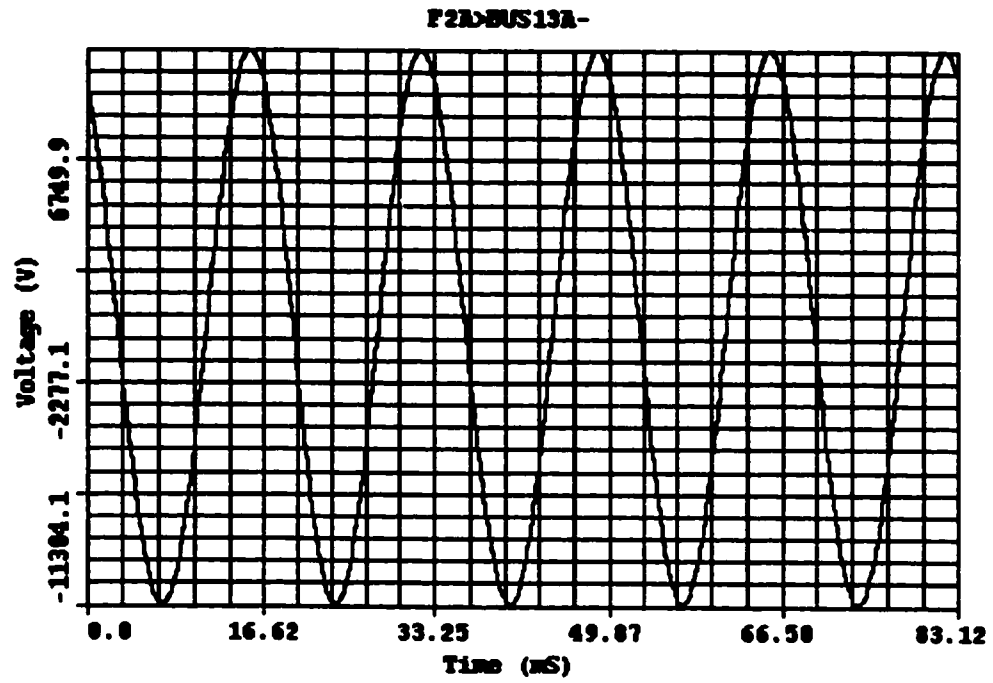


**Figure B.3.3: Phase-A Voltage Waveform for HIF on Phase-A at Node-2**

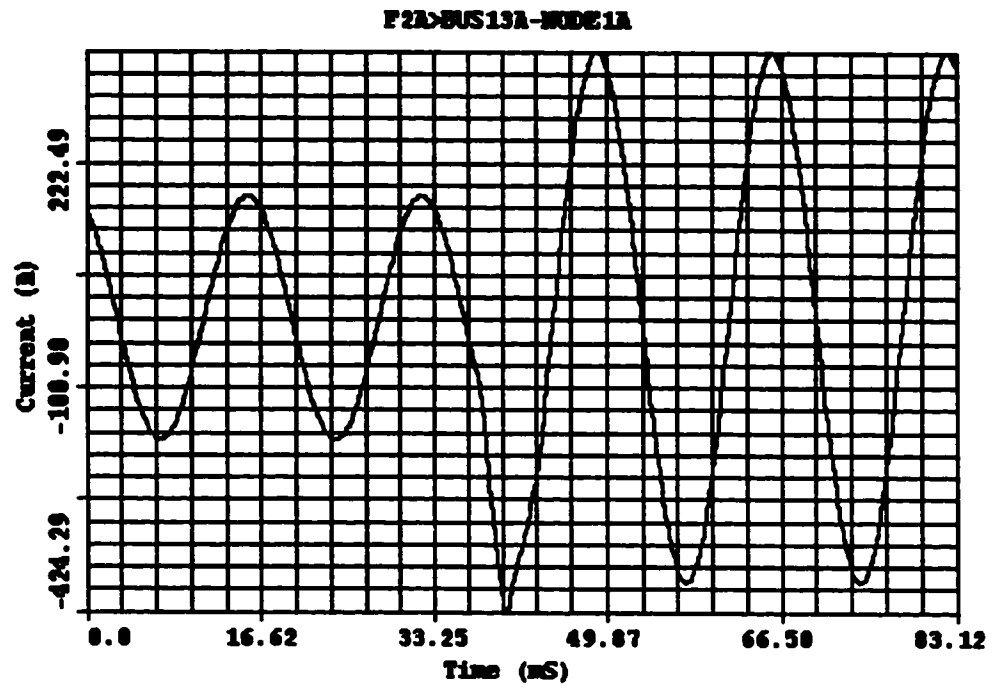


**Figure B.3.4: Phase-A Current Waveform for HIF on Phase-A at Node-2**

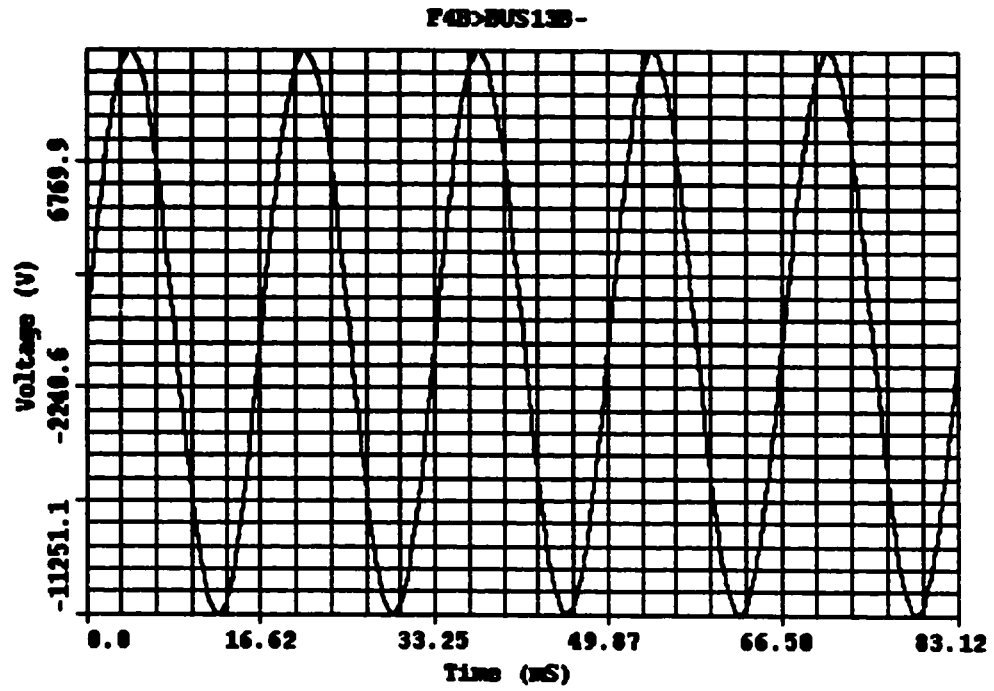


**Figure B.3.5: Phase-B Voltage Waveform for HIF on Phase-B at Node-4**

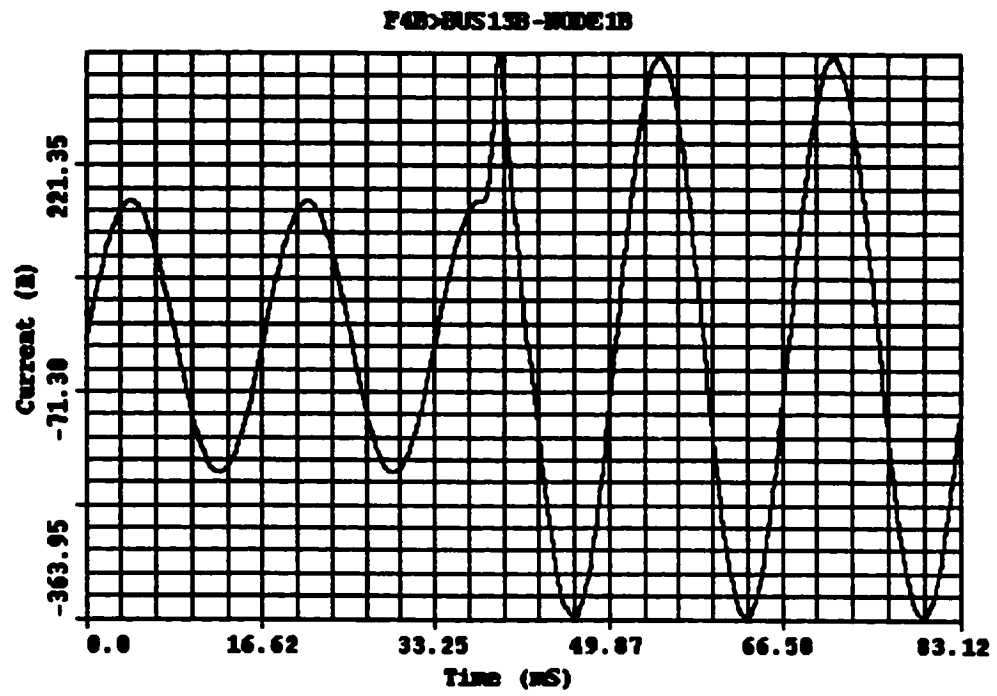


**Figure B.3.6: Phase-B Current Waveform for HIF on Phase-B at Node-4**

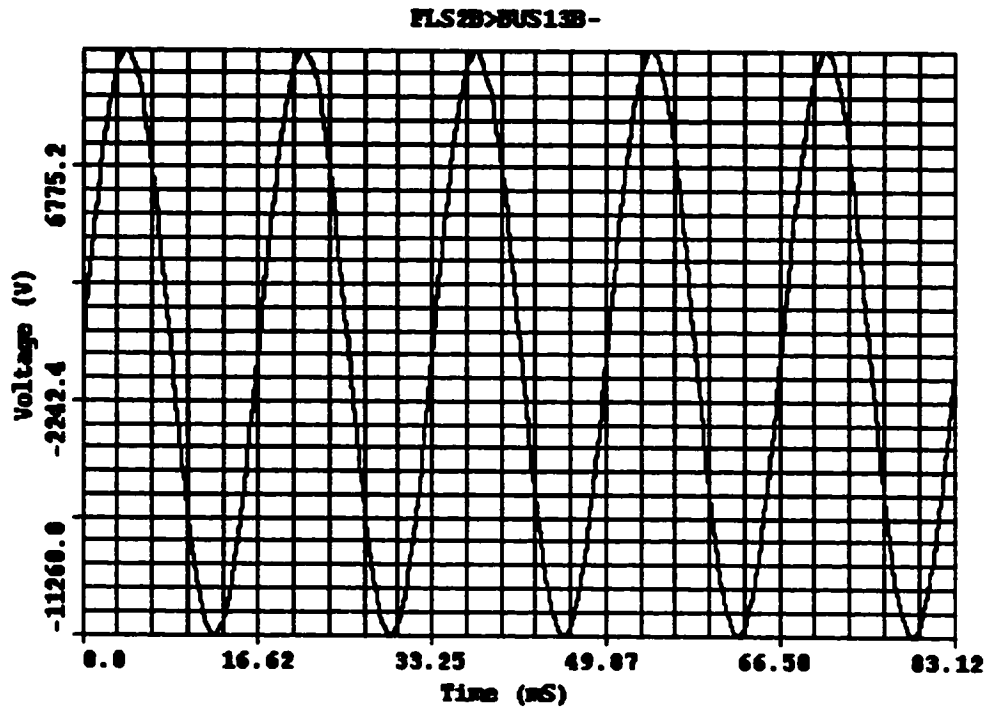


**Figure B.4.1: Phase-B Voltage Waveform for HIF on Phase-B at Node-2  
with Load-2 Switching**

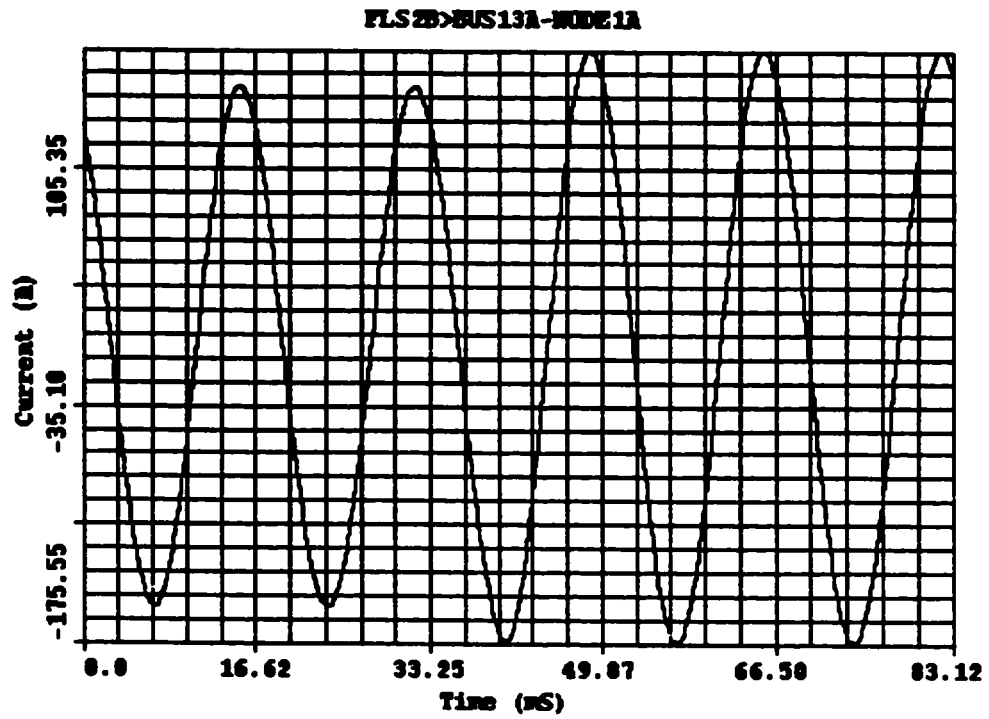


**Figure B.4.2: Phase-A Current Waveform for HIF on Phase-B at Node-2  
with Load-2 Switching**



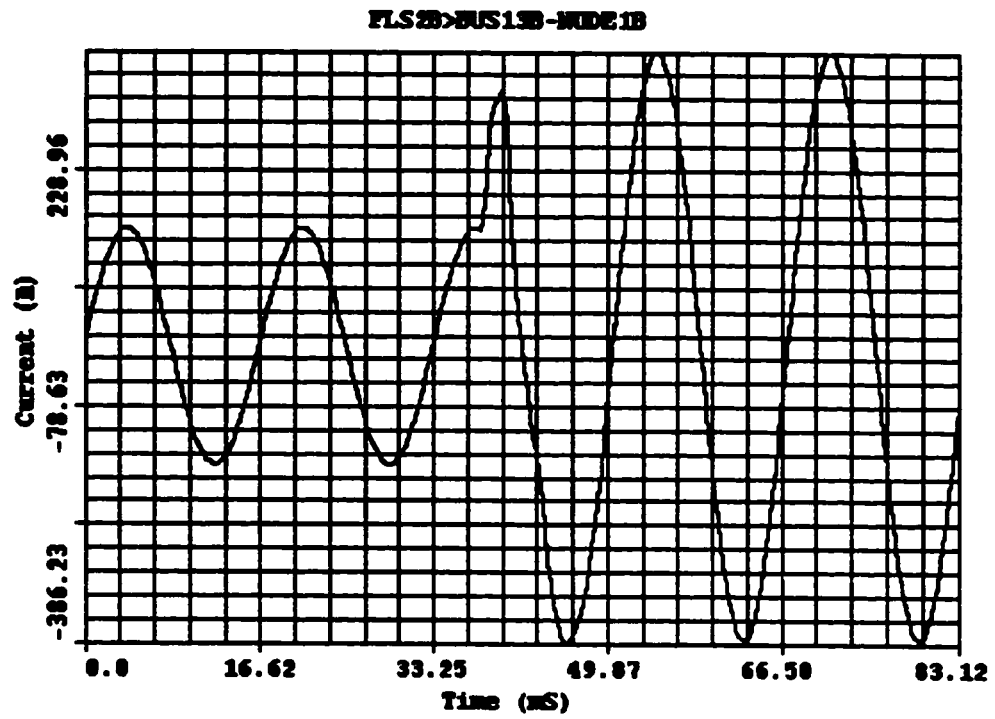


**Figure B.4.3: Phase-B Current Waveform for HIF on Phase-B at Node-2  
with Load-2 Switching**

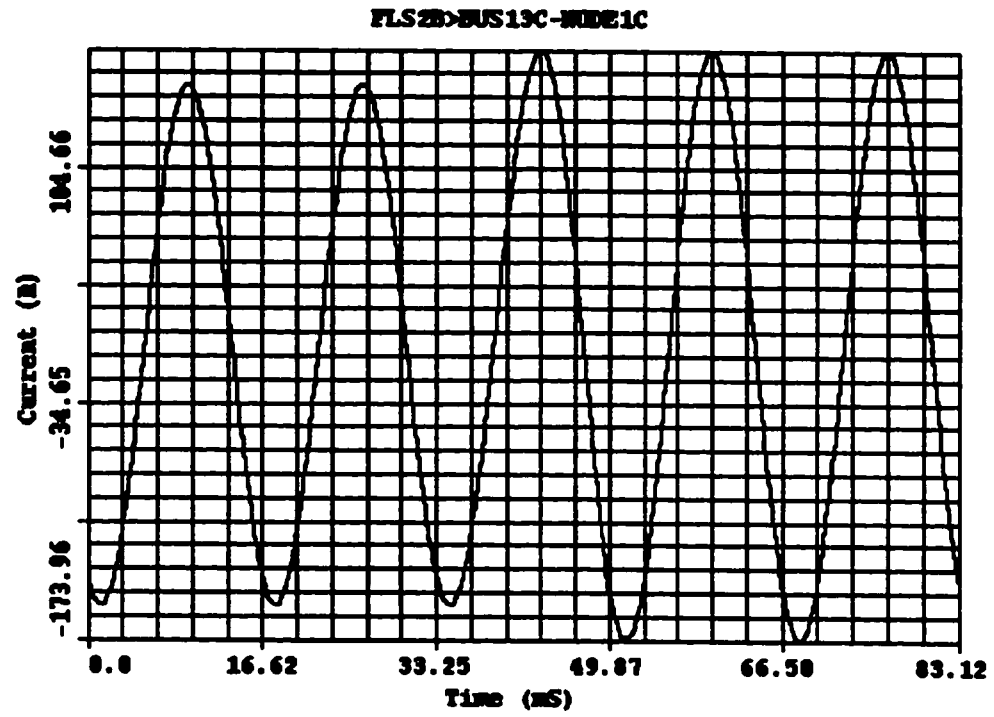


**Figure B.4.4: Phase-C Current Waveform for HIF on Phase-B at Node-2  
with Load-2 Switching**

## **B.5 HIF with Load and Capacitor Switching**

Figures B.5.1 to B.5.4 show the voltage and current waveforms due to a HIF on Phase-A at Node-1, with switching of Load-1 and Capacitor C1.

## **B.6 Mid-span HIFs**

Waveforms for HIFs that take place midway between Node-3 and Node-4 are shown in Figures B.6.1 to B.6.4.

## **B.7 HIF with Varying Fault Current**

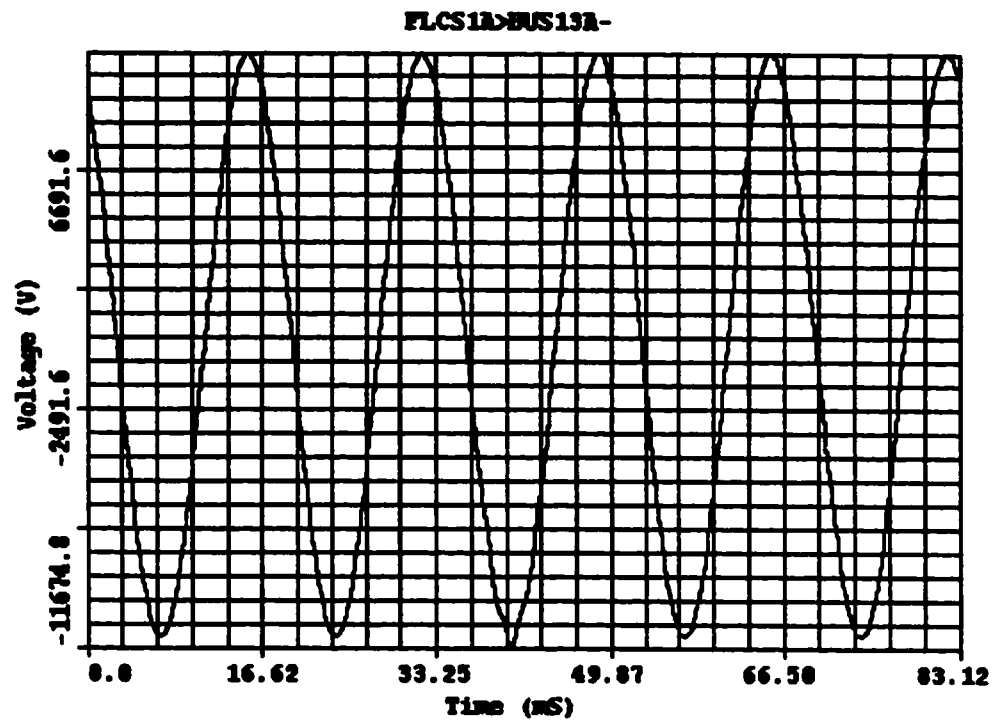
For HIFs that passes to ground a 50 % fault current, the voltage and current waveforms are illustrated in Figures B.7.1 to B.7.4.

## **B.8 HIF with Varying Line Impedance**

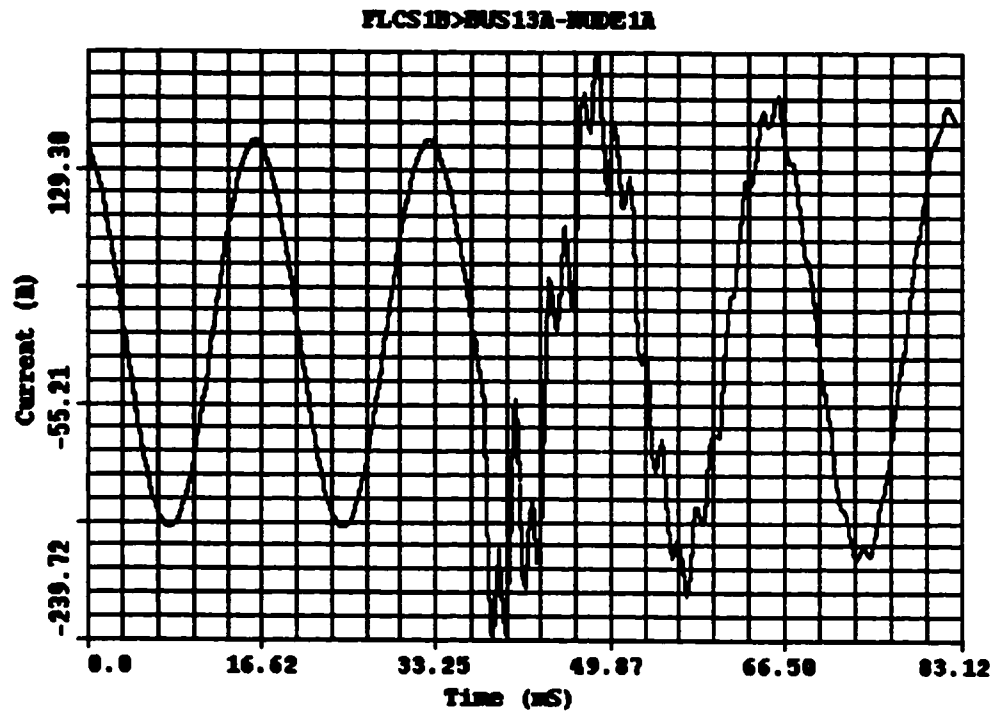
Figures B.8.1 to B.8.4 show waveforms for a HIF at Node-1 when the overhead line impedance is increased by 20 % above the line impedance used for simulation of the feeder model of Figure 4.1.

## **B.9 HIF for Extended Feeder**

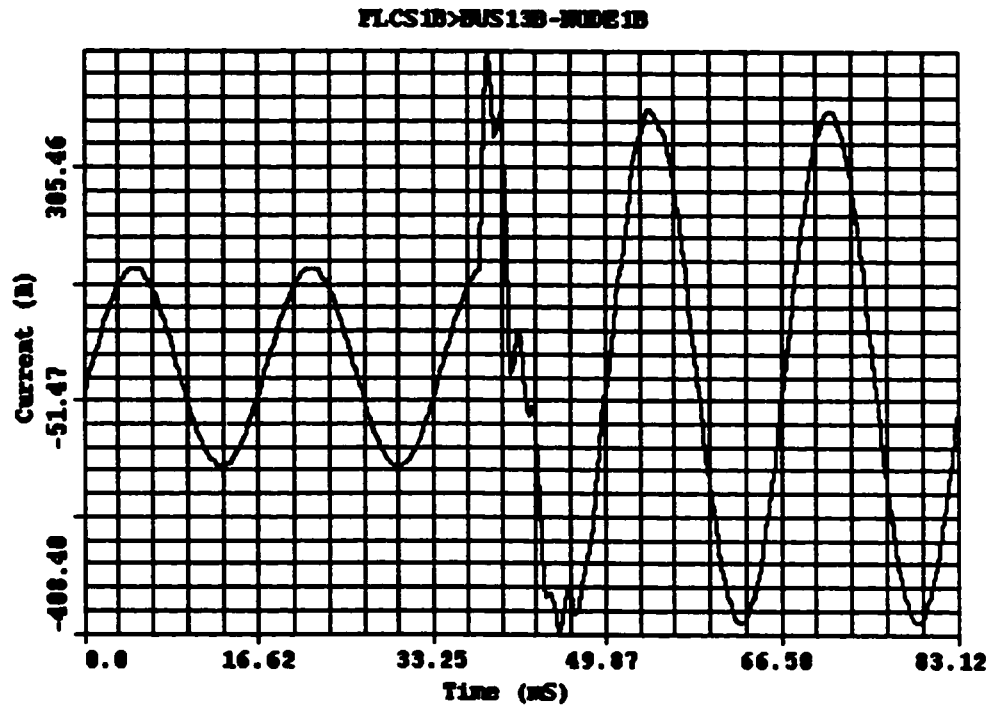
Figures B.9.1 and B.9.2 show the voltage and current waveforms for a HIF at Node-4 simulated on the model feeder of Figure 4.1, but with an additional branch added at the end of the feeder. This is just like simulating a different feeder from the feeder model. The



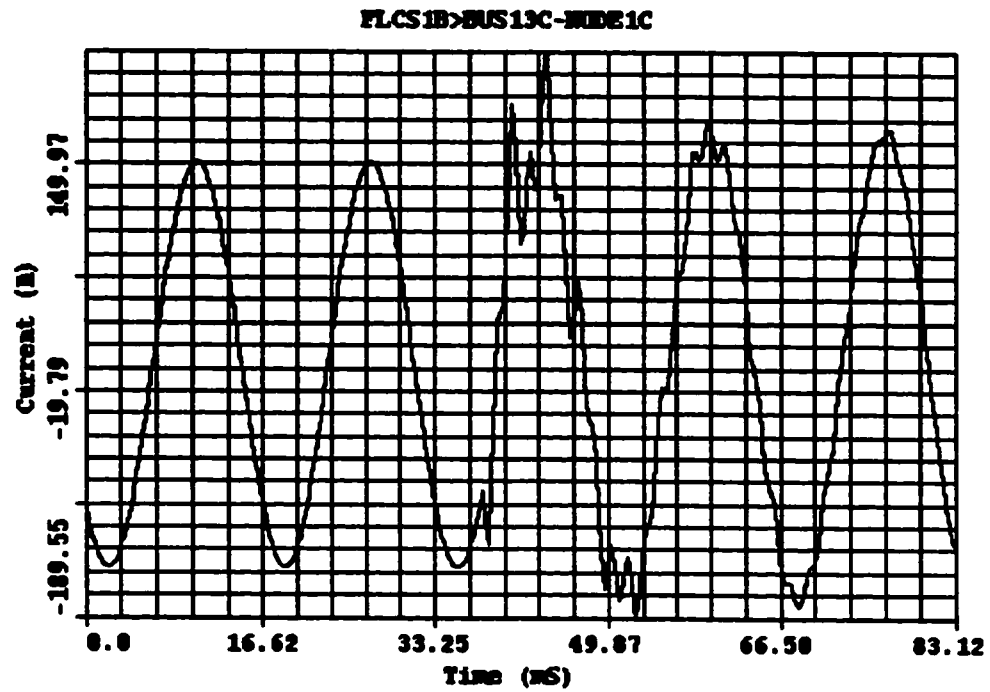
**Figure B.5.1: Phase-A Voltage Waveform for HIF on Phase-A at Node-1  
with Load-1 and Capacitor C1 Switching**



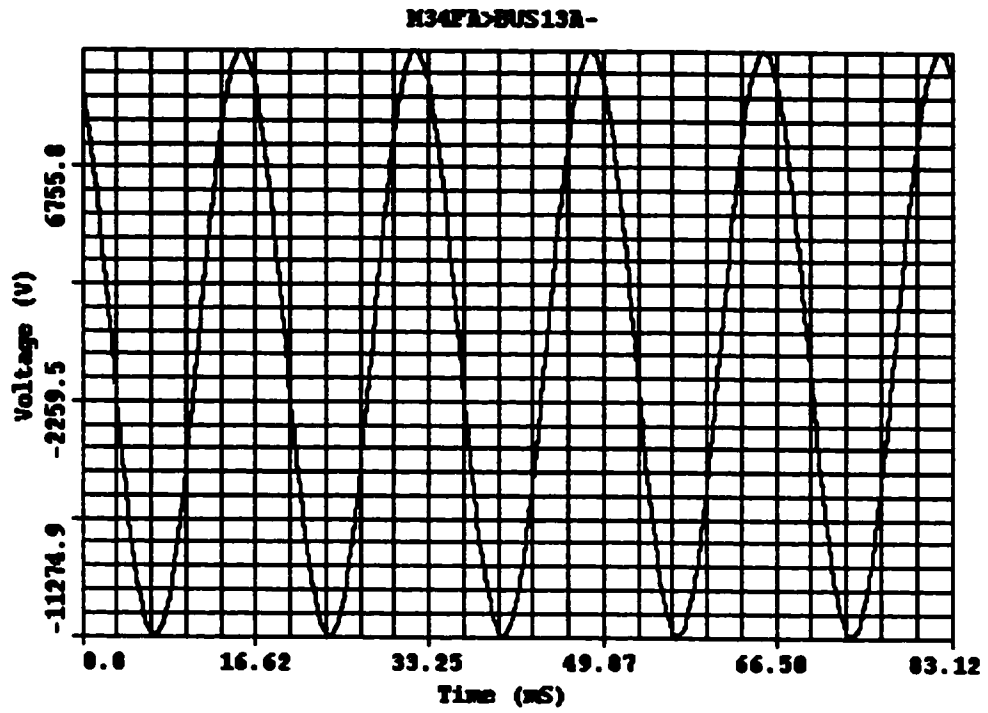
**Figure B.5.2: Phase-A Current Waveform for HIF on Phase-A at Node-1  
with Load-1 and Capacitor C1 Switching**



**Figure B.5.3: Phase-B Current Waveform for HIF on Phase-A at Node-1  
with Load-1 and Capacitor C1 Switching**

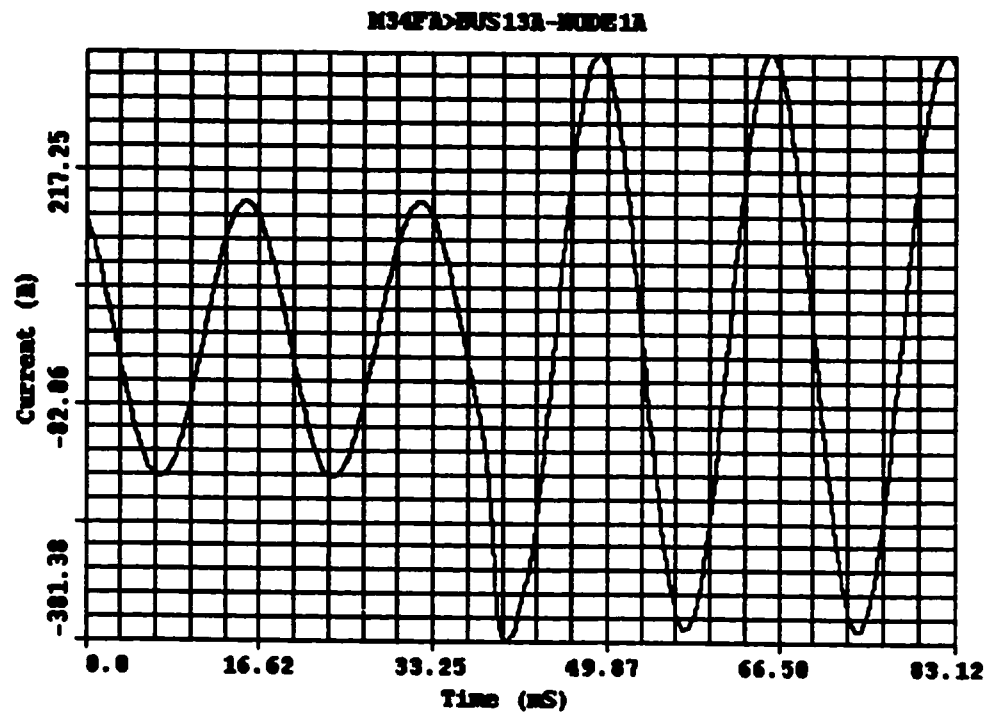


**Figure B.5.4: Phase-C Current Waveform for HIF on Phase-A at Node-1  
with Load-1 and Capacitor C1 Switching**



**Figure B.6.1: Phase-A Voltage Waveform for HIF on Phase-A  
Between Nodes-3 and 4**





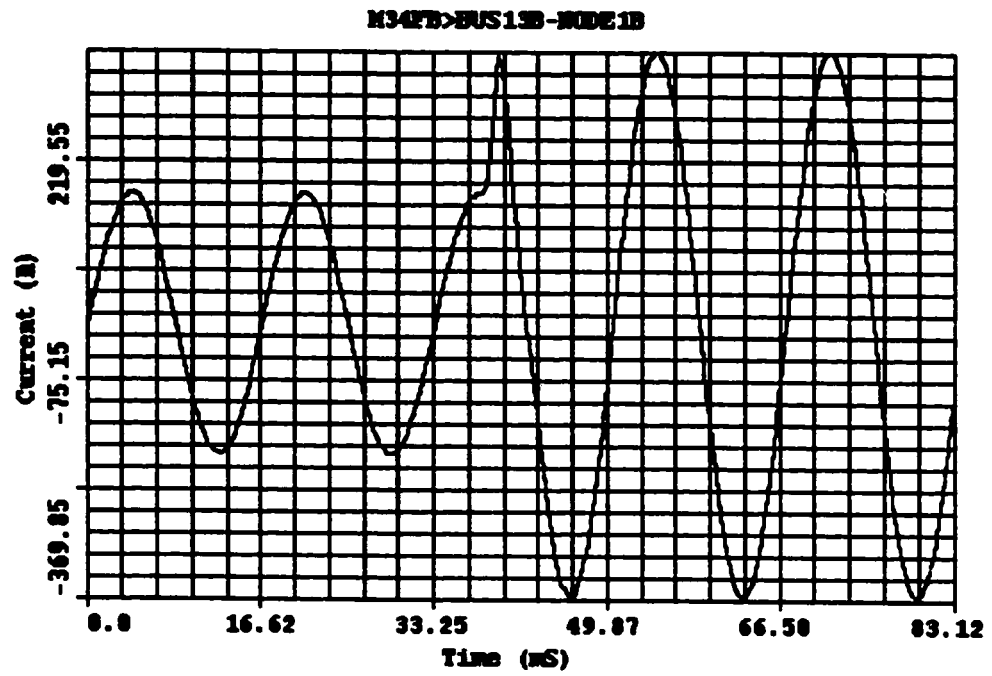


**Figure B.6.3: Phase-B Current Waveform for HIF on Phase-B  
Between Nodes-3 and 4**

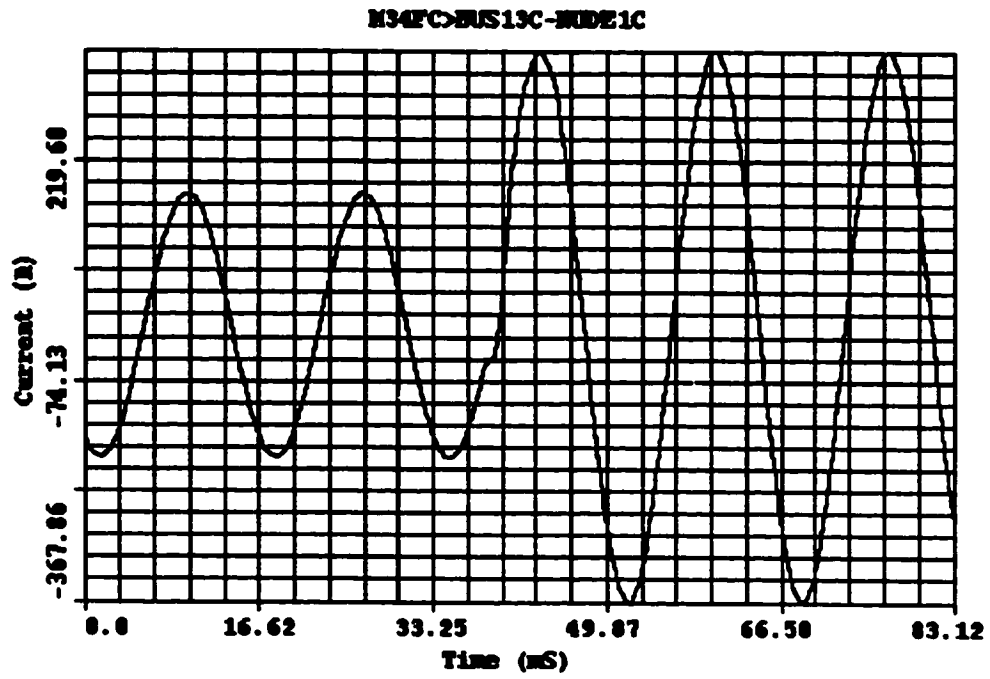


**Figure B.6.4: Phase-C Current Waveform for HIF on Phase-C**

**Between Nodes-3 and 4**

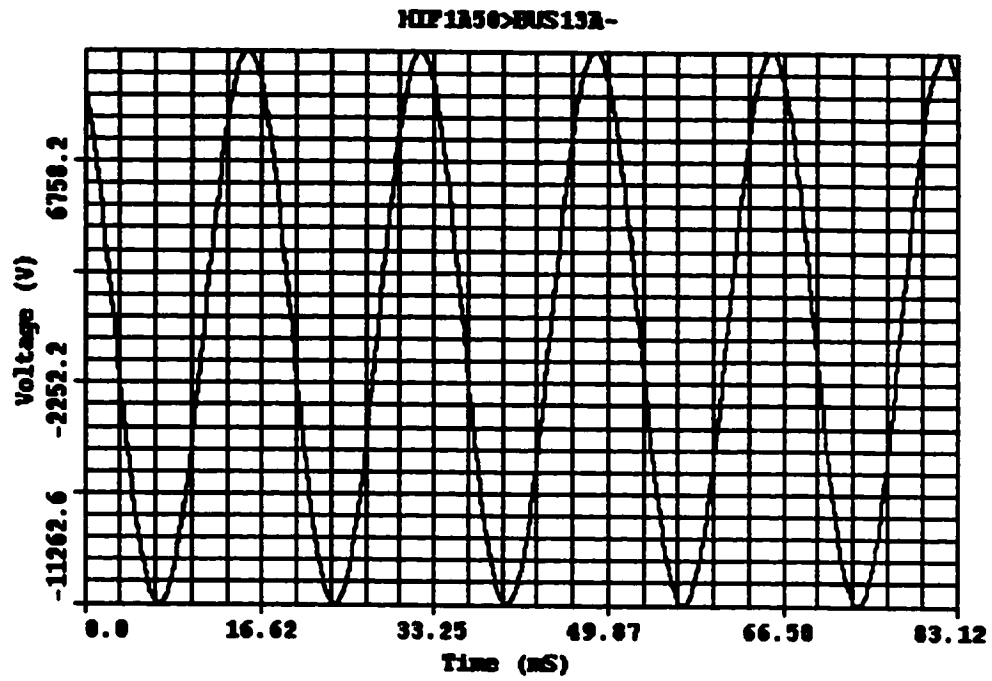


**Figure B.7.1: Phase-A Voltage Waveform for HIF at Node-1 (Phase-A)  
with 50 % Fault Current**

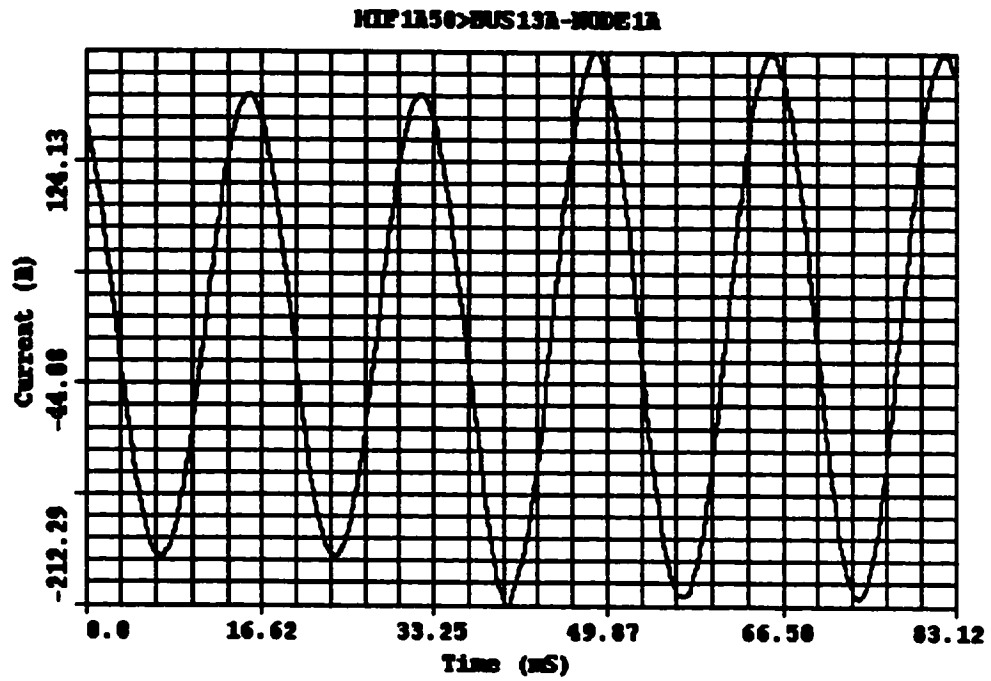


**Figure B.7.2: Phase-A Current Waveform for HIF at Node-1 (Phase-A)**

**with 50 % Fault Current**

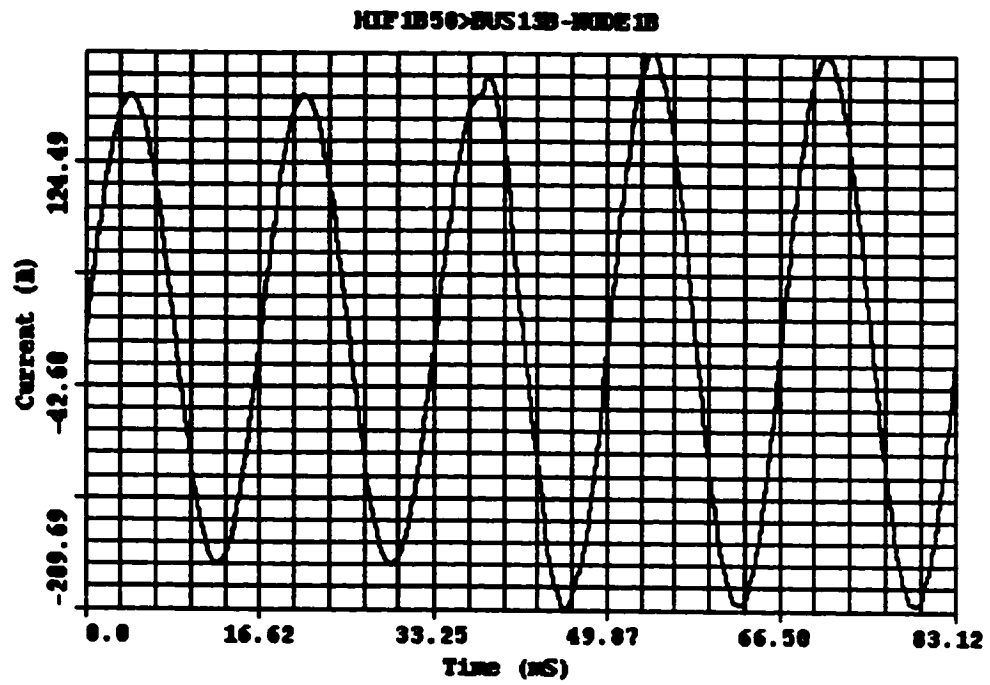


**Figure B.7.3: Phase-B Current Waveform for HIF at Node-1 (Phase-B)  
with 50 % Fault Current**

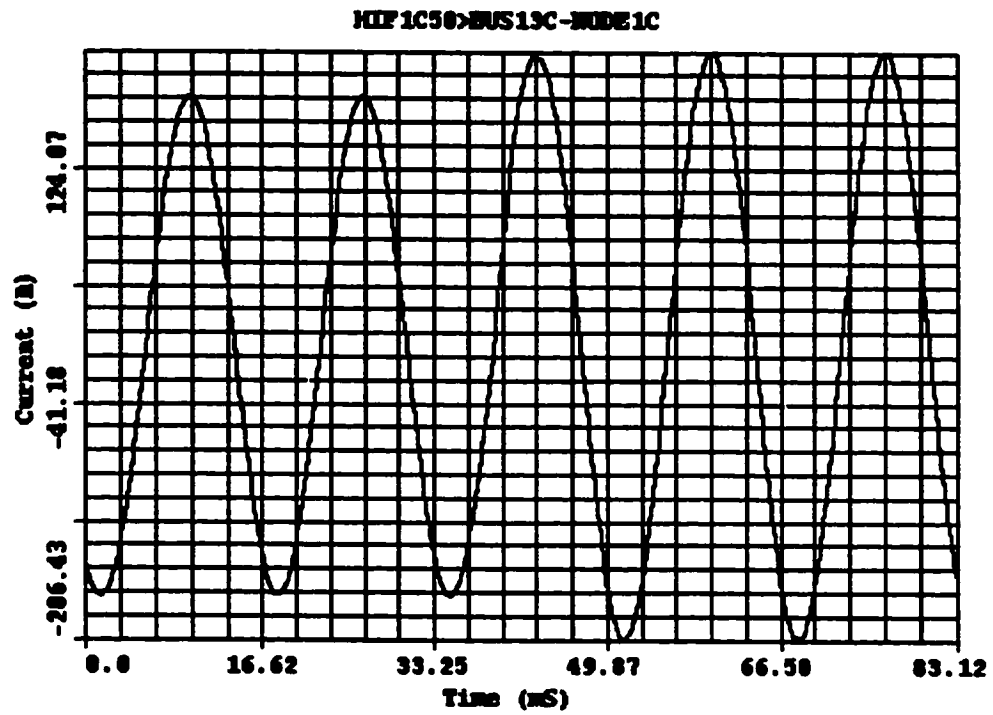


**Figure B.7.4: Phase-C Current Waveform for HIF at Node-1 (Phase-C)  
with 50 % Fault Current**

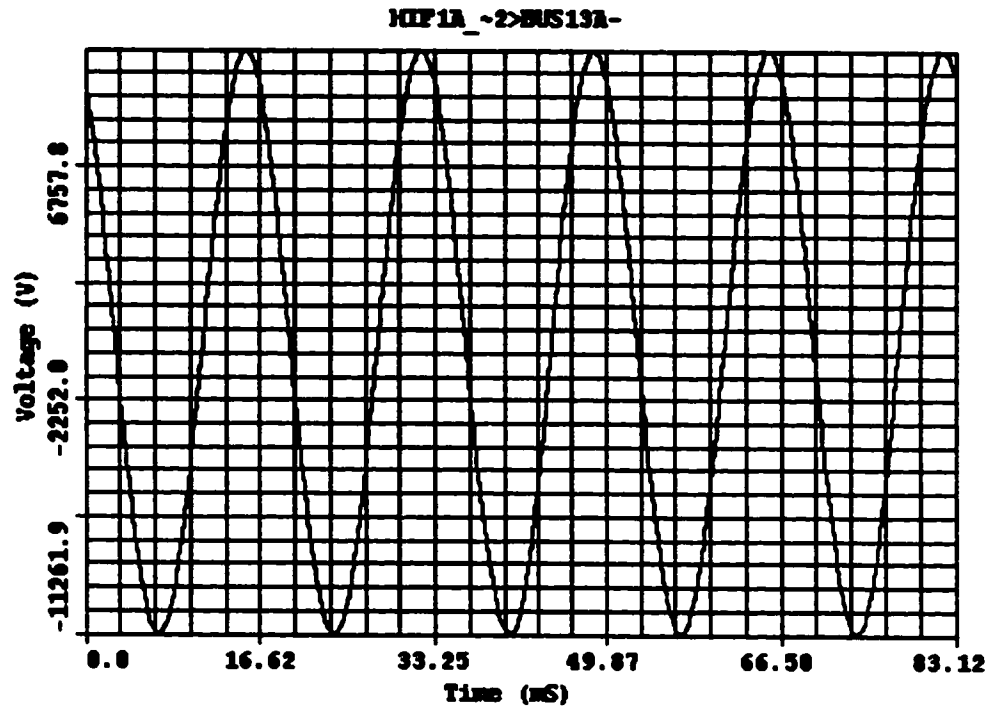


**Figure B.8.1: Phase-A Voltage Waveform for HIF at Node-1 (Phase-A)  
with Line Impedance Increased by 20 %**



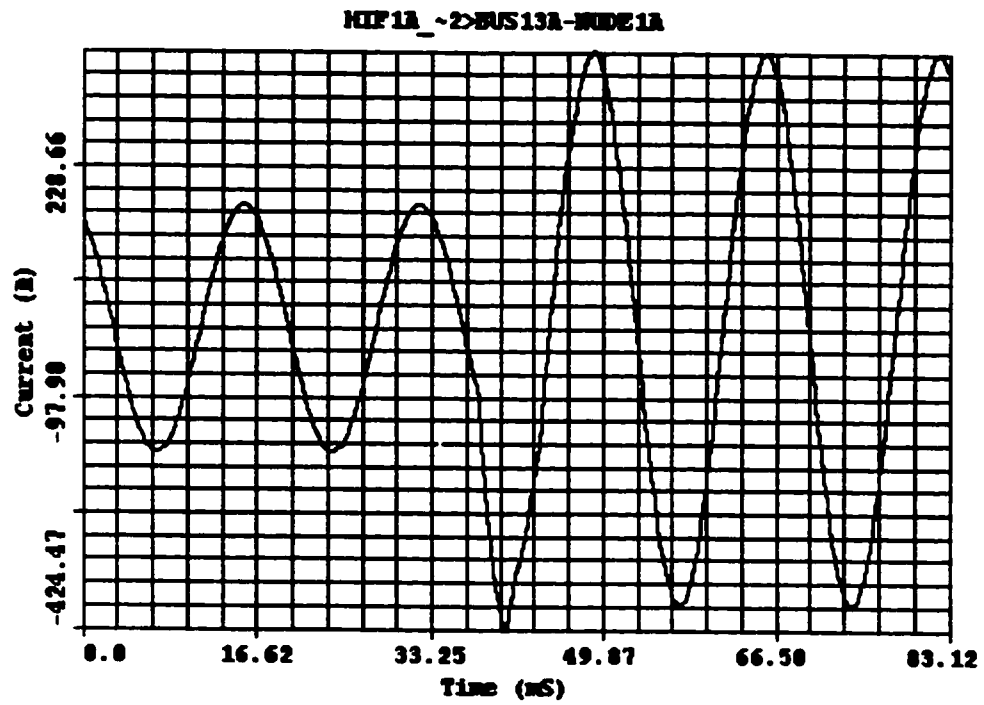


**Figure B.8.2: Phase-A Current Waveform for HIF at Node-1 (Phase-A)  
with Line Impedance Increased by 20 %**

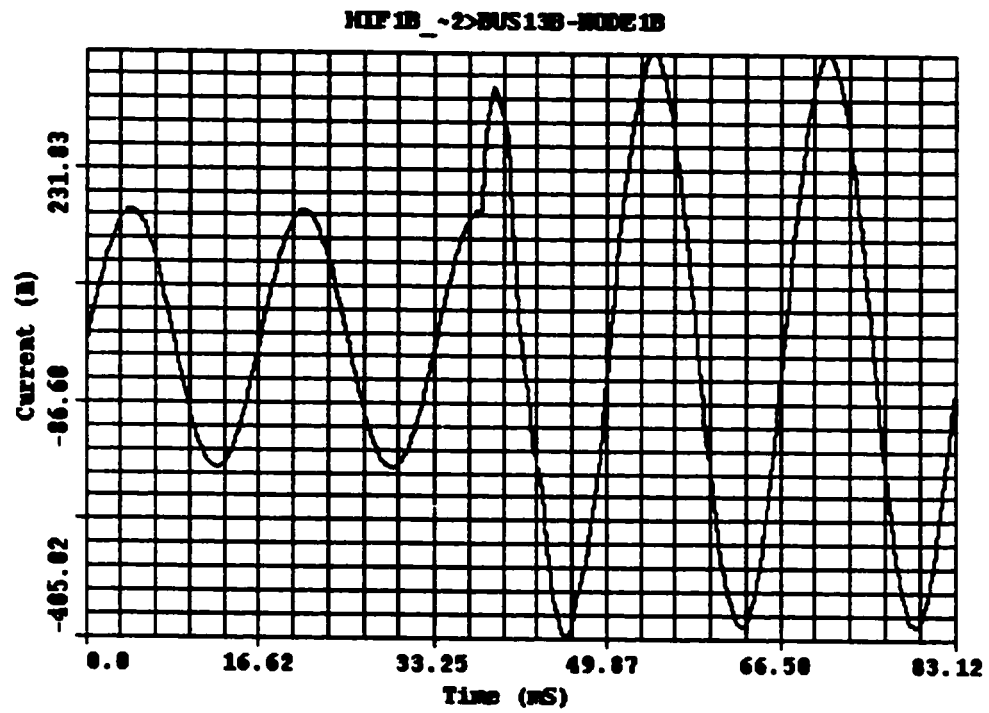


**Figure B.8.3: Phase-B Current Waveform for HIF at Node-1 (Phase-B)  
with Line Impedance Increased by 20 %**

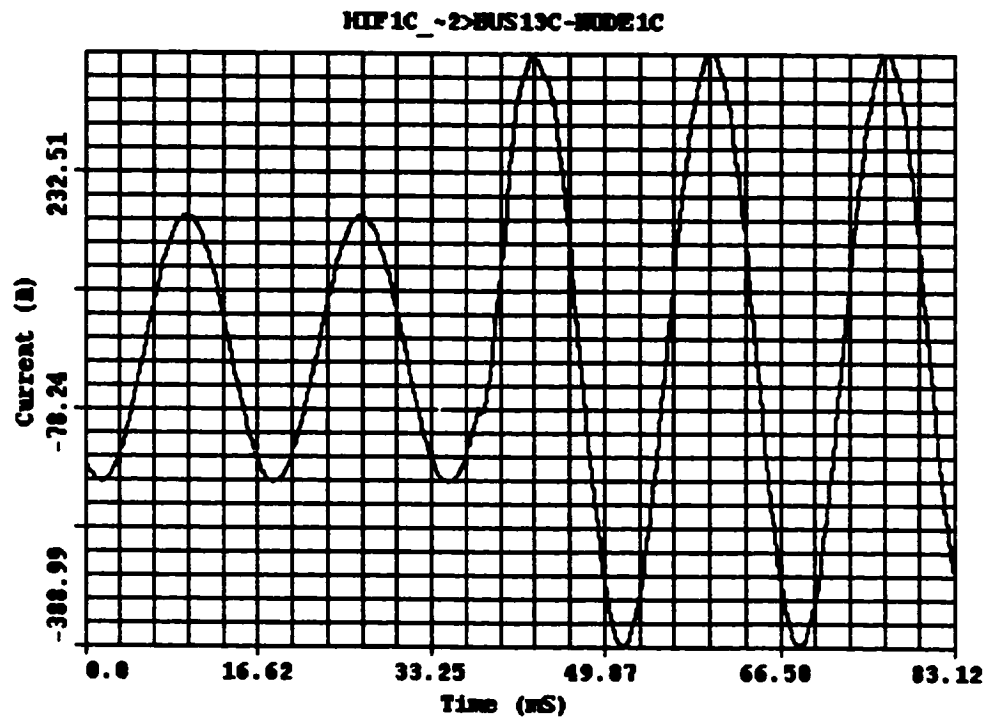


**Figure B.8.4: Phase-C Current Waveform for HIF at Node-1 (Phase-C)  
with Line Impedance Increased by 20 %**

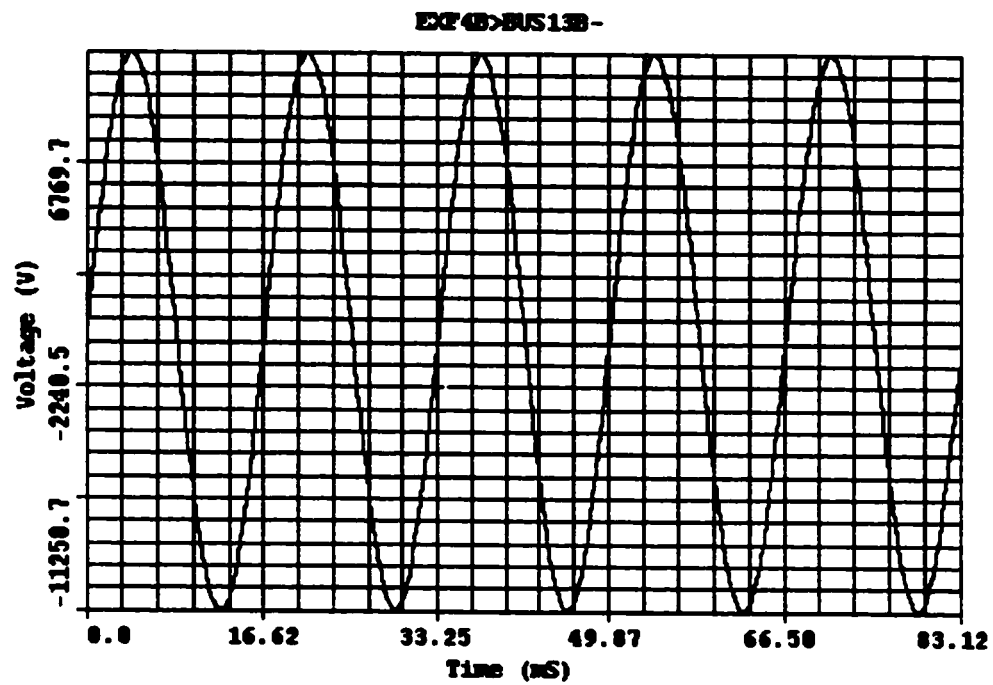


**Figure B.9.1: Phase-B Voltage Waveform for HIF on Phase-B at Node-4  
with Extended Feeder**

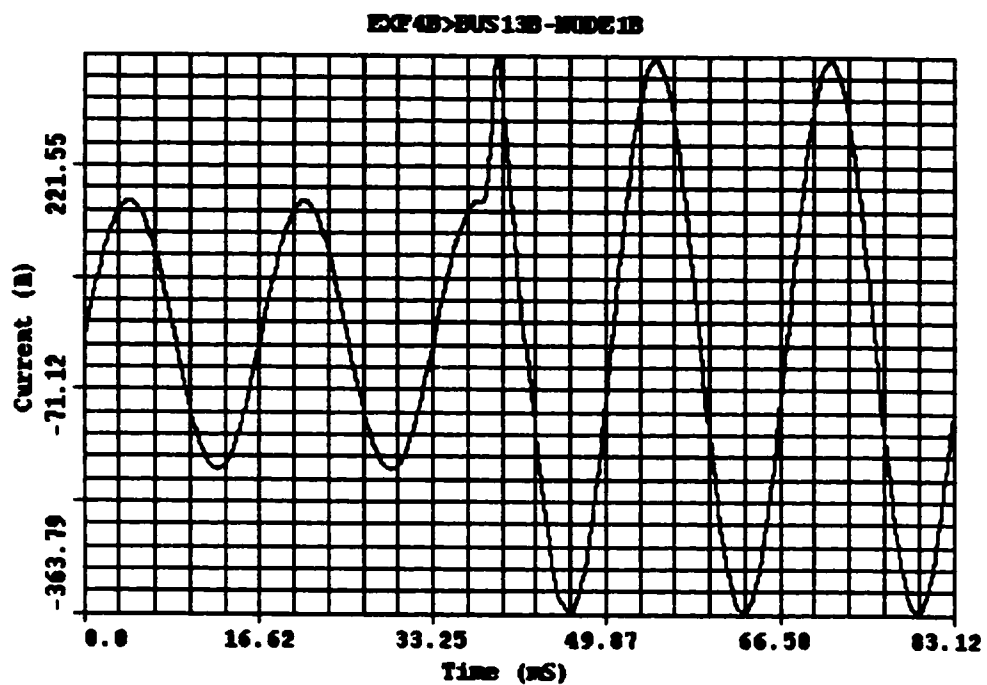


**Figure B.9.2: Phase-B Current Waveform for HIF on Phase-B at Node-4  
with Extended Feeder**

resulting waveforms are utilized for checking the generalization capability of the proposed ANN-based HIF diagnosis system.

### **B.10 HIF for Lightly Loaded Feeder**

The waveforms indicated in Figures B.10.1 to B.10.4 are those resulted from simulating HIFs at Node-1 with transformer T2 and Capacitor C1 disconnected. Again this is performed to obtain waveforms for a totally different feeder from the feeder model. These have been used for generalization check of the proposed HIF diagnosis systems.

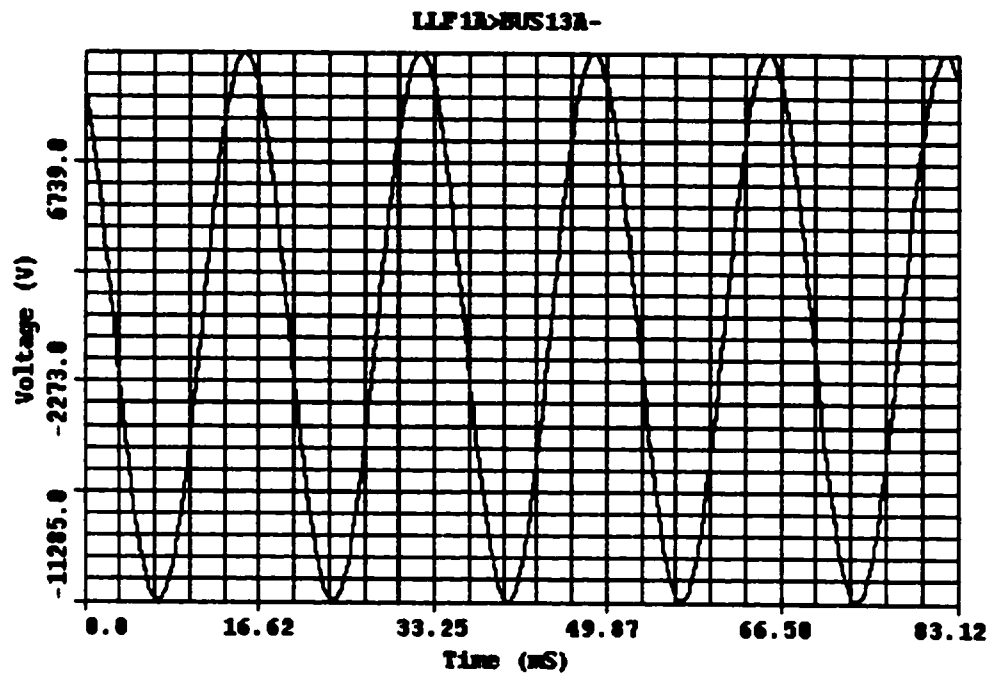


**Figure B.10.1: Phase-A Voltage Waveform for HIF on Phase-A at Node-1  
with T2 and C1 Disconnected**

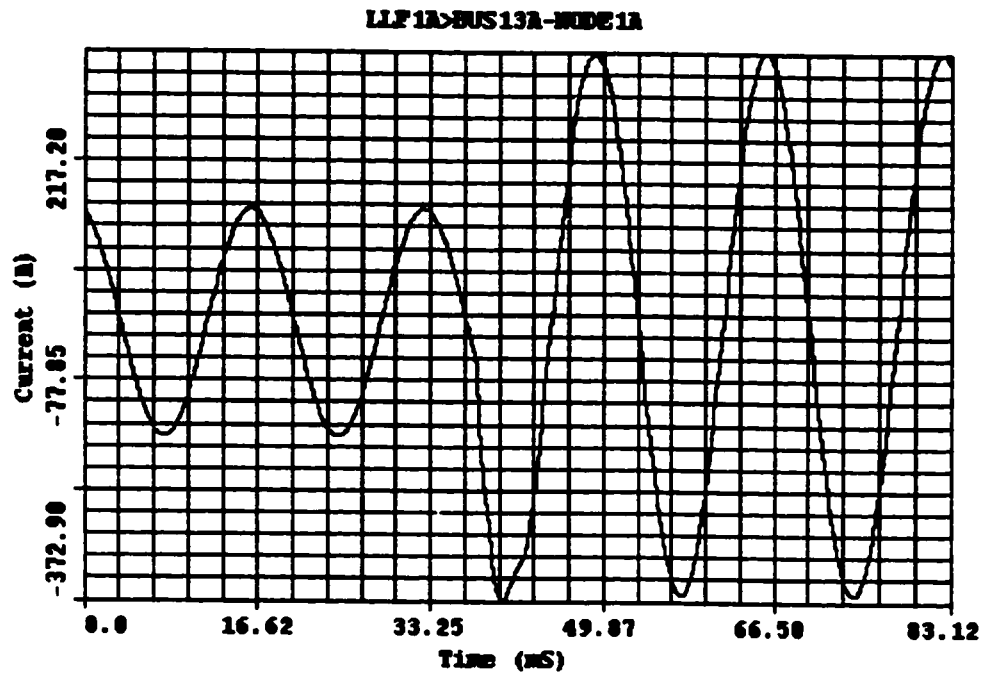


**Figure B.10.2: Phase-A Current Waveform for HIF on Phase-A at Node-1  
with T2 and C1 Disconnected**



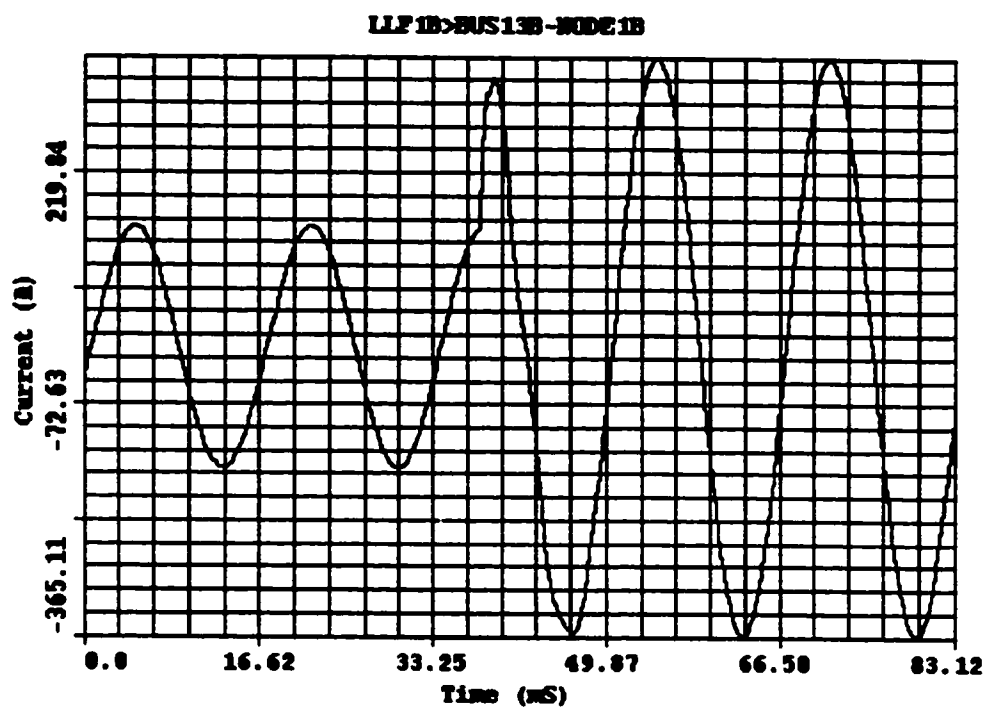


**Figure B.10.3: Phase-B Current Waveform for HIF on Phase-B at Node-1  
with T2 and C1 Disconnected**

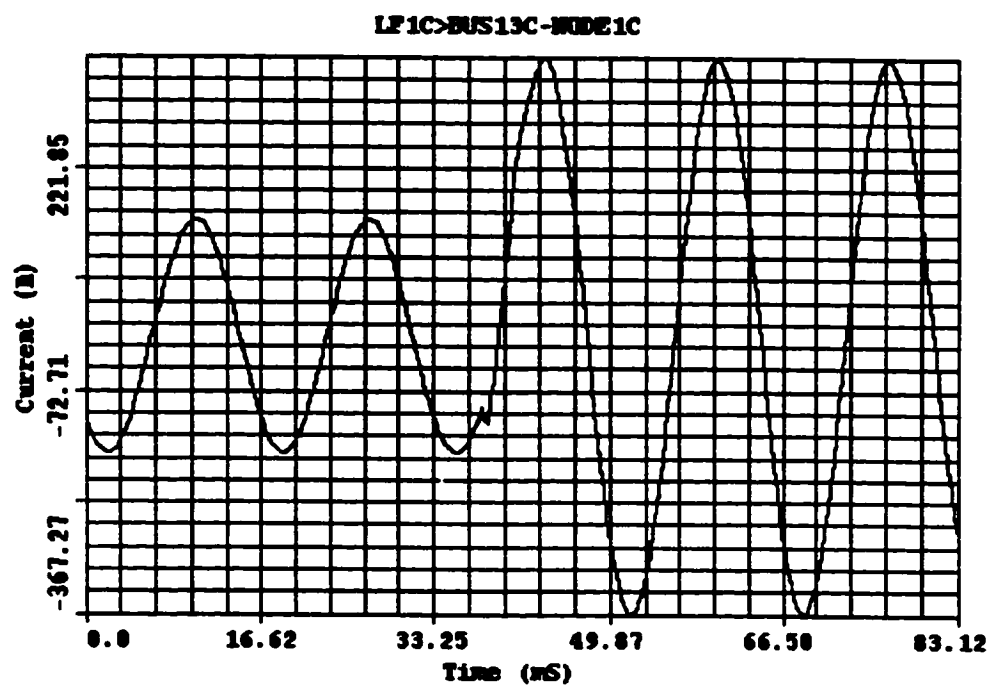


**Figure B.10.4: Phase-C Current Waveform for HIF on Phase-C at Node-1  
with T2 and C1 Disconnected**

## **Appendix C**

### **MATLAB M-FILES**

This appendix describes the M-files that have been used for reading and building the input matrices to the ANN. It also includes the M-files used for training the ANN and testing it with the test and generalization (or validation) cases. Only the m-files that are created for design D1F are presented here as an example.

#### **C.1 M-File for Reading the Case Matrices for Design D1F**

The sampled data of the voltage and current waveforms that result from the EMTP simulations are first converted to MS-Excel sheets. Next, an m-file is created for each EMTP case in the form of a 300X6 matrix. The m-file (called bigmaty1.m) used for reading these m-files is shown in the box hereunder with description of the names used for the m-files of the cases that were used for training, testing and checking the generalization of the ANN for design D1F.

```

clear all
NLS1;
NLS2;
NLS3;
NLS4;
NLCS11;
NLCS12;
NLCS13;
NLCS21;
NLCS22;
NLCS23;
NLCS31;
NLCS32;
NLCS33;
NLCS41;
NLCS42;
NLCS43;
F1A;
F1B;
F1C;
F2A;
F2B;
F2C;
F3A;
F3B;
F3C;
F4A;
F4B;
F4C;
FLS1A;
FLS1B;
FLS1C;
FLS2A;
FLS2B;
FLS2C;
FLS3A;
FLS3B;
FLS3C;
FLS4A;
FLS4B;
FLS4C;
FLCS1A;
FLCS1B;
FLCS1C;
FLCS2A;
FLCS2B;
FLCS2C;
FLCS3A;
FLCS3B;
FLCS3C;
FLCS4A;
FLCS4B;
FLCS4C;

```

Reading normal load switching cases

Reading normal load and capacitor switching cases

Reading high impedance fault with no load or capacitor switching cases

Reading high impedance fault with load switching cases

Reading high impedance fault with load and capacitor switching cases

## C.2 M-File for Building the ANN Input and Test Matrices for Design D1F

The next m-file (called PT4.m) is used to manipulate the 300X6 matrices that were created using the bigmaty1.m m-file into vectors each of which is sized 1800X1. Each of these vectors represent a case of feeder simulation. Next, the m-file combines these vectors to form two matrices. The first matrix (p), sized 1800X39, is used for ANN training. The second matrix (ptest) is sized 1800X13 and used for testing the ANN design D1F. The m-file also defines the target output vector (t) which is used for training the ANN to recognize the desired outputs for each of the 39 cases used during the learning phase.

**File Name: PT4.m**

### % Building the 52 Vectors for ANN Training and Testing

```
p1=[NLS1(:,1);NLS1(:,3);NLS1(:,5);NLS1(:,2);NLS1(:,4);NLS1(:,6)];
p2=[NLS2(:,1);NLS2(:,3);NLS2(:,5);NLS2(:,2);NLS2(:,4);NLS2(:,6)];
p3=[NLS3(:,1);NLS3(:,3);NLS3(:,5);NLS3(:,2);NLS3(:,4);NLS3(:,6)];
p4=[NLS4(:,1);NLS4(:,3);NLS4(:,5);NLS4(:,2);NLS4(:,4);NLS4(:,6)];
p5=[NLCS11(:,1);NLCS11(:,3);NLCS11(:,5);NLCS11(:,2);NLCS11(:,4);NLCS11(:,6)];
p6=[NLCS12(:,1);NLCS12(:,3);NLCS12(:,5);NLCS12(:,2);NLCS12(:,4);NLCS12(:,6)];
p7=[NLCS13(:,1);NLCS13(:,3);NLCS13(:,5);NLCS13(:,2);NLCS13(:,4);NLCS13(:,6)];
p8=[NLCS21(:,1);NLCS21(:,3);NLCS21(:,5);NLCS21(:,2);NLCS21(:,4);NLCS21(:,6)];
p9=[NLCS22(:,1);NLCS22(:,3);NLCS22(:,5);NLCS22(:,2);NLCS22(:,4);NLCS22(:,6)];
p10=[NLCS23(:,1);NLCS23(:,3);NLCS23(:,5);NLCS23(:,2);NLCS23(:,4);NLCS23(:,6)];
p11=[NLCS31(:,1);NLCS31(:,3);NLCS31(:,5);NLCS31(:,2);NLCS31(:,4);NLCS31(:,6)];
p12=[NLCS32(:,1);NLCS32(:,3);NLCS32(:,5);NLCS32(:,2);NLCS32(:,4);NLCS32(:,6)];
p13=[NLCS33(:,1);NLCS33(:,3);NLCS33(:,5);NLCS33(:,2);NLCS33(:,4);NLCS33(:,6)];
p14=[NLCS41(:,1);NLCS41(:,3);NLCS41(:,5);NLCS41(:,2);NLCS41(:,4);NLCS41(:,6)];
p15=[NLCS42(:,1);NLCS42(:,3);NLCS42(:,5);NLCS42(:,2);NLCS42(:,4);NLCS42(:,6)];
p16=[NLCS43(:,1);NLCS43(:,3);NLCS43(:,5);NLCS43(:,2);NLCS43(:,4);NLCS43(:,6)];
p17=[F1A(:,1);F1A(:,3);F1A(:,5);F1A(:,2);F1A(:,4);F1A(:,6)];
p18=[F1B(:,1);F1B(:,3);F1B(:,5);F1B(:,2);F1B(:,4);F1B(:,6)];
p19=[F1C(:,1);F1C(:,3);F1C(:,5);F1C(:,2);F1C(:,4);F1C(:,6)];
p20=[F2A(:,1);F2A(:,3);F2A(:,5);F2A(:,2);F2A(:,4);F2A(:,6)];
p21=[F2B(:,1);F2B(:,3);F2B(:,5);F2B(:,2);F2B(:,4);F2B(:,6)];
p22=[F2C(:,1);F2C(:,3);F2C(:,5);F2C(:,2);F2C(:,4);F2C(:,6)];
p23=[F3A(:,1);F3A(:,3);F3A(:,5);F3A(:,2);F3A(:,4);F3A(:,6)];
```

**Continuation of PC Program**

```
p24=[F3B(:,1);F3B(:,3);F3B(:,5);F3B(:,2);F3B(:,4);F3B(:,6)];
p25=[F3C(:,1);F3C(:,3);F3C(:,5);F3C(:,2);F3C(:,4);F3C(:,6)];
p26=[F4A(:,1);F4A(:,3);F4A(:,5);F4A(:,2);F4A(:,4);F4A(:,6)];
p27=[F4B(:,1);F4B(:,3);F4B(:,5);F4B(:,2);F4B(:,4);F4B(:,6)];
p28=[F4C(:,1);F4C(:,3);F4C(:,5);F4C(:,2);F4C(:,4);F4C(:,6)];
p29=[FLS1A(:,1);FLS1A(:,3);FLS1A(:,5);FLS1A(:,2);FLS1A(:,4);FLS1A(:,6)];
p30=[FLS1B(:,1);FLS1B(:,3);FLS1B(:,5);FLS1B(:,2);FLS1B(:,4);FLS1B(:,6)];
p31=[FLS1C(:,1);FLS1C(:,3);FLS1C(:,5);FLS1C(:,2);FLS1C(:,4);FLS1C(:,6)];
p32=[FLS2A(:,1);FLS2A(:,3);FLS2A(:,5);FLS2A(:,2);FLS2A(:,4);FLS2A(:,6)];
p33=[FLS2B(:,1);FLS2B(:,3);FLS2B(:,5);FLS2B(:,2);FLS2B(:,4);FLS2B(:,6)];
p34=[FLS2C(:,1);FLS2C(:,3);FLS2C(:,5);FLS2C(:,2);FLS2C(:,4);FLS2C(:,6)];
p35=[FLS3A(:,1);FLS3A(:,3);FLS3A(:,5);FLS3A(:,2);FLS3A(:,4);FLS3A(:,6)];
p36=[FLS3B(:,1);FLS3B(:,3);FLS3B(:,5);FLS3B(:,2);FLS3B(:,4);FLS3B(:,6)];
p37=[FLS3C(:,1);FLS3C(:,3);FLS3C(:,5);FLS3C(:,2);FLS3C(:,4);FLS3C(:,6)];
p38=[FLS4A(:,1);FLS4A(:,3);FLS4A(:,5);FLS4A(:,2);FLS4A(:,4);FLS4A(:,6)];
p39=[FLS4B(:,1);FLS4B(:,3);FLS4B(:,5);FLS4B(:,2);FLS4B(:,4);FLS4B(:,6)];
p40=[FLS4C(:,1);FLS4C(:,3);FLS4C(:,5);FLS4C(:,2);FLS4C(:,4);FLS4C(:,6)];
p41=[FLCS1A(:,1);FLCS1A(:,3);FLCS1A(:,5);FLCS1A(:,2);FLCS1A(:,4);FLCS1A(:,6)];
p42=[FLCS1B(:,1);FLCS1B(:,3);FLCS1B(:,5);FLCS1B(:,2);FLCS1B(:,4);FLCS1B(:,6)];
p43=[FLCS1C(:,1);FLCS1C(:,3);FLCS1C(:,5);FLCS1C(:,2);FLCS1C(:,4);FLCS1C(:,6)];
p44=[FLCS2A(:,1);FLCS2A(:,3);FLCS2A(:,5);FLCS2A(:,2);FLCS2A(:,4);FLCS2A(:,6)];
p45=[FLCS2B(:,1);FLCS2B(:,3);FLCS2B(:,5);FLCS2B(:,2);FLCS2B(:,4);FLCS2B(:,6)];
p46=[FLCS2C(:,1);FLCS2C(:,3);FLCS2C(:,5);FLCS2C(:,2);FLCS2C(:,4);FLCS2C(:,6)];
p47=[FLCS3A(:,1);FLCS3A(:,3);FLCS3A(:,5);FLCS3A(:,2);FLCS3A(:,4);FLCS3A(:,6)];
p48=[FLCS3B(:,1);FLCS3B(:,3);FLCS3B(:,5);FLCS3B(:,2);FLCS3B(:,4);FLCS3B(:,6)];
p49=[FLCS3C(:,1);FLCS3C(:,3);FLCS3C(:,5);FLCS3C(:,2);FLCS3C(:,4);FLCS3C(:,6)];
p50=[FLCS4A(:,1);FLCS4A(:,3);FLCS4A(:,5);FLCS4A(:,2);FLCS4A(:,4);FLCS4A(:,6)];
p51=[FLCS4B(:,1);FLCS4B(:,3);FLCS4B(:,5);FLCS4B(:,2);FLCS4B(:,4);FLCS4B(:,6)];
p52=[FLCS4C(:,1);FLCS4C(:,3);FLCS4C(:,5);FLCS4C(:,2);FLCS4C(:,4);FLCS4C(:,6)];
```

### % Forming the (p) Matrix for ANN Training

```
p=[p1 p2 p4 p6 p7 p8 p10 p11 p12 p14 p15 p16 p17 p18 p19 p21 p22 p23 p25 p26 p27 ...
    p30 p31 p32 p34 p35 p36 p38 p39 p40 p41 p42 p43 p45 p46 p47 p49 p50 p51];
```

### % Forming the (ptest) Matrix for ANN Testing

```
ptest=[p3 p5 p9 p13 p20 p24 p28 p29 p33 p37 p44 p48 p52];
```

### % Defining the Desired Output Matrix (t)

```
t=[0 0 0 0 0 0 0 0 0 0 0 0 1 1 1 1 1 1 1 1 1 1 1 1 1 1 1 1 1 1 1 1 1 1 1 1; ...
    0 0 0 0 0 0 0 0 0 0 0 0 1 1 1 2 2 3 3 4 4 1 1 2 2 3 3 4 4 4 1 1 1 2 2 3 3 4 4; ...
    0 0 0 1 1 1 1 1 1 1 1 1 2 2 2 2 2 2 2 2 3 3 3 3 3 3 3 3 4 4 4 4 4 4 4 4; ...
    0 0 0 0 0 0 0 0 0 0 0 0 1 2 3 2 3 1 3 1 2 2 3 1 3 1 2 1 2 3 1 2 3 2 3 1 3 1 2];
```

### C.3 M-File for ANN Training for Design D1F

The next short m-file (named Train4.m) calls the above two m-files (bigmaty1.m and PT4.m) and train the four-layer feedforward ANN using the scaled conjugate gradient (TRAINSCG) training algorithm with tan-sigmoid (TANSIG) transfer functions.

**File Name: Train4.m**

```
clear all;
load bigmaty1;
load PT4;
[pn,minp,maxp,tn,mint,maxt] = premnmx(p,t);
net=newff(minmax(pn),[35,20,30,4],{'tansig','tansig','tansig','tansig'}...
,'trainscg');
net.trainParam.epochs = 1000;
net.trainParam.goal = 1e-5;
net = train(net,pn,tn);
```

### C.4 M-File for ANN Testing for Design D1F

The last m-file (named Ptest.m) is used for testing the ANN design D1F for cases in the (ptest) matrix (13 cases) which were not presented to the ANN during its training.

**File Name: Ptest.m**

```
% Testing ANN for cases not presented to it during training

pnewn = tramnmx(ptest,minp,maxp);
anewn = sim(net,pnewn);
anew = postmnmx(anewn,mint,maxt)
```

# **Bibliography**

- [1] B. M. Aucoin, and R. H. Jones, "High Impedance Fault Detection Implementation Issues", *IEEE Transactions on Power Delivery*, Vol. 11, No. 1, January 1996, pp. 139-148.
- [2] Craig G. Wester, "High Impedance Fault Detection on Distribution Systems", *The Internet, GE Power Management WEB Site*, December 1998, pp.1-5.
- [3] Mike Aucoin, "Status of High Impedance Fault Detection", *IEEE Transactions on Power Apparatus and Systems*, Vol. PAS-104, No. 3, March 1985, pp. 638-644.
- [4] Report of IEEE PSRC Working Group D15, "High Impedance Fault Detection Technology", *The Internet, GE Power Management WEB Site*, March 2001, pp.1-11.
- [5] J. T. Tengdin, E. E. Baker, J. J. Burke, B. D. Russell, R. H. Jones, T. E. Wiedman, and N. J. Johnson, "Application of High Impedance Fault Detectors - A Summary of the Panel Session Held at the 1995 IEEE PES Summer Meeting", *Proceedings of the IEEE Transmission and Distribution Conference*, September 1996, pp. 116-122.



- [6] E. A. Mohamed, and N. D. Rao, "Artificial Neural Network Based Fault Diagnostic System for Electric Power Distribution Feeders", *Electric Power Systems Research*, Vol. 35, 1995, pp. 1-10.
- [7] T. S. Sidhu, H. Singh, and M. S. Sachdev, "Design, Implementation and Testing of an Artificial Neural Network Based Fault Direction Discriminator for Protecting Transmission Lines", *IEEE Transactions on Power Delivery* , Vol. 10, No. 2, April 1995, pp. 697-706.
- [8] Saudi Electricity Company (SEC-ERB) Intranet, Operating Areas WEB Site, 2001 (1422 H).
- [9] "Distribution Fault Current Analysis" , EPRI Report RP-1209-1, Vol. 1-2, Prepared by Power Technologies Inc., January 1983.
- [10] J. A. Momoh, L. G. Dias, and D. N. Laird, "An Implementation of a Hybrid Intelligent Tool for Distribution System Fault Diagnosis", *IEEE Transactions on Power Delivery* , Vol. 12, No. 2, April 1997, pp. 1035-1040.
- [11] Sonja Ebron, David L. Lubkeman, and Mark White, "Neural Network Approach to the Incipient Faults on Power Distribution Feeders" , *IEEE Transactions on Power Delivery* , Vol. 5, No. 2, April 1990, pp. 905-914.
- [12] J. Carr, "Detection of High Impedance Faults on Multi-Grounded Primary Distribution Systems", *IEEE Transactions on Power Apparatus and Systems* , Vol. PAS-100, No. 4, April 1981, pp. 2008-2016.

- [13] Howard Calhoun, Martin T. Bishop, and Charles H. Eicher, "Development and Testing of an Electro-Mechanical Relay to Detect Fallen Distribution Conductors", *IEEE Transactions on Power Apparatus and Systems*, Vol. PAS-101, No. 6, June 1982, pp. 1643-1650.
- [14] S. J. Balser, K. A. Clements, and D. J. Lawrence, "A Microprocessor-Based Technique for Detection of High Impedance Faults", *IEEE Transactions on Power Delivery* , Vol. PWRD-1, No. 3, July 1986, pp. 252-258.
- [15] B. M. Aucoin, and B. D. Russell, "Detection of Distribution High Impedance Faults Using Burst Noise Signals Near 60 Hz", *IEEE Transactions on Power Delivery* , Vol. PWRD-2, No. 2, April 1987, pp. 347-348.
- [16] B. M. Aucoin, and B. D. Russell, "Distribution High Impedance Fault Detection Utilizing High Frequency Current Components", *IEEE Transactions on Power Apparatus and Systems* , Vol. PAS-101, No. 6, June 1982, pp. 1596-1606.
- [17] David C. Yu, and Shoukat H. Khan, "An Adaptive High and Low Impedance Fault Detection Method", *IEEE Transaction on Power Delivery*, Vol. 9, No. 4, October 1994, pp.1812-1821.
- [18] P. R. Silva, and A. Santos Jr., "Impulse Response Analysis of a Real Feeder for High Impedance Fault Detection", *Proceedings of the IEEE Transmission and Distribution Conference*, April 1994, Chicago, pp. 276-283.

- [19] J. A. Momoh, L. G. Dias, T. Thor, and D. Laird, "Rule Based Decision Support System for Single-Line Fault Detection in a Delta-Delta Connected Distribution System", *IEEE Transactions on Power Systems*, Vol. 9, No. 2, May 1994, pp. 782-788.
- [20] A. F. Sultan, G. W. Swift, and D. J. Fedirchuk, "Detection of High Impedance Arcing Faults Using a Multi-Layer Perceptron", *IEEE Transactions on Power Delivery*, Vol. 7, No. 4, October 1992, pp. 1871-1877.
- [21] Yasmine Assef, Patrick Bastard, and Michel Meunier, "Artificial Neural Networks for Single Phase Fault Detection in Resonant Grounded Power Distribution Systems", *Proceedings of the IEEE Transmission and Distribution Conference*, September 1996, pp. 566-572.
- [22] K. L. Butler, and J. A. Mamoh, "A Neural Net Based Approach for Fault Diagnosis in Distribution Networks", *Proceedings of the IEEE PES Winter Meeting*, January 2000, Singapore, pp. 23-26.
- [23] A. Mohamed, and M. D. A. Mazumder, "A Neural Network Approach to Fault Diagnosis in a Distribution System", *International Journal of Power and Energy Systems*, Vol. 19, No. 2, 1999, pp. 129-134.
- [24] Shyh-Jier Huang, and Cheng-Tao Hsieh, "High Impedance Fault Detection Utilizing a Morlet Wavelet Transform Approach", *IEEE Transaction on Power Delivery*, Vol. 14, Mo. 4, October 1999, pp. 1401-1410.

- [25] A. M. Sharat, L. A. Snider, and K. Debnath, "A Neural Network Based Back Error Propagation Relay Algorithm For Distribution System High Impedance Fault Detection", *Proceedings of the 2nd International Conference on Advances in Power System Control, Operation and Management, APSCOM – 1993*, pp. 613-620.
- [26] A. P. Apostolov, J. Bronfeld, C. H. M. Saylor, and P. B. Snow, "An Artificial Neural Network Approach To The Detection Of High Impedance Faults", *Proceedings of the International Conference and Exhibition on Expert Systems Applications for the Electric Power Industry*, 1993, USA.
- [27] Howard Demuth, and Mark Beale, *Neural Network Toolbox for Use with MATLAB® - User's Guide Version 3.0*, The Math Works Inc., Natick, MA, USA, 1997.
- [28] C. Rodriguez, S. Rementeria, J. I. Martin, A. Lafuente, J. Muguerza, and J. Perez, "Fault Analysis with Modular Neural Networks", *Electric Power and Energy Systems*, Vol. 18, No. 2, 1996, pp. 99-110.
- [29] Anne-Johan Annema, *Feed-Forward Neural Networks – Vector Decomposition Analysis, Modeling and Analog Implementation*, Kluwer Academic Publishers, Norwell, Massachusetts, USA, 1995.
- [30] Dimitris C. Dracopoulos, *Evolutionary Learning Algorithms for Neural Adaptive Control - Perspective in Neural Computing*, Springer - Verlag, London, UK, 1997.

- [31] Mladen Kezunovic and Igor Ricalo, "Detect and Classify Faults Using Neural Nets", *IEEE Computer Applications in Power*, October 1996, pp. 42-47.
- [32] R. C. Eberhart and R. W. Dobbins, *Neural Network PC Tools*, Academic Press Inc., California, USA, 1990.
- [33] "*Electromagnetic Transients Program (EMTP) Primer*", EPRI Report EL-4202, Prepared by Westinghouse Electric Corporation, Pennsylvania, USA, September 1985.
- [34] "*Electromagnetic Transients Program (EMTP) Revised Rule Book, Version 2, Volume 1: Main Program*", EPRI Report EL-6421-L, Research Project 2149-4, Prepared by Systems Control Division of Power Automation Inc., California, USA, June 1989.
- [35] Hydro-Quebec Research Institute (IREC), Teqsim International Inc., Ecole de Technologie Supérieure and Université Laval, *Power System Blockset for Use with SIMULINK® - User's Guide Version 1*, The Math Works Inc., Natick, MA, USA, January 1999.
- [36] Michel Misiti, Yves Misiti, George Oppenheim, and Jean-Michel Poggi, *Wavelet Toolbox for Use with MATLAB® - User's Guide Version 1*, The Math Works Inc., Natick, MA, USA, 1996.

## **V i t a**

- **Mohammad Hasan Mohammad Al-Mubarak**
- **Born in Al-Hassa, Saudi Arabia in October 1969.**
- **Received Degree of Bachelor of Science in Electrical Engineering, with high honors, from King Fahd University of Petroleum and Minerals, Dhahran, Saudi Arabia in July 1992.**
- **Working in the Saudi Electricity Company-Eastern Region Branch (SEC-ERB), Dammam, Saudi Arabia as Supervisor, Engineering Standards Unit.**
- **Completed Master's degree requirements in Electrical Engineering at King Fahd University of Petroleum and Minerals, Dhahran, Saudi Arabia in September 2001.**